NOTE TO USERS

This reproduction is the best copy available.

UMI®

CFD Study of Balcony Spill Plumes: Focused on the Balcony Area

by
Yoon J. Ko

Supervised by
George Hadjisophocleous

January 2006
A thesis submitted in partial fulfillment of the requirements for the degree of
Master of Applied Science in Civil Engineering
Department of Civil Engineering
Carleton University
Ottawa, Ontario Canada

Your file Votre référence
ISBN: 0-494-13445-3
Our file Notre référence
ISBN: 0-494-13445-3

ABSTRACT

This thesis presents the results of an in-depth investigation of air entrainment in balcony spill plumes. The focus of this research was the smoke flow under the balcony area and the rotating regions using CFD modelling and full-scale experiments. Comparisons between model predictions and experimental data indicate that the CFD predictions agree well with experimental data both of which show a large degree of air entrainment into the rotating flow. Mass flow rates of vertical spill plumes near the balcony area were examined to evaluate the applicability of existing balcony spill plume correlations. The results of this study were used to develop an empirical correlation to calculate air entrainment rate at the spill edge. The correlation considers the various factors affecting air entrainment under the balcony area and the rotating region.

ACKNOWLEDGEMENT

Foremost, I would like to thank Dr. George Hadjisophocleous for his hard work, scientific knowledge, patience, and dedication during the process of developing the ideas presented in this thesis, especially during the extended process of completing the thesis.

I wish to express my sincere gratitude and appreciation to the Fire Risk Management Program of the National Research Council's Institute for Research in Construction, and most especially to Dr. Gary D. Lougheed, Cameron McCartney, and Eric Gibbs for their support.

The faculty in the Fire Engineering Program, Dr. Proulx, Dr. Benichou, have been an invaluable resource for me. Their unsurpassed expertise significantly broadened my knowledge and fuelled my enthusiasm to carry out further research. Specifically, I need to recognize Dr. Jim R. Mehaffey, for his advice and assistance.

Finally, I would like to thank my family for their limitless love and support throughout this endeavour.

TABLE OF CONTENTS

1 INTRODUCTION 1

1.1 BACKGROUND 1

1.1.1 Atrium Smoke Management 1

1.1.1.1 What is smoke? 1

1.1.1.2 Smoke management system design objectives 2

1.1.1.3 Clear layer height 3

1.1.1.4 Types of plume in the atrium 4

1.1.2 Balcony Spill Plume 6

1.1.3 Balcony Spill Plume vs. Axisymmetric Plume 8

1.2 THE PROBLEM 11

1.2.1 Factors affecting air entrainment of balcony spill plumes 11

1.2.2 The problem of the initial approach flow 13

1.3 OBJECTIVES 14

2 LITERATURE REVIEW 16

2.1 BALCONY SPILL PLUME CORRELATIONS 16

2.1.1 Existing Correlations 16

2.1.2 Limitation and uncertainties of spill plume equations 20

2.2 AIR ENTRAINMENT UNDER THE BALCONY AND THE ROTATING REGION 23

2.2.1 Method: Amount of air entrainment, δm 23

2.2.1.1 Morgan and Marshall [1975] 23

2.2.1.2 Thomas [1987] 25

2.2.1.3 Hansell [1993] 25

2.2.2 Method 2: Layer depth 27

2.2.2.1 Poreh, Morgan, Marshall, and Harrison [1998] 27

2.2.2.2 Thomas, Morgan and Marshall [1998] 29

2.2.2.3 Harrison [2004] 31

2.2.3 Method 3: The virtual origin, Δ 33

2.2.3.1 Law [1986, 1995] 33

2.2.3.2 Thomas [1987] 35

2.3 EXPERIMENTAL STUDIES 35

2.3.1 Balcony spill plume from channelled flow: Morgan and Marshall [1975] *35*

2.3.2 Morgan and Marshall [1979] *36*

2.3.2.1 Effective layer depth 37

2.3.3 Hansell, Morgan and Marshall [1993] *37*

2.3.3.1 Temperature and balcony breadth limitation 38

2.3.4 Marshall and Harrison [1996] *39*

2.3.4.1 Effect of atrium size 40

2.3.5 Harrison [2004] *40*

2.3.5.1 Downstand at the spill edge 41

2.4 CFD MODELLING WORK 42

2.4.1 Miles, Kumar, and Cox [1996] *42*

2.4.2 Chow [1998] *42*

2.4.3 Chow [1999] *42*

2.4.4 Chow and Li [2001] *43*

2.4.5 Harrison [2004] *43*

2.5 SUMMARY 44

3 SCOPE OF WORK 46

4 SIMPLE MODELLING STUDY 48

4.1 GENERAL 48

4.1.1 CFD modelling of smoke movement *48*

4.1.2 FDS (Fire Dynamics Simulator) *48*

4.1.3 The simplified problem of balcony spill plume *49*

4.1.4 Objectives *50*

4.2 DOMAIN SIZE TESTING 51

4.2.1 Description of modelling *51*

4.2.2 Results *53*

4.3 TEMPERATURE AND VELOCITY EFFECTS 56

4.3.1 Description of modelling *56*

4.3.2 Results *58*

4.3.2.1 Flow behaviour 58

4.3.2.2 M_s / M_b and Ri 60

4.4 PARAMETER SENSITIVITY TESTING 61

4.4.1 Description of modelling *62*

4.4.2 Results *63*

4.4.2.1 Parameter effects 63

4.4.2.2 Parameter effect on flow characteristics and the air entrainment 65

4.5 SUMMARY OF RESULTS AND DISCUSSION 67

5 CFD MODELLING: DESCRIPTION AND PROCEDURE 69

5.1 CFD MODELLING DESCRIPTION 69

5.1.1 Model geometry *69*

5.1.2 Fire simulation *70*

5.1.3 Computational domain and grid size *73*

5.2 SIMULATIONS 75

5.2.1 Parameters of interest and variations *75*

5.3 OUTPUT DATA 78

5.3.1 Calculation of the mass flow rate of gases *78*

5.3.1.1 FDS code modification 78

5.3.1.2 Planes of interest 79

5.3.2 Calculation of the layer depth *81*

5.3.3 Error Analysis *81*

6 FULL-SCALE EXPERIMENTS: THE TEST FACILITY 82

6.1.1 Model geometry: Fire compartment *82*

6.1.2 Fire simulation *83*

6.1.3 Instrumentation *83*

6.1.4 The series of experiments *87*

7 RESULTS 88

7.1 GENERAL 88

7.1.1 Flow behaviour *88*

7.1.1.1 Typical flow behaviour 88

7.1.1.2 Turbulent motion at the balcony area 91

7.1.1.3 Mass loss for unchanneled flows 92

7.1.2 The onset of steady-state conditions *94*

7.2 COMPARISON OF FDS RESULTS WITH EXPERIMENTAL RESULTS 95

7.2.1.1 Temperature and velocity profiles at the doorway 96

7.2.1.2 Temperature and velocity profiles at the end of the balcony 98

7.2.1.3 Temperature and velocity profiles at the balcony edge 99

7.2.1.4 Temperature and velocity profile 1 m above the balcony 101

7.2.1.5 Discussion 102

7.3 MASS FLOW RATE RESULTS 103

7.3.1 Summary of the results from CFD modelling *103*

7.3.2 Mass flow rates over the flow path *106*

7.4 INITIAL ANALYSIS OF RESULTS 110

7.4.1 Overview of the mass flow rate of the balcony spill plume *110*

7.4.2 The limiting height of rise of the spill plume correlation *113*

7.4.3 Comparison with existing methods *117*

7.4.3.1 Method 1: Amount of air entrainment, δm 119

7.4.3.2 Method 2: Layer depth 120

7.4.3.3 Method 3: The virtual origin 123

7.4.3.4 Discussion 124

8 ANALYSIS AND DISCUSSION **126**

8.1 TEMPERATURE AND VELOCITY TRANSITION UNDER THE BALCONY AREA 126

8.1.1 Behaviour at the door opening *127*

8.1.2 The end of the balcony *129*

8.1.3 At the balcony edge *131*

8.1.4 Characteristics of approach flow *133*

8.2 AIR ENTRAINMENT RATE INTO THE ROTATING FLOW 134

8.2.1 Overview of air entrainment into rotating flow *134*

8.2.2 Initial source conditions *137*

8.2.2.1 Characteristic source strength 137

8.2.2.2 Layer width –depth effect 138

8.2.3 Parameter effects *138*

8.2.3.1 Fascia and Draft curtain effect 138

8.2.3.2 Balcony effect 139

8.2.4 Empirical correlation of air entrainment rate of rotating flow *139*

8.3 AIR ENTRAINMENT RATE UNDER THE BALCONY 141

8.3.1 Overview of air entrainment rate under the balcony area *141*

8.3.2 Empirical correlation of air entrainment rate under the balcony area for case with draft curtains 143

8.4 VALIDATION OF EMPIRICAL CORRELATION 144

8.4.1 Comparison of experimental and simulated results *144*

8.4.2 Comparison with previous studies *145*

8.5 EMPIRICAL CORRELATION OF THE MASS FLOW RATE AT THE SPILL EDGE 148

8.5.1 Model limitations *149*

9 CONCLUSION AND RECOMMENDATION **150**

10 REFERENCES **153**

APPENDIX A. CODE MODIFICATION OF FDS FOR CALCULATING MASS FLOW RATE OF SMOKE 157

APPENDIX B. EXAMPLE FDS INPUT DATA 159

APPENDIX C. COMPARISON OF FDS PREDICTIONS WITH EXPERIMENTAL DATA 165

APPENDIX D. TEMPERATURE CORRELATION WITH Q/W : RESULTS FROM CASES WITHOUT DRAFT CURTAIN 186

LIST OF FIGURES

Figure 1.1 Atrium smoke filling and clear layer height [Lougheed and Hadjisophocleous 2001] 3
Figure 1.2 Free balcony spill plume scenario 7
Figure 1.3 Axisymmetric plume 8
Figure 1.4 Comparison of smoke production rate for axisymmetric plumes and balcony spill plumes (Q = 3.5 MW, h_b = 5m) 10
Figure 1.5 The problem of the flow under the balcony area and in the rotating region 12
Figure 2.1 Comparison of existing balcony spill plume formula 21
Figure 2.2 Schematic description of the proposed model by Poreh et al [1998] 28
Figure 2.3 The variation of Db with temperature [Tomas et al 1998] 30
Figure 2.4 Correlation between M_s and M_b at z = 0 [Tomas et al 1998] 31
Figure 2.5 Mass flow rate correlation with z (height of rise) [Law 1986] 34
Figure 2.6 Experimental configuration [Marshall and Harrison 1996] 40
Figure 4.1 The problem of the buoyant jet in the simple modelling study 50
Figure 4.2 Mass flow rate measurements at planes of interest 52
Figure 4.3 Mass flow rates at z = 4 m over time for computational domain size tests 53
Figure 4.4 Mass flow rate variation with respect to computational domain size 54
Figure 4.5 The air entrainment rates at the rotating region using various computational domain sizes 55
Figure 4.6 Vector slice of simulation TV2 (1) and T2V2 (2) 59
Figure 4.7 Simple model results displayed as a plot of M_s / M_b with respect to Ri 60
Figure 4.8 Velocity vector slices of simulation of the sensitivity test 65
Figure 4.9 A plot of M_s/M_b with respect to Ri : from parameter sensitivity tests 65
Figure 5.1 Model geometry 70
Figure 5.2 Plot of results of grid convergence test 74
Figure 5.3 Computational domain and grid size 74
Figure 5.4 Comparison of calculations of mass flow rate between the modified FDS and the FDS model. (M_w from HRR = 4 MW, W = 5m) 79
Figure 5.5 Definition of planes of interest to calculate mass flows 80
Figure 6.1 Full-scale test facility at the NRC: the fire compartment 82
Figure 6.2 Fire simulation in the fire compartment 83
Figure 6.3 A sketch of locations of the instrumentaion trees 84
Figure 6.4 Side view of the instrumentation map under the balcony area 85
Figure 6.5 Side view of instrumentation tree at the balcony edge tilted through 90 degrees to the perpendicular 86
Figure 6.6 Tilting down the measuring tree 86
Figure 7.1 Velocity vectors of the flow under the balcony (from Simulation S2M75NN) 89
Figure 7.2 Velocity vector of the flow under the balcony S2M75YN 89
Figure 7.3 Flow behaviour for channelled flow with fascia and draft curtains (from simulation S2M75YY) 90
Figure 7.4 Turbulent motion in the balcony area 91
Figure 7.5 Mass loss through both sides of the balcony 92
Figure 7.6 Mass loss observed for unchanneled flows (from simulation S3M75YN) 93
Figure 7.7 Mass loss observed in S1M75YN and areas to calculate the mass flow rate 93

Figure 7.8 Mass flow rate over time (Simulation S4M5NY) 94

Figure 7.9 Mass flow rate over time (Simulation-S1M12NY) 95
Figure 7.10 Temperature and velocity measurements at the opening, at the end of the balcony and at the balcony edge 96
Figure 7.11 Temperature rise profiles at the opening (S3M5YY and T3M5YY) 97
Figure 7.12 U-Velocity profiles at the compartment opening (S3M5YY and T3M5YY) 97
Figure 7.13 Temperature rise profile at the balcony end (S3M5YY and T3M5YY) 98
Figure 7.14 U-Velocity profile at the balcony end (S3M5YY and T3M5YY) 99
Figure 7.15 Temperature rise profile at the balcony edge (S3M5YY and T3M5YY) 100
Figure 7.16 W-Velocity profile of the vertical spill plume at the balcony edge (z = 0m) 100
Figure 7.17 Temperature rise profile at z = 1 m (R5M5YY and RT5M5YY) 101
Figure 7.18 W-Velocity profile at z = 1 m (R5M5YY and RT5M5YY) 102
Figure 7.19 Mass flow rates over the flow path (Q = 3 MW, W = 7.5m) 108
Figure 7.20 Mass flow rate over the flow path (Q = 4 MW, W = 12m) 109
Figure 7.21 Variations of mass flow rates normalized to mass flow rate at the opening over the flow path (m) 112
Figure 7.22 Variation of mass flow rate normalized to $(Q_c L_e^2)^{1/3}$ against flow path 114
Figure 7.23 Max. Temperature rise at every 1 m above the balcony, plotted with respect to (Q_c/L) , (Simulation with draft curtain) 115
Figure 7.24 Comparison of ΔT (at z = 0 m and 1m) between experiment and simulation (cases with draft curtain) 117
Figure 7.25 Mass flow rate of the spill plume normalized to $(Q_c L^2)^{1/3}$ 117
Figure 7.26 Comparison between FDS results with method by Morgan and Marshall [1975], Thomas [1987] 119
Figure 7.27 Comparison between FDS results from current study and methods by Poreh et al [1998], Harrison [2004] 121
Figure 7.28 Correlated FDS results by method of Harrison 122
Figure 7.29 Comparison between FDS results from current study with those from method used by Thomas (modified) 123
Figure 7.30 Comparison of FDS results with methods of Law(modified), NFPA 92B(modified) 124
Figure 8.1 The maximum temperature rise at the doorway 127
Figure 8.2 The maximum U-Velocity at the doorway 128
Figure 8.3 The maximum temperature rise at the balcony end 130
Figure 8.4 The maximum velocity at the balcony end 131
Figure 8.5 The maximum temperature rise at the spill edge 132
Figure 8.6 The maximum W-Velocity at the balcony edge 132
Figure 8.7 Variation of air entrainment rate at the rotating region with Ri of the initial flow 134
Figure 8.8 Air entrainment rate at rotation region 135
Figure 8.9 Correlated FDS predictions 140
Figure 8.10 The mass flow rate normalized to the mass flow rate at the door way 142
Figure 8.11 Correlated air entrainment rate under the balcony (for channelled flows) 143
Figure 8.12 Comparison of correlated experimental results with FDS results 144
Figure 8.13 Validation of empirical correlation to parameter variation 148

LIST OF TABLES

Table 2.1 Limiting Temperature for the BRE spill plume method....38
Table 4.1 Computational domain size test (D, W, and H are depicted in Figure 4.2)....52
Table 4.2 Series of simple simulation : temperature and velocity effects....57
Table 4.3 Series of simple model used for sensitivity testing....62
Table 4.4 Flow characteristics at the end of the balcony and *Ms/Mb*....65
Table 5.1 Parameters of interest and variations....75
Table 5.2 Parameter conditions used in the modelling....75
Table 5.3 The series of FDS simulations....77
Table 6.1 Experiments conducted at the NRC....87
Table 7.1 Summary of results from CFD modelling (a)....104
Table 8.1 Parameter variation of small scale experiments by Harrison, Marshall and Harrison....146

NOMENCLATURE

Symbol Description

A	Area (m^2)
b	Balcony breadth (m)
B	A constant of spill plume (kg $s^{-1}m^{-5/3}kw^{-1/3}$)
C_m	Dimensionless entrainment coefficient
C_p	Specific heat (J $kg^{-1}K^{-1}$)
C_d	Discharge coefficient
D	Depth (m)
D_{fuel}	Fuel diameter (m)
d_e	Effective smoke layer depth in an atrium or reservoir (m)
g	Acceleration due to gravity (m s^{-2})
h	Height above floor (m)
k	Thermal conductivity (W $m^{-1}K^{-1}$)
L	Lateral width of spill plume layer (m)
l_b	the total lateral width of the balcony (m)
M	Mass flow rate of gases (kg s^{-1})
m_p	Mass flow rate of an axisymmetric plume evaluated at an arbitrary height of rise (kg s^{-1})
P	Parameter effect
Ri	Richardson number
Q	Total heat release rate (kW)
Q_r	Radiative heat loss (kW)
Q_c	Convective heat release rate (kW)
Q_{con}	Conduction heat loss (kW)
T	Absolute gas temperature (K)
ΔT	Temperature rise of gases above ambient temperature (^oC)
$U\text{-}Vel$	Horizontal velocity of the flow (U- Velocity) (m s^{-1})
W	Width of opening (m)
$W\text{-}Vel$	Vertical velocity of the flow (W-Velocity) (m s^{-1})
z	Height of rise of plume from the spill edge to the smoke layer base in the reservoir (m)

Greek symbol

a	Entrainment constant for plume
a'	Entrainment constant for air mixing into rotating gases at a horizontal edge
ΔT	Temperature rise of gases above ambient temperature (^oC)
ρ	Density (kg m^{-3})

κ_M	Profile correction factor for mass flow (approx 1.3)
Δ	Virtual origin (m)
Ψ	Characteristic source strength of the flow
δm	Mass flow rate of air entrained into rotating flow (kg s^{-1})

List of subscripts

0	An ambient property
a	Variable evaluated in an atrium or smoke reservoir
b	Variable evaluated in the horizontal layer flow at the end of balcony
c	Property of the draft curtain
comp	property of the fire compartment
d	Property of the downstand
e	An effective property of the smoke layer
f	Variable evaluated at the fascia
max	A maximum value
s	Variable evaluated in the vertical flow at the spill edge (at the edge of balcony)
w	Variable evaluated in the horizontal layer flow at the compartment opening

1 Introduction

1.1 Background

An atrium is a large space often found in shopping malls, airport terminals, office buildings, apartment buildings, and hotels. Enclosing multi-stories, the atrium presents an entrance hall, connects units of a complex building, and covers pedestrian malls.

This open concept design can result in fire safety problems. A fire from a single unit could possibly threaten the occupants of the entire building since smoke from a fire compartment could easily travel into to the connected large atrium space and the interconnected space, which may be used as means of egress.

Since safety measures for preventing smoke from entering the atrium space are expensive and difficult to design, a smoke ventilation system is commonly used, which exhausts smoke from the atrium [Morgan et al 1999]. The key to the effective performance of this system is estimating the required amount of smoke that should be extracted from the atrium.

1.1.1 Atrium Smoke Management

1.1.1.1 What is smoke?

Before proceeding to a discussion of smoke management in an atrium, it is necessary to define the term "smoke". NFPA 92B (Guide for Smoke Management Systems in Malls, Atria, and Large Areas) [NFPA 2000] defines smoke as

"The airborne solid particulates and gases evolved when a material undergoes pyrolysis or combustion, together with air that is entrained or otherwise mixed into the mass."

Smoke is the mixture of the combustion products and air. Smoke consists mostly of air, which is entrained along the smoke flow path [Milke 2002]. Smoke contaminates the ambient environment during its dilution. As smoke rises due to its buoyancy, it entrains air, and the mass flow rate of smoke increases whereas the concentration of combustion gases decreases [Milke 2002].

1.1.1.2 Smoke management system design objectives

Smoke contains toxic and irritant gases and is the main cause of fatalities in fires [Klote 2002]. In addition, smoke reduces visibility, which makes it difficult for occupants to escape the building [Lougheed and Hadjisophocleous 2001]. Milke gives five design objectives for smoke control systems in atrium buildings [Milke 1990].

1) Maintain a tenable environment in the means of egress in the atrium during the time required for evacuation
2) Confine the smoke in the atrium to a limited region in that space.
3) Limit the migration of smoke from the atrium into adjacent spaces.
4) Provide conditions in the atrium that will assist emergency response personnel in conducting search-and-rescue operations, and in locating and controlling the fire
5) Contribute to the overall protection of life and to the reduction of property loss

1.1.1.3 Clear layer height

A smoke-management system often used for covered shopping malls and atria is a system that exhausts gases from the buoyant hot layer near the ceiling of the atrium.

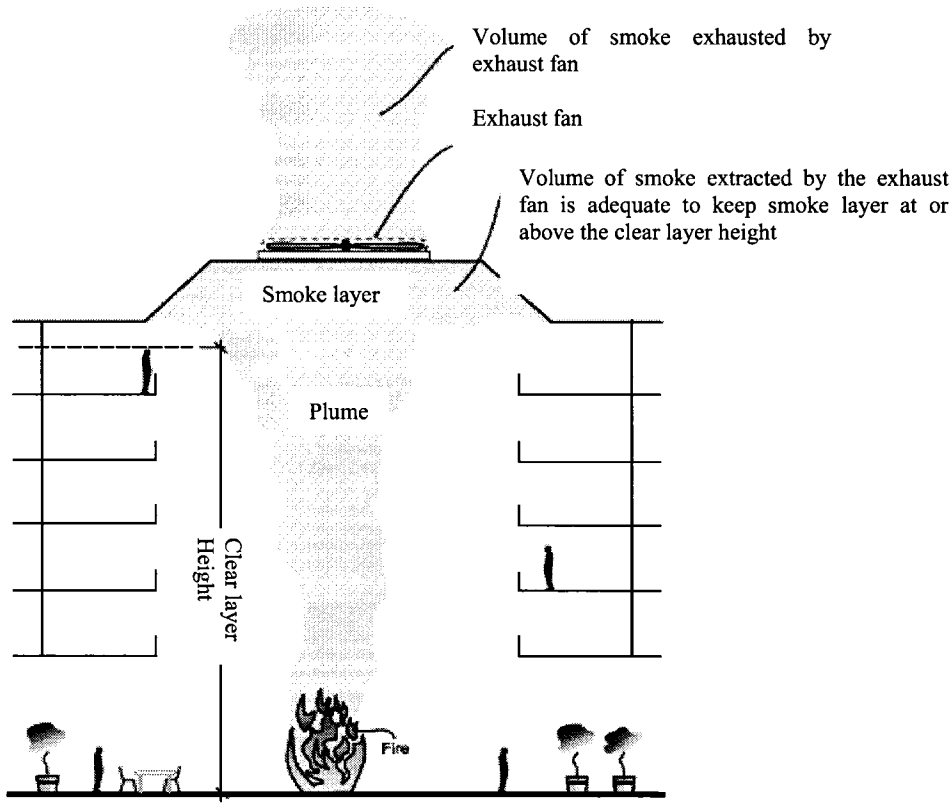

Figure 1.1 Atrium smoke filling and clear layer height [Lougheed and Hadjisophocleous 2001]

Smoke from a fire rises as a plume with subsequent air entrainment and fills the upper region of the space. Once the smoke layer has been formed, its depth increases with time as more gases from the fire plume enter the hot layer. A critical design parameter of this smoke management system is maintenance of the required minimum height of the smoke layer, which allows safe conditions for egress, and which confines

the smoke in the atrium. To maintain this clear layer height, it is necessary to arrest the descent of the smoke layer by using a natural or a mechanical ventilation system [Milke 2002].

1.1.1.4 Types of plume in the atrium

The exhaust rate required to maintain the design height can be estimated from the mass flow rate of the plume at the level of the design height. The mass flow rate of the plume depends on the plume configuration. Milke recognized five configurations of smoke plume [Milke 1990].

1) Axisymmetric plume

An axisymmetric plume is an unbounded free plume, which comes from the fire near the centre of an atrium. A cone-shaped plume entrains air from all sides of the plume. There is a well-established model to estimate the mass flow rate of axisymmetric plumes, which should be applied to a plume situated away from walls and overhead obstructions.

2) Wall plume

A wall plume is a plume which rises against a wall when the fire source is located near a wall. A wall plume entrains air from its half-unbounded sides, so the mass flow rate of a wall plume is considered to be half of that of an axisymmetric plume.

3) Corner plume

Using a similar argument, as for the wall plume, a plume rising from a fire located near a corner of a room is considered to entrain a quarter of the possible amount of air that an axisymmetric plume can entrain.

4) Balcony spill plume

A balcony spill plume refers to the vertical plume generated from the horizontally moving smoke layer at the spill edge of a balcony. Balcony spill plume scenarios involve ceiling, balcony and other horizontal obstructions, which block the initial buoyant (upward) movement of the plume, and which cause the plume to run horizontally along the obstruction. At the edge of the obstruction, the horizontally moving smoke rises up into the atrium. This is the type of plume which is considered in this study.

5) Window plume

A window plume is established when smoke moves out from the room of origin and enters the adjacent atrium through an opening. NFPA 92B [1991], and International Building Code (IBC) [International Code Council, Inc. 2000] identify the window plume after flashover, so the correlation is based on fires controlled by ventilation not by fuel surface area [Klote 2000].

1.1.2 Balcony Spill Plume

Figure 1.2 shows the typical smoke movement of a balcony spill plume originating from a room that is adjacent to an atrium. The plume from the fire initially forms the smoke layer in the upper part of the fire compartment. If there is no means to confine the smoke in the room of origin, the buoyant layer moves horizontally beneath the balcony and enters the atrium area. At the spill edge, the horizontally moving layer rotates and this region is known as the "rotating region" or "turning region". After

rotation, the plume rises vertically in the atrium, and this plume is now knows as a "spill plume". The spill plume is quite flat (two-dimensional) immediately after rotating, so the term "line plume" is also used. When Morgan and Marshall [1979] first developed the BRE (Building Research Establishment) spill plume method, it was recognized that there are three discrete regions, namely, the under the balcony region, the rotating region and the spill plume region. Mass flow rates were studied in each region, and the spill plume method was completed by coupling the method to estimate entrainment at the rotating region to the method of the spill plume.

In general, balcony spill plumes are categorized as either "free balcony spill plumes" or "adhered balcony spill plumes" [Morgan and Marshall 1975, Hansell et al 1993]. This is, in fact, an important feature of the balcony spill plume as it determines the amount of air entrainment. Most existing spill plume methods only consider free balcony spill plumes.

An adhered balcony spill plume is likely to occur if the projection of the balcony is relatively short or the plume temperature is exceedingly high [Hansell et al 1993]. In these cases, the vertical spill plume rises close to the wall and tends to adhere to the wall above the balcony, so that the rising plume entrains air only from the side that is unbounded. On the other hand, in the case of a free balcony spill plume, air entrainment occurs from all sides of the plume. Figure 1.2 shows the free balcony spill plume scenario. Most studies to date have considered this type of spill plume, and this current study also focuses on free balcony spill plumes.

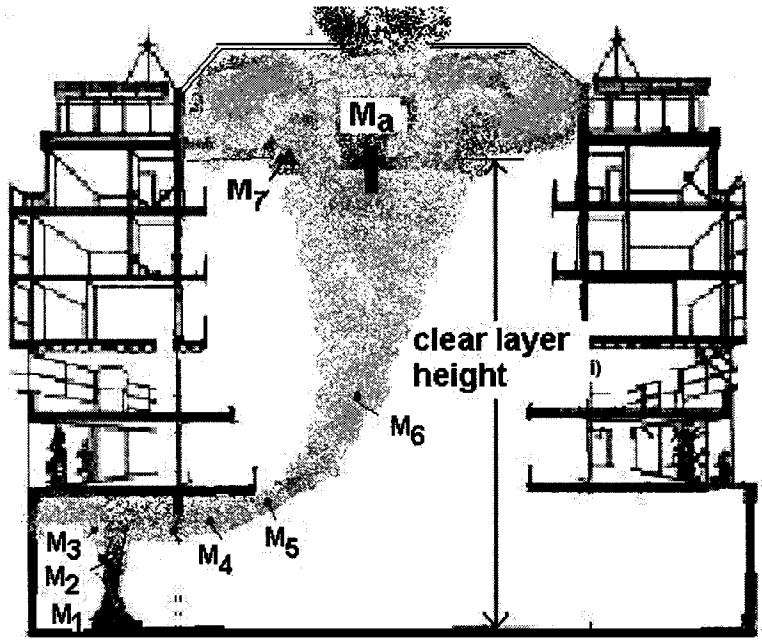

Figure 1.2 Free balcony spill plume scenario

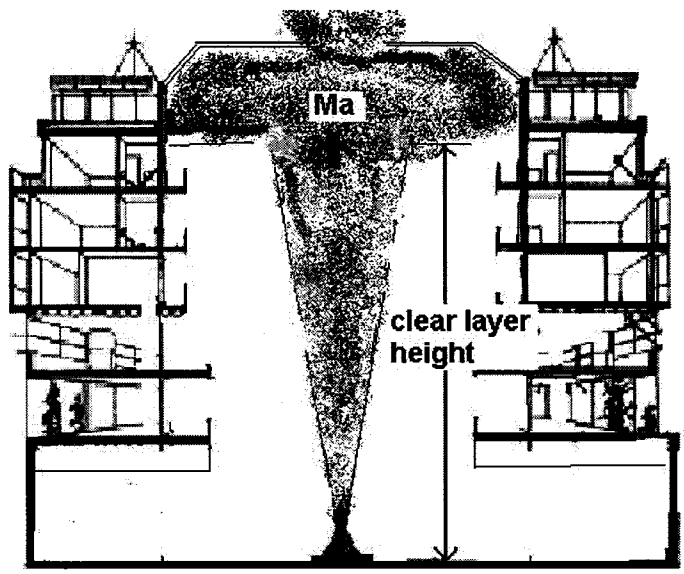

Figure 1.3 Axisymmetric plume

1.1.3 Balcony Spill Plume vs. Axisymmetric Plume

The mass flow rate of an axisymmetric plume, as shown in Figure 1.3, is a function of the fire size and the height of rise [Milke 2002].

$$m_p = 0.071 Q_c^{1/3} (z - \Delta)^{5/3} + 0.002 Q_C$$
$$\Delta = 0.083 Q^{2/5} - 1.02 D_{fuel} \qquad (1.1)$$

where
m_p = mass flow rate of an axisymmetric plume (kg s^{-1})
Q_c = convective heat release rate (kW)
z = the height of rise (m)
Δ = the virtual origin
D_{fuel} = fuel diameter (m)

Air entrainment in balcony spill plumes is affected by several factors in addition to fire size and height of rise. A number of calculation methods used for balcony spill plumes have been developed based on small-scale experiments, and will be discussed in detail in the literature review (Chapter 2). Equation 1.2 is the established general form of the correlation of balcony spill plumes.

$$M_a = B Q_c^{1/3} L^{2/3} z + M_s \qquad (1.2)$$

where
M_a = the mass flow rate of the balcony spill plume (kg s^{-1})
B = an empirical constant of the spill plume (kg $s^{-1} m^{-5/3} kw^{-1/3}$)
Q_c = convective heat release rate (kW)
L = the lateral width of the spill plume layer (m)
z = the height of rise (m)
M_s = the mass flow rate of the initial approach flow at the spill edge (kg s^{-1})

Mike [2002] compared the smoke production rate of axisymmetric plumes and balcony spill plumes by using the simple balcony spill plume correlation developed by Law [1986] based on Morgan and Marshall's small-scale experiments [1979]. Using the same way by Mike [2002], the smoke production rate of axisymmetric plumes and

balcony spill plumes was compared in Figure 1.4. Equation 1.3 by Law [1986] was used to predict the smoke production rate for balcony spill plumes.

$$M_a = 0.34Q^{1/3}L^{2/3}(z + 0.15h_b) \tag{1.3}$$

where
Q = total heat release rate (kW)
h_b = balcony height above the floor

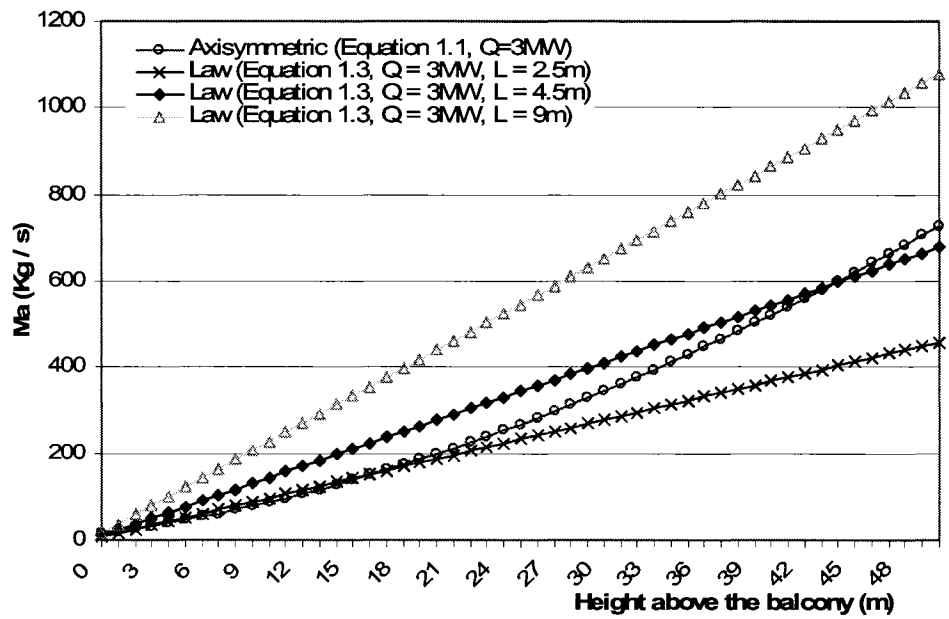

Figure 1.4 Comparison of smoke production rate for axisymmetric plumes and balcony spill plumes (Q = 3.5 MW, h_b = 5m)

Figure 1.4 shows that, for the same fire size and a balcony width of 4. 5m, the balcony spill plume generates more smoke than the axisymmetric plume up to a certain height. With increasing height, the mass flow rate of the balcony spill plume becomes comparable with that of the axisymmetric plume [Milke 2002]. As suggested by Milke [2002], the applicability of the correlation of balcony spill plumes is questionable,

especially for greater heights. Milke commented that the smoke production rate from a balcony spill plume should be estimated using the axisymmetric plume equation with z evaluated from the balcony to the smoke layer [Milke 2002]. The Figure also shows the balcony spill plume for 9 m width generates much more smoke than the axisymmetric plume, and for the 2.5 m width, it generates much less. The balcony spill plume correlation should be further validated for various widths of the spill plume layer (L) and height of rise (z).

1.2 The problem

1.2.1 Factors affecting air entrainment of balcony spill plumes

It has been shown that the mass flow rate of balcony spill plumes is greater than that of axisymmetric plumes. This increased entrainment for balcony spill plumes is due to entrainment in the rotating region and mixing at the locations of obstructions, such as the ceiling, the balcony and the fascia. Poreh et al identified several causes of air entrainment for balcony spill plumes, which are depicted in Figure 1.2. The total mass flow rate required for the ventilation system can be written as [Poreh et al 1998]

$$M_a = M_1 + M_2 + M_3 + M_4 + M_5 + M_6 + M_7 \qquad (1.4)$$

where
M_1: entrainment by the flame
M_2: entrainment into the rising plume above the fire
M_3: entrainment due to disturbance created by plume as it plunges into the upper layer of the compartment
M_4: entrainment into the horizontal layer that flows toward the atrium
M_5: entrainment into the curved section of the plume as it rounds the edge of the balcony
M_6: entrainment into the spill plume that rises vertically
M_7: entrainment when the spill plume enters the buoyant layer in the atrium

The above analysis suggests that possible factors affecting the air entrainment of the initial approach flow include the atrium size, the size of the fire compartment, the size of the door, the depth of fascia, and the presence of draft curtains, as well as the length of balcony projection. Figure 1.5 shows the problem of the flow under the balcony and in the rotating region and depicts the characteristics of the balcony spill problem.

To model this complicated problem of balcony spill plume, previous studies considered the vertically rising spill plume as being separate from the fire, so that the source of the spill plume was a wide layer emerging from the spill edge [Thomas et al 1998]. This approach, in fact, was an important assumption that provided the framework for the analysis of balcony spill plumes.

The established correlation of balcony spill plumes (Equation 1.2) incorporates the width of the initial layer at the end of the balcony, and the mass flow rate of the initial approach flow at the spill edge in addition to the heat release rate of fire, and the height of rise of the plume.

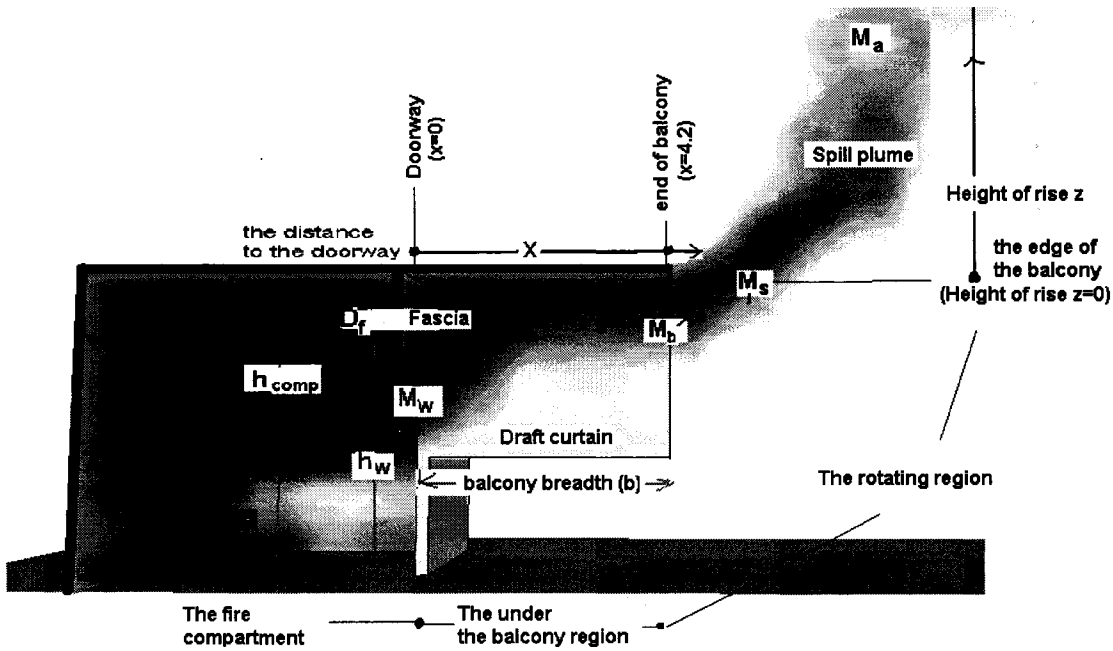

Figure 1.5 The problem of the flow under the balcony area and in the rotating region

1.2.2 The problem of the initial approach flow

Based on the approach described above, a number of correlations were developed to estimate the mass flow rate of the balcony spill plume (M_a). All correlations developed by previous studies have tried to find the empirical constant 'B' in Equation 1.2. Another important parameter that requires further investigation is the initial mass flow rate (M_s) at the spill edge. The initial approach flow rate is the focus of this study.

The importance of the initial approach flow comes from the fact that it is the source of the spill plume. The initial properties of the source flow affect the mass flow rate of the spill plume; in particular, the width of the source layer is the key factor governing entrainment of line plumes. However, very few studies have specifically looked at this source flow at the end of the balcony.

As will be discussed in detail in the literature review, there are a number of methods to estimate the mass flow rate of the initial approach flow (M_s), yet a considerable discrepancy exists among these methods. Indeed, current design guidance suggests a rough estimation of the mass flow rate at the spill edge (M_s). Comprehensive studies are necessary to clarify the problem of estimating the flow under the balcony and in the rotating region.

Another problem in quantifying the initial mass flow rate at the spill edge is the lack of sufficient data that covers the various configurations. The existing simple correlations of balcony spill plumes have been primarily based on the common case of channelled flow, so that the extent of applicability of the spill plume correlations and methods to calculate M_s are questionable. Therefore, it is necessary to develop a new empirical correlation to estimate M_s that addresses various factors affecting the air entrainment under the balcony area.

1.3 Objectives

A balcony spill plume should be considered when designing a smoke management system in most atria, where low-level rooms are open to the atrium. The reasons are

1) Most low–level compartments, which are typically used as commercial stores, restaurants or offices, and are adjacent to the atrium, generally have greater fire loads than the atrium itself.
2) Smoke from a fire in these compartments could easily travel into the connected large atrium space, since there is often no compartmentation and no

vertical separation between adjacent rooms and the atrium.

3) The balcony spill plume generates a greater amount of smoke than an axisymmetric plume for the same size of fire in general.

For estimating the smoke production rate of balcony spill plumes, there are several design methods, which have been developed based on small-scale experiments; however, a significant discrepancy exists among these methods in the estimation of the mass flow rate of the initial approach flow (M_s). In this regard, this study addresses the issue of estimating M_s. By focusing on the flow under the balcony area and the edge of the balcony, the horizontal flow and the rotating flow of free balcony spill plumes are examined.

The objectives of this study are described below.

1) To better understand the flow under a balcony and in the rotating area of balcony spill plumes.

2) To asses the extent of applicability of existing methods for estimating the initial mass flow rate at the spill edge.

3) To develop an empirical correlation to quantify the factors affecting air entrainment rate at the spill edge.

2 Literature Review

There are a number of published experimental investigations on balcony spill plumes; however published work on the rotating region and under the balcony area is very limited. Our interest is focused on investigations that deal with air entrainment under the balcony and in the rotating region. This chapter reviews existing models and previous work addressing the problem of balcony spill plumes. It specifically covers various approaches that previous studies have taken to solve the air entrainment rate of the initial flow. At the end, a summary is given, which outlines how this study deals with issues arising from this literature review.

2.1 Balcony spill plume correlations

2.1.1 Existing Correlations

The starting point for modelling the balcony spill plume was the Lee and Emmons theory of two-dimensional line plumes in a uniform stationary ambient environment [Lee and Emmons 1961]. Analytical expressions were obtained for plume width, the buoyancy and gas velocities as a function of height above the source by solving conservation equations of momentum and energy.

Morgan and Marshall first applied this theory to correlate data which were obtained from $1/10^{th}$ physical scale experiments of balcony spill plumes [Morgan and Marshall 1975]. Thomas and Poreh also used this theory to develop correlations [Thomas et al 1998, Poreh et al 1998].

The resulting analytical equations developed by Morgan et al and Thomas et al are shown below.

$$M_a = BQ_c^{1/3} L^{2/3} z + M_s \tag{1.2}$$

$$B = C_m \rho_0 \left(\frac{g}{\rho_0 C_p T_0} \right)^{1/3} \tag{2.1}$$

where
ρ_0 = density of ambient air (kg m^{-3})
g = acceleration due to gravity (m s^{-2})
C_p = specific heat (J kg^{-1}K^{-1})
C_m = dimensionless entrainment coefficient
T_0 = temperature of ambient air (K)

Law re-analyzed data from Morgan and Marshall's experiments with a different interpretation. Law was able to find a temperature correlation with $(Q/L)^{2/3}$ for the region underneath the balcony and 3 m (full-scale equivalent) above the balcony [Law 1986], which was consistent with Yokoi's plume correlation for a flow from an opening [Yokoi 1960]. Law simplified the spill plume formula by applying conservation of heat energy shown below, rather than coupling it with the Lee and Emmons plume theory, and obtained the same form of correlation of M_a with $Q^{1/3} L^{2/3} z$.

$$\begin{aligned} Q &= C_p M_b \Delta T_b = C_p M_a \Delta T_a \\ \Delta T_b, \quad \Delta T_a &\propto (Q/L)^{2/3} \\ M_a &= BQ^{1/3} L^{2/3} z + M_s \end{aligned} \tag{2.2}$$

where
M_b = the mass flow rate at the end of the balcony (kg s^{-1})
ΔT_b = Temperature rise at the end of the balcony (K)
ΔT_a = Temperature rise of the spill plume (K)
z = the height of rise (m)

Morgan et al and Law provided the conceptual framework for spill plumes.

Subsequent work updated the method by adding correction factors and suggested various formulas. All correlations developed by previous studies found the empirical constant 'B' based on small-scale experiments and incorporated the mass flow rate at the edge of the balcony by adopting a virtual origin (Δ) or mass flow rate at the end of the balcony (M_b).

1) Law [1986]

$$M_a = 0.34Q^{1/3}L^{2/3}(z+\Delta) \tag{2.3}$$

where
$\Delta = 0.15h_b$
h_b = balcony height above the floor

2) Morgan and Hansell [1987]

$$M_a = 0.40Q_c^{1/3}L^{2/3}(h_a - d_e) + 0.061Q_c^{1/3}L^{2/3} \tag{2.4}$$

where
$d_e = 1.26d_a$ when $d_a < 0.67A_a^{0.5}$
$d_e = d_a$ when $d_a > 0.67A_a^{0.5}$
A_a = area of the atrium (m^2)
d_e = effective smoke layer depth in the atrium (m)
h_a = the height of the atrium (m)
d_a = smoke layer depth in the atrium height of the atrium (m)

3) Thomas [1987]

$$M_a = 0.58\rho_0\left(\frac{gQ_cL^2}{\rho_0 C_p T_0}\right)^{1/3}(z+\Delta) \tag{2.5}$$

where
$\Delta = 0.15h_b$

4) Law [1995]

$$M_a = 0.31Q^{1/3}L_e^{2/3}(z+\Delta) \tag{2.6}$$

where

L_e(effective layer depth) = $W+b$
W = width of the opening (m)
b = balcony breadth (m)
Δ = 0.205 or $0.25h_{comp}$ (h_{comp} : compartment height above the floor)

5) NFPA 92B [1991]

$$M_a = 0.41 Q_c^{1/3} L^{2/3} (z+\Delta)\left\{1+\frac{0.063(z+0.6h_{comp})}{L}\right\} \tag{2.7}$$

NFPA 92B [2000]

$$M_a = 0.36 Q_c^{1/3} L^{2/3} (z+\Delta) \tag{2.8}$$

where
{ } = large height correction.
$\Delta = 0.25h_{comp}$

6) Poreh et al [1998]

$$M_a = 0.16 Q_c^{1/3} L^{2/3}\left(z+\frac{M_b}{0.16 Q_c^{1/3} L^{2/3}}+D_b\right) \tag{2.9}$$

$$\therefore M_a = M_b + 0.16 Q_c^{1/3} L^{2/3} (z+D_b)$$

where
D_b = the layer depth of the flow at the end of the balcony (m)

7) Thomas et al [1998]

$$M_a = 0.16 z Q_c^{1/3} L^{2/3} + 1.4 M_b + 0.0014 Q_c \tag{2.10}$$

Despite the variation of their methods, there seems to be a general agreement on the following key aspects of the mass flow rate of spill plumes.

1) The mass flow rate of the balcony spill plume (M_a) has a linear correlation with plume height z

2) The slope of the linear correlation with z depends on $Q_c^{1/3}L^{2/3}$, as shown in Equation 1.2.

3) The balcony spill plume incorporates the mass flow rate of the vertically moving spill plume and the mass flow rate of the horizontally approaching initial flow at the spill edge.

2.1.2 Limitation and uncertainties of spill plume equations

The existing balcony spill plume formulas listed above are compared in Figure 2.1. Despite the successful overall analytical framework of spill plumes, there are considerable differences in each method.

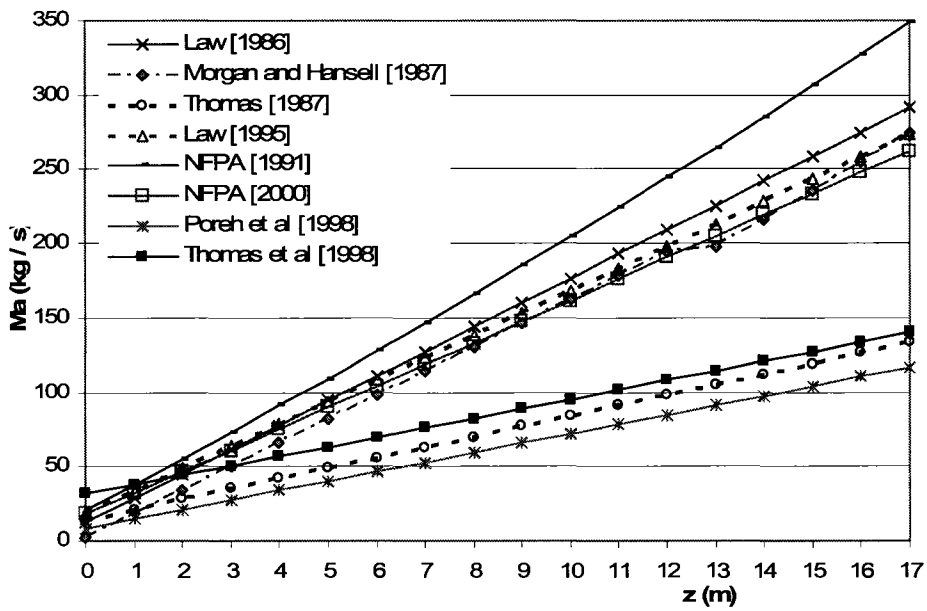

Figure 2.1 Comparison of existing balcony spill plume formula

Methods by Poreh et al [1998], Thomas [1987], and Thomas et al [1998] result in similar predictions because these methods have the same value for the spill plume

constant '*B*' at about 0.16.

Methods by Law [1986] and Law [1995] predict relatively high mass flow rates at a high height of rise, since these methods are empirically obtained based on data obtained near the balcony, where additional entrainments are observed. Using a high value for the spill plume constant (B = 0.4), methods by Morgan and Hansell [1987] and NFPA 92B [2000] predict high values of the mass flow rate with increasing height. To reduce mass flow rates at great heights, the method by Morgan and Hansell [1987] uses an effective layer depth correction (see the kink in the curve in Figure 2.1), while the method by NFPA 92B [1991] enhances the increase using a large height correction.

There are some important problems and questions that remain unanswered, and theses bring about various uncertainties and consequent limitations of the balcony spill plume formula.

The main problem is that the spill plume constant B in the linear function of the spill plume formula is valid only for a certain range of 'height of rise'. At great heights of rise, the effect of the width of the spill plume becomes weak, and the plume behaves more like an axisymmetric plume. The method in previous edition of NFPA 92B [1991] enhances the increase using a large height correction, for extra entrainments due to the three-dimensional behaviour of plumes at large heights. Additional problems encountered in the 'far' field are entrainment due to the free end of vertically rising spill plumes and effective layer depth correction, which are associated with the atrium size.

Near the source of the plume (near the balcony), there is also a discrepancy among methods as shown in Figure 2.1. Morgan and Marshall [1975] recognized that the

theoretical treatment of the spill plume revealed a problem in the region immediately after the rotation of the flow. If the temperature and velocity are not in a Gaussian distribution across the balcony area, Lee and Emmons' theory is not valid for this region. As a result, estimating the initial mass flow rate at the spill edge is another difficult problem related to the spill plume formula.

2.2 Air entrainment under the balcony and the rotating region

Studies on air entrainment into the flow under the balcony and the rotating region considered several approaches to calculate the initial mass flows and to couple it to the spill plume correlations.

2.2.1 Method: Amount of air entrainment, δm

Some studies sought to calculate the amount of air entrainment, δm, into the horizontally approaching flow which rotates around the spill edge. Combining the mass flow rate at the doorway, the mass flow rate at the balcony edge can be described as below [Morgan and Marshall 1975]

$$M_s = M_w + \delta m \tag{2.11}$$

Where
M_w = mass flow rate at the doorway (kg s^{-1})
δm = entrainment into the rotating flow (kg s^{-1})

2.2.1.1 Morgan and Marshall [1975]

Morgan and Marshall recognized three discrete regions in the balcony spill plume and suggested a model for the horizontal approach flow and rotating flow in their BRE spill plume method [Morgan and Marshall 1975]. The suggested equation for the

entrainment into the rotating flow, δm, uses parameters of the approach flow, temperature rise and layer depth.

$$\delta m = \frac{2}{3}\alpha' L\rho_0 \left(\frac{2g\Delta T}{T_0}\right)^{1/2} D^{3/2} \tag{2.12}$$

Where
δm = entrainment into the rotating flow (kg s^{-1})
α' = entrainment constant for air mixing into rotating gases at the horizontal edge
D = layer depth (m)

They empirically found the best fit entrainment constant (α') to be 0.9, implying a high entrainment rate at the rotating region. Morgan and Hansell found this constant to be 1.1 [Morgan and Hansell 1987]. The mass flow rate of vertical flow at the balcony edge is

$$M_s = M_w + \delta m = M_w + \frac{2}{3}\alpha' L\rho_0 \left(\frac{2g\Delta T}{T_0}\right)^{1/2} D^{3/2} \tag{2.13}$$

Morgan suggested the buoyancy-driven mass flow rate of gases at the doorway as [Morgan 1986]

$$M_w = \frac{2}{3} C_d^{3/2} (2g\Delta T_w T_0)^{1/2} \frac{W\rho_0}{T_w} D_w^{3/2} K_m \tag{2.14}$$

Where
M_w = mass flow rate at the doorway (kg s^{-1})
C_d = discharge coefficient
K_m = profile correction factor (K_m =1.3, for most typical flow layers)
W = width of the door (m)
T_w = temperature of the flow at the doorway (K)
D_w=depth of the flow layer at the doorway (m)

Morgan and Marshall coupled Equation 2.12 to the 2-D line strip of the vertical plume following Lee and Emmons' theory [1961]. The equation estimates a large amount

of air entrainment into the rotating flow, which disagrees with the finding of CFD studies by Miles et al [1996].

2.2.1.2 Thomas [1987]

Thomas modified the equation of Morgan and Marshall, adopting the conventional view that entrainment is 0.16 times the maximum velocity of the flow [Thomas 1987].

$$M_s = C_m \rho D \left(\frac{gQ_c}{\rho C_p T_0 W} \right)^{1/3} + \frac{2}{3} \alpha' L \rho_0 \left(\frac{2g\Delta T}{T_0} \right)^{1/2} D^{3/2} \tag{2.15}$$

The mass flow rate at the edge of the balcony was estimated by adding the initial mass of the layer flow to the amount of entrainment into the rotating flow. The entrainment constant (α') is 0.16. The equation was then reduced by replacing the temperature rise term (ΔT) with $(Q_c / W)^{2/3}$ and setting β as 0.9.

$$M_s = \beta \rho D \left(\frac{gQ_c}{\rho C_p T_0 L} \right)^{1/3} \tag{2.16}$$

The equation estimates entrainments of up to 22% of the flow, or higher if β is set at 1.56.

2.2.1.3 Hansell [1993]

Hansell conducted limited full-scale experiments on balcony spill plumes, and updated the model to calculate the air entrainment at the rotating region [Hansell 1993].

Equation 2.12 of the mass flow entrained at the rotating region developed by Morgan and Marshall [1975] was modified. A correcting function sin Ψ was developed

to calculate the accurate air entrainment at the rotating region by taking into account D_b (the layer depth) and ΔT_b (the temperature rise) at the end of the balcony. However, to determine D_b and ΔT_b, one needs to know M_s. Hansel's suggestion was to assume M_s and then carry out the entire calculation until the value of M_s has converged, using the following steps.

1) Calculate the value of D_b after assuming a value for M_s

2) Calculate an effective rotational entrainment constant α″

Effective rotational entrainment constant, $\alpha'' = \alpha \cos \chi$

Angle, $\chi = 93.5 - 58.75\mu$

Velocity ratio, $\mu = \dfrac{(M_s - M_w)T_b}{LD_b\rho_0(2g\Delta T_b T_0 X_u)}$

Height parameter, $X_u = 0.5D_w + D_d - D_b$

3) If $D_b \leq D_d$ and $(D_d - D_b) \leq 1$,

$$\delta m = \frac{2}{3}\rho_0 L\alpha''\left(2g\frac{\Delta T}{T}\right)^{1/2} D_w^{3/2}$$

4) If $D_b > D_d$,

$$\alpha'' = \alpha \cos \chi$$

$$\chi = 93.5 - 58.75\mu$$

$$\mu = \frac{(M_s - M_w)T_b}{LD_b\rho_0(2g\Delta T_b T_0 X_u)}$$

$$X_u = 0.5D_w + D_d - D_b$$

$$\delta m = \frac{2}{3}\rho_0 L\alpha''\left(2g\frac{\Delta T}{T}\right)^{1/2} D_w^{3/2}\sin\Psi$$

$$\sin\Psi = \left[1 - \left(\frac{D_b - D_d}{D_w}\right)^2\right]^{1/2}$$

5) $M_s = M_w + \delta m$

6) Repeat the entire procedure until M_s converges.

This method is not simple and requires many sub-calculations, such as determining the layer depths D_b and D_w, the temperature rise ΔT, and the mass flow rate at the door, M_w.

Some of the above equations are questionable and involve many variables and coefficients. Convergence is difficult to achieve and the method is reported to be unsuitable for many different scenarios [Harrison 2004]. Indeed, Hansell developed the model based on experiments with a relatively narrow compartment opening. Therefore, this method is only valid for limited cases.

2.2.2 Method 2: Layer depth

2.2.2.1 Poreh, Morgan, Marshall, and Harrison [1998]

The proposed model used the initial layer depth of approach flow to solve the air entrainment into the curved section. The model presumed $M_b = M_a(\Delta - D_b)$ when the atrium smoke layer descends down to the height of the elevated layer in the store, as depicted in Figure 2.2. The virtual origin was found using the layer depth at the end of the balcony.

$$M_b = M_a(\Delta - D_b) = BQ_c^{1/3}L^{2/3}(\Delta - D_b)$$
$$\therefore \Delta = \frac{M_b}{BQ_c^{1/3}L^{2/3}} + D_b \tag{2.17}$$

The final correlation was suggested as Equation 2.18.

$$M_a = 0.16 Q_c^{1/3} L^{2/3} (z + \frac{M_b}{B Q_c^{1/3} L^{2/3}} + D_b)$$

$$\therefore M_a = M_b + 0.16 Q_c^{1/3} L^{2/3} (z + D_b)$$

$$M_s = M_b + 0.16 Q_c^{1/3} L^{2/3} D_b \tag{2.18}$$

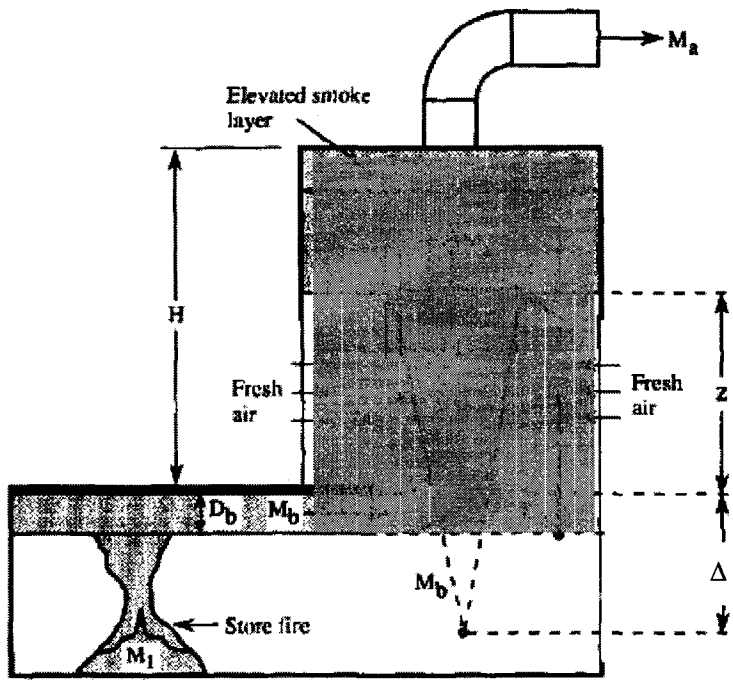

Figure 2.2 Schematic description of the proposed model by Poreh et al [1998]

This approach is quite plausible as long as the air entrainment from the lower part of the interface height in the atrium is small enough to ignore. However, this method requires additional calculation of the layer depth and the mass flow rate at the end of the balcony, which are also unidentified functions of Q_c and L.

2.2.2.2 Thomas, Morgan and Marshall [1998]

Thomas et al [1998] tried to complete the correlation (Equation 2.18) of Poreh et

al [1998] by using the theoretical layer depth formula. Thomas et al further explored the layer depth approach to the problem of rotating flow.

Further analysis on the layer depth was attempted by applying the theoretical layer depth correlation that Morgan [1986] developed.

$$\frac{D_b Q_c'^{1/3}}{M'_b} = \alpha\left(1+\beta\frac{Q_c}{C_p T_0 M'_b}\right)^{2/3}$$
$$\alpha = \left(\frac{9C_p K_Q T_0}{8\rho_0^2 g}\right)^{1/3}\frac{1}{K_m C_d} \tag{2.19}$$

where
$\beta = K_m/K_g$
K_m = profile correction factor for mass flow (approximately 1.3)
K_g = profile correction factor for heat flux (approximately 0.95)
$Q'_c = Q_c/W$
$M'_b = M_b/W$

Figure 2.3 shows that experimental data for the layer depth do not agree with the theoretical correlation. Instead, the following empirical correlation with the layer depth was found by Thomas et al [1998].

$$\frac{D_b Q_c'^{1/3}}{M'_b} = 2.5\left(1+\frac{Q_c}{C_p T_0 M_b}\right) \tag{2.20}$$

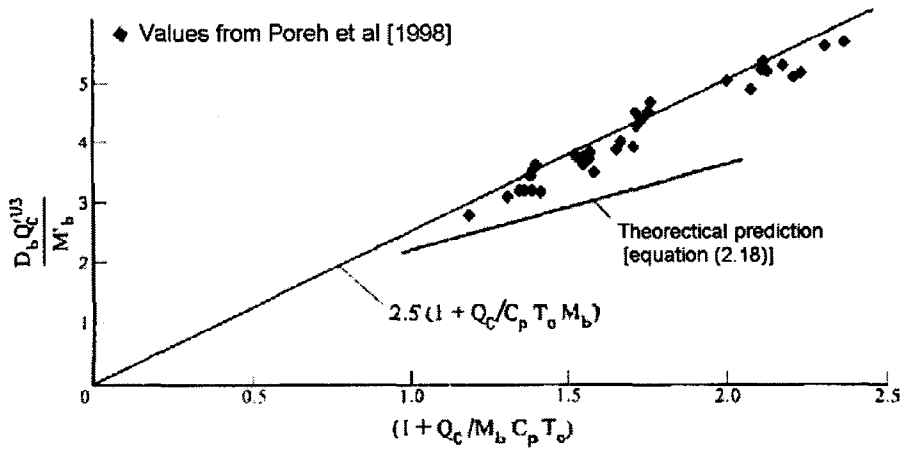

Figure 2.3 The variation of Db with temperature [Tomas et al 1998]

Thomas et al suggested that a possible reason for the discrepancy between the theoretical prediction (Equation 2.19) and experimental results was the lower Reynolds number of the layer in reduced scale experiments, which might have influenced the layer just before rotation. No further analysis of this issue was pursued by Thomas et al, rather a new correlation (Equation 2.10) of spill plume was sought by introducing the layer depth correlation (Equation 2.20).

$$M_a = 0.16 z Q_c^{1/3} L^{2/3} + 1.4 M_b + 0.0014 Q_c \tag{2.10}$$

Thomas et al obtained Equation 2.21 by statistical analysis of experimental data.

$$M_a = 0.16\, z Q_c^{1/3} L^{2/3} + 1.2 M_b + 0.0027 Q_c \tag{2.21}$$

It is not surprising that the two correlations are very similar because both equations were obtained from the same experimental data set. For the spill edge (z = 0), the mass flow rate at the spill edge (M_s) can be obtained from the two above equations.

$$M_s = 1.4 M_b + 0.0014 Q_c \tag{2.22}$$

$$M_s = 1.2 M_b + 0.0027 Q_c \tag{2.23}$$

Thomas et al concluded that the difference was acceptable after comparing the two correlations with experimental data, as in Figure 2.4.

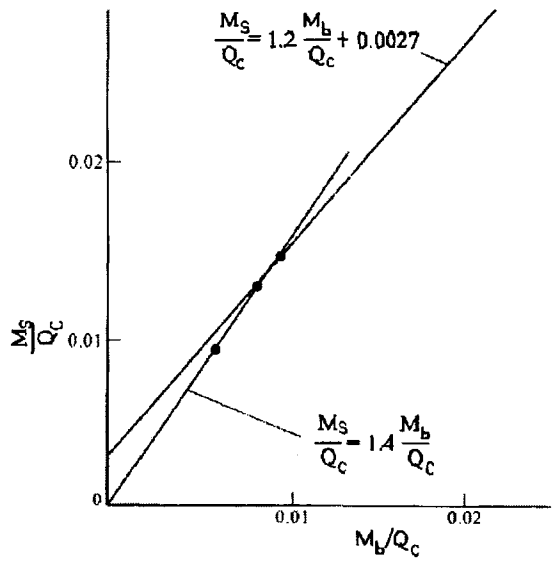

Figure 2.4 Correlation between M_s and M_b at z = 0 [Tomas et al 1998]

Thomas et al [1998] also raised doubts about the correlation of the air entrainment rate at the rotating area after it was found that flow rates had been overestimated. It was suggested that further study is necessary on this issue since the nature of the problem at the rotating area also involves other possible factors, such as imposed initial momentum, and surface friction.

2.2.2.3 Harrison [2004]

Harrison updated the method by Poreh et al [1998] and Thomas et al[1998] with data obtained from a series of 1/10th scale experiments and CFD modelling.

Harrison found the best-fit correlation as follows:

$$M_a - M_b = 0.195 Q_c^{1/3} L^{2/3} (z + D_b) \tag{2.24}$$

$$M_s = 0.2Q_c^{1/3}L^{2/3}D_b + M_b \tag{2.25}$$

Harrison suggested an acceptable alternative equation in the form of Thomas et al [1998].

$$M_a = 0.2\, zQ_c^{1/3}L^{2/3} + 1.5M_b + 0.0017Q$$

$$M_s = 1.5M_b + 0.0017Q_c \tag{2.26}$$

To complete the spill plume method, a model to predict M_b was developed by Harrison, based on a CFD study exclusively aimed at determining the mass flow rate at the end of the balcony. The resulting equation is:

$$M_b = 0.89\left(\frac{h_w}{W}\right)^{-0.92}\left(\frac{h_{comp}M_w}{W}\right) \tag{2.27}$$

$$M_b = 0.89\left(\frac{h_{comp}M_w}{h_w}\right) \tag{2.28}$$

$$M_s = 0.2Q_c^{1/3}L^{2/3}D_b + 0.89\left(\frac{h_{comp}M_w}{h_w}\right) \tag{2.29}$$

A simplified alternative formula (Equation 2.28) is proposed, yet it appears to predict a smaller value of M_b than M_w for cases with no fascia ($h_{comp} = h_w$). Equation 2.27 is compared with simulated results of this current study in Section 7.4.3.2. Considerable disagreement was found in Harrison's model because it was developed based on small scale modelling and one nominal total heat output was mostly used.

2.2.3 Method 3: The virtual origin, Δ

2.2.3.1 Law [1986, 1995]

Law found the virtual origin of the plume by exploiting experimental data instead of relying only on a complicated theory. Δ was experimentally determined and expressed as a fraction of height.

$$M_a = 0.34 Q^{1/3} L^{2/3} (z + \Delta) \tag{2.3}$$

where
$\Delta = 0.075$ or $0.15 h_b$ (balcony height above the floor)

In Figure 2.5, Law showed that the M_s value (marked with '●'), which was predicted using the heat energy conservation, fell on the line of the spill plume correlation as above.

$$\begin{aligned} \Delta T_b &= 40(Q/L)^{2/3} \\ M_s &= Q/\Delta T_b C_p = 0.025 Q^{1/3} L^{2/3} \end{aligned} \tag{2.30}$$

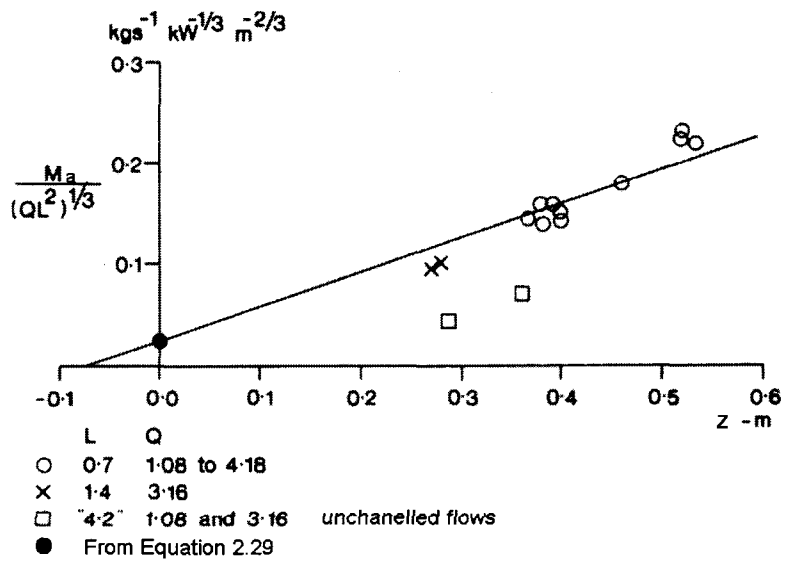

Figure 2.5 Mass flow rate correlation with z (height of rise) [Law 1986]

For unchanneled flow (marked with '□'), Law later developed a revised correlation with further experimental data from Hansell et al Law noted that with no channelling curtain, the flow became diffuse and ill-defined. Law introduced an effective balcony plume width L_e, and found the general correlation for both channelled and unchanneled flows [Law 1995].

$$L_e = W + b \tag{2.31}$$

where
L_e = effective layer depth (m)
b = balcony breadth (m)

$$M_a = 0.31 Q^{1/3} L_e^{2/3} (z + \Delta) \tag{2.6}$$

where
$\Delta = 0.205$ or $0.25h_{comp}$ (compartment height above the floor)

The entrainment coefficient, 0.31 is similar to 0.34 of the earlier correlation whereas the virtual origin, $0.25h_{comp}$, was found to be different from the earlier value, $0.15h_{comp}$. Law commented that the location of the virtual source of the balcony plume is expected to be a function of the layer depth, temperature, and perhaps the opening height.

2.2.3.2 Thomas [1987]

Thomas re-examined data from the 1/10th scale experiments conducted by Morgan and Marshall in an attempt to extend the work of Law [1986], which tried to locate the position of the virtual origin from experimental data.

Thomas adjusted the Lee and Emmons [1961] plume temperature correlation using experimental data to locate the virtual origin. The result was found to be in a form similar to Yokoi's window plume correlation [1960], which was used by Law [1986].

Estimated values of Δ lay between $0.3h_{comp}$ to $0.8h_{comp}$. Values were not consistent over the series of measurements. A number of possible estimates for the position of the virtual origin were presented, and it was commented that Δ was expected to be dependent on the size of fire and geometry of experimental set-up.

2.3 Experimental studies

2.3.1 Balcony spill plume from channelled flow: Morgan and Marshall [1975]

Recognizing the potential hazard of balcony spill plumes in a covered shopping mall, Morgan and Marshall conducted a number of 1/10th scale experiments to examine the mass flow rate of hot gases. Two different sizes of compartments were examined. The width of the compartment was either 0.7 m or 1.4 m and both compartments were 0.5 m deep and 0.5 m high. The balcony breadth was 0.4 m, and the balcony was fully channelled by draft curtains. For selected cases, a fascia was used.

The heat source was industrial methylated spirits contained in a 0.2 m by 0.2 m tray, and the heat output was varied by controlling the fuel flow rate.

The maximum temperature rise at the balcony end (ΔT_b) was measured 10 mm below the balcony edge, and the maximum temperature rise was measured at a distance of either 0.31 m or 0.4 m above the balcony edge.

2.3.2 Morgan and Marshall [1979]

Another set of 1/10th scale experiments was conducted by Morgan and Marshall [1979]. A compartment of width 0.7 m was used for these experiments, and the

compartment was linked to the atrium (of dimensions, 4.2 m (W) × 1.4 m (D) × 1.5 m (H)). The hot gas flow originating in the compartment was allowed to enter the atrium by passing under the 0.4 m long balcony. The distance between the draft curtains for most experiments was either 0.7 m or 1.4 m. Two experiments were conducted without draft curtains. The heat sources used were electric convective heaters, and Q varied from 1.08 kW to 4.18 kW.

The mass flow rate of gases was directly measured by a carbon dioxide tracer gas technique, which evolves injections of a volume-weighted tracer gas into the zone, and then making a measurement at a point some distance away from the injection point [McWilliams 2002].

The temperature was only measured at locations above the balcony to determine the hot layer depth in the atrium.

2.3.2.1 Effective layer depth

From the results of this study, Morgan and Marshall developed the effective layer depth theory, which corrects the height of rise when there is warming of surrounding air. Experiments showed that when the width of the atrium was large compared to the depth of the buoyant layer, the temperature of the ambient air beneath the visible smoke layer was higher than the normal ambient temperature, which is in violation of the fundamental assumption of the Lee and Emmons 2-D line plume theory [1961]. This effective layer depth correction was included in the BRE spill plume method and regarded as an important design factor for balcony spill plumes [Morgan and Marshall 1979].

2.3.3 Hansell, Morgan and Marshall [1993]

1/10th scale experiments similar to those of Morgan and Marshall [1979] were conducted, but the geometry of the model atrium was tall and narrow compared to the atrium used by Morgan and Marshall [1979]. Various balcony breadths, 1.25 m, 2.5 m, and 5 m (full-scale equivalent), were examined.

The fire source was an electrical heater, and the heat release rate was varied from 1 MW to 5 MW (full-scale equivalent).

Temperatures and mass flow rates were measured at various locations including the doorway.

2.3.3.1 Temperature and balcony breadth limitation

The balcony effect was examined by using three different balcony breadths (1.25 m, 2.5 m, 5 m, full-scale equivalent) in this experiment.

Hansell et al [1993] found that the balcony breadth needed to be at least 2 m to ensure a free balcony spill plume, and a shorter projection of balcony caused the spill plume to adhere to the wall behind. Hansell et al [1993] found that the free balcony spill plume method could be applied to adhered spill plumes by taking approximately half the entrainment coefficient of free plumes.

In addition to the breadth of the balcony, Hansell et al [1993] found that there are limiting temperature conditions of the approach flow for the spill plume method. The balcony spill plume formula is valid only for flows with lower temperatures than these limiting temperature criteria.

Table 2.1 Limiting temperature for the BRE spill plume method

Type	Limiting temperature
Free spill plume	250°C for door width 4 m to 5 m 330°C for door width 7 m
Adhered spill plume	280°C for door width 4 m

2.3.4 Marshall and Harrison [1996]

Five series of 1/10th scale experiments with varying fire compartment and atrium configurations were examined. As shown in Figure 2.6, the widths of the atria and the compartment in all configurations were the same in all cases, i.e., W = 0.91 m for all cases. In series I, a relatively small atrium with dimensions, 0.91 m (W) × 1.0 m (D) × 1.59 m (H) was used. At the compartment opening, a sliding air shutter was installed to prevent counter flow back from the atrium. In series II, the same compartment was used but in a relatively larger atrium [dimensions 0.91 m (W) × 2.0 m (D) × 2.59 m (H)]. In series III, the atrium length was reduced to 1.0 m (D) (but W was still 0.91 m and H was 2.59 m). Counter flow was allowed at the doorway. In series IV and V, the same compartment configuration of Series III was examined in the large atrium, 0.91 m (W) × 2.0 m (D) × 2.59 m (H).

The vertical distribution of the horizontal velocity and temperature below the balcony were measured to determine the heat flux generated by the industrial methylated spirits, and the mass flow rate under the balcony.

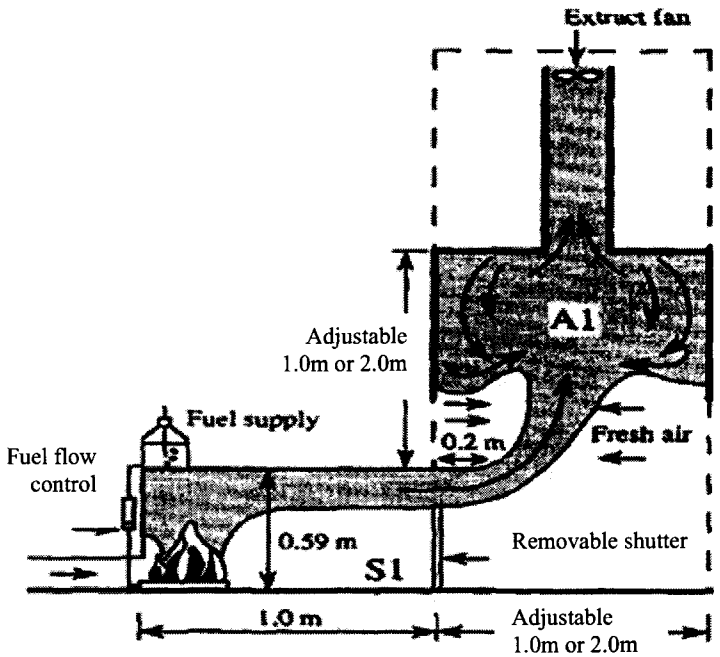

Figure 2.6 Experimental configuration [Marshall and Harrison 1996]

2.3.4.1 Effect of atrium size

Through five series of experiments, three different sizes of atria were examined. Results showed that air entrainment rates were greater for relatively small atria. Marshall and Harrison [1996] noted that flows were more turbulent in relatively small atria, and the buoyant layer was unstable. The effect of atrium size on air entrainment was addressed in the BRE method and was taken into account in the form of an effective layer depth correction.

2.3.5 Harrison [2004]

To explore the limitations and uncertainties of the spill plume method, Harrison conducted a series of 1/10th scale experiments. Mass flow rates of balcony spill plumes generated from a fire compartment, with dimensions 1.0 m (D) × 1.0 m (W) × 1.0 m (H),

were measured at various heights of rise in a relatively tall atrium (dimensions 2.0 m (D) × 1.0 m (W) × 2.5 m (H)). The balcony breadth was 0.3 m, and the flow was fully channelled by draft curtains. The effect of a downstand at the spill edge was examined, using these configurations: either no downstand (0 m), downstand of 0.1 m or 0.2 m.

The heat source was industrial methylated spirits contained in a 0.25 m by 0.25 m tray, and the heat output was adjusted to 6, 9, or 12 kW equating to a fire size of 1.9, 2.8, and 3.8 MW respectively for a full scale equivalent.

The mass flow rate of gases entering the buoyant layer was determined by using a CO_2 tracer measurement technique and a subsequent calculation method. Gas temperatures and velocities were measured and analyzed to calculate the mass flow rate at the doorway and the end of the balcony.

2.3.5.1 Downstand at the spill edge

Harrison found that the presence of a downstand at the spill edge had little impact on the entrainment of air into the spill plume, but caused the emerging plume to rise vertically, leading to smoke logging at higher heights of rise. Harrison developed a spill plume formula incorporating the approach flows, which have a deep down stand at the spill edge.

2.4 CFD modelling work

2.4.1 Miles, Kumar, and Cox [1996]

Numerical simulations of balcony spill plumes were carried out by Miles et al

[1996] using the CFD program, JASMINE. The 1/10th scale model used by Marshall and Harrison [1996] was modelled. Miles et al found that there were differences in the mass flow rates at greater heights of rise. For the rotation region, the study found a small degree of air entrainment and their correlation was identical to that of Poreh et al [1998].

2.4.2 Chow [1998]

The CFD model, CC-EXACT was used to examine the entrainment of air into a spill plume. The same 1/10th physical scale model tested by Marshall and Harrison [1996] was simulated with two heat release rates and three ventilation conditions. A linear correlation of the entrainment rates into the spill plume was derived, which was similar to that described by Poreh et al. Chow suggested that a CFD study on the balcony spill plume be limited to the lower part of the plume, and concluded that the CC-EXACT model is a suitable tool to study smoke filling in atria from a spill plume.

2.4.3 Chow [1999]

In this study, the CFD program PHOENICS 3.1 was used to simulate the same 1/10th physical scale model similar to that in the test of Marshall and Harrison's tests [1996]. The computational domain enclosing the model atrium and compartment was set back in order to properly attain the free boundary conditions.

The result showed that there was a very high air intake from the surroundings. Chow found that the free boundary conditions have to be clearly specified in order to carry out meaningful simulations.

2.4.4 Chow and Li [2001]

Chow and Li developed the two-zone model CL-Atrium to model the smoke filling process in atria from a balcony spill plume. The balcony spill plume correlation developed by Poreh et al [1998], Thomas et al [1998], and the correlation in NFPA-92B [2000] were coded in the program , and the results were compared with another zone model, CFAST.

Both steady-state fires and transient fires were considered, and the correlations by Poreh et al [1998] and Thomas et al [1998] showed similar results for the layer temperature and interface height in the atrium. The results from the NFPA 92B analysis were similar to those predicted by CFAST under both steady-state and transient fire conditions.

2.4.5 Harrison [2004]

Harrison simulated 1/10th scale models using FDS (Fire Dynamics Simulator), in order to examine the mass flow rate of the initial approach flow at the end of the balcony. In this study, five different opening widths (0.2, 0.4, 0.6, 0.8 and 1.0 m) and five different fascia depths (0.1, 0.16, 0.2, 0.25, and 0.3 m) were used. For most cases, the breadth of the balcony was 0.3 m, and for selected cases, a breadth of 0.2 m or 0.5 m was used.

For the majority of the simulations, the fire size was 10.3 kW. However, 6 kW and 16 kW fire sizes were also explored for selected cases.

The mass flow rate of the initial approach flow at the end of the balcony was calculated from the velocity and temperature profiles. Based on the FDS results, Harrison

determined an empirical correlation to estimate M_b (mass flow rate of the approach flow at the end of the balcony), which only applies to a channelled flow.

2.5 Summary

Some of the issues discussed in the literature review are considered in this study.

1) The atrium size

Previous CFD studies have found that the mass flow rate is sensitive to the size of the computational domain, which can be relevant to the issue of extra entrainment at great heights in large atria. In Section 4.2, the impact of the computational domain size is investigated to ensure that it does not affect the flow near the balcony area, so that reliable estimates of the mass flow rates can be obtained.

2) The rotation point (the limiting height of rise)

Morgan and Marshall [1975], in their first 1/10th scale investigation, measured the maximum temperature rise 3 m or 4 m (full-scale equivalent) above the balcony. In subsequent experiments, data from points near the balcony were insufficient to give the exact plume behaviour. Therefore, the question raised is the uncertainty in determining a limiting height of rise, near the balcony edge, above which the spill plume formula has a linear relationship with height. In this study, mass flow rates near the balcony area are fully examined in Chapter 7, in order to determine the point nearest to the balcony at which the spill plume correlation is still valid.

3) Assessing existing methods of calculating M_s by comparison with model results

Existing methods reviewed above are assessed by comparison with model results in Section 7.4.3, in order to examine the performance of each approach and accuracy of the prediction.

4) Entrainment into rotating flows

There is disagreement on the amount of air entrainment into the rotating flow. In the initial work, Morgan and Marshall [1975] found a large degree of air entrainment into the rotation region, while later studies found a small degree of entrainment. Thus, a focused study on air entrainment at the rotating region is conducted in Section 8.2.1. Factors affecting the air entrainment rate at this region are identified, and a new correlation is developed.

3 Scope of Work

With an increasing demand for consideration of the balcony spill plume in the design of atrium smoke exhaust systems, the American Society of Heating, Refrigerating and Air-Conditioning Engineers (ASHRAE) and the National Research Council of Canada (NRC) have recently initiated a joint research project to study balcony spill plumes in-depth. There are several design methods, as outlined in the literature review, for estimating the smoke-production rate of balcony spill plumes, which are based on reduced-scale physical testing. However, there are considerable differences in the estimates obtained, and these differences become particularly significant when applied to the large atria often found in North American buildings [Lougheed 2004].

Therefore, the joint research project also includes full-scale testing, which was conducted at NRC, in addition to computational analysis. The fire compartment was built in the NRC Burn Hall. The project includes CFD modelling investigations of the spill plume behaviour in tall atria and CFD simulation of the balcony spill plume under the balcony area.

As part of the joint project, this study focuses on smoke flow under the balcony and the rotating region. The CFD model, FDS (Fire Dynamics Simulator) [McGrattan and Forney 2004], is used in this study to model the NRC facility used to perform the full-scale experiments and to calculate air entrainment rates in the area under the balcony and the rotating region.

Experimental data obtained from full-scale experiments conducted at NRC were used for the validation of the CFD model predictions. An attempt has been made to develop a correlation using the results of the model.

This study consists of three parts

1) Simple modelling study

Since there are few fundamental explanations of the problem of flow near the balcony, this study conducted simple simulations to understand the physical system of such flows. Without explicit fire modelling, balcony spill plumes were modelled as if the layer of hot gas horizontally flowed into the large reservoir.

2) Full scale CFD simulation

In order to investigate the air entrainment rate under the balcony and the rotating region, this study modelled a full-scale balcony spill plume induced by a fire, and has exploited extensive simulated data and visualization of plume behaviour. CFD model prediction of mass flow rates of the balcony spill plume are compared with existing methods, and data are used to develop a new empirical correlation.

3) Full scale experiments

Experimental results have been used to validate the CFD results.

4 Simple Modelling Study

4.1 General

4.1.1 CFD modelling of smoke movement

CFD modelling has been used for the study of the behaviour of fire, and it has been demonstrated that it can be used for the study of smoke movement. A CFD program, Fire Dynamics Simulator (FDS) developed by NIST (National Institute of Standards and Technology), is used with some modification to calculate the mass flow rate of the gas through various planes.

4.1.2 FDS (Fire Dynamics Simulator)

FDS is a computational fluid dynamics (CFD) model of fire driven fluid flow developed by NIST (National Institute of Standards and Technology), which solves numerically a form of the Navier-Stokes equations appropriate for low-speed, thermally-driven flow with an emphasis on smoke and heat transport from fires [McGrattan and Forney 2004].

The formulation of the equations and the numerical algorithm are in the Fire Dynamics Simulator – Technical Reference Guide [McGrattan 2004].

Main features;

1) Hydrodynamic Model

- The fundamental conservation equations of mass, momentum, and energy
- Large Eddy Simulation (LES) approach for turbulence [Baum et al 1998]
- Direct Numerical Simulation (DNS) if the numerical grid is fine enough

- Limited to low Mach number flows

2) Combustion Model

- Mixture fraction based, equilibrium chemistry model for combustion

3) Thermal Radiation Transport Model

- The Radiative Transport Equation (RTE)

4) Numerical methods

- Finite difference scheme (1st-2nd order); predictor corrector time integrator (2nd order); rectangular Cartesian grid; multi-block grid.

4.1.3 The simplified problem of balcony spill plume

Smoke-movement simulations are very sensitive to the computational domain size and grid size [McGrattan and Forney 2004]. A coarse grid size is used in this simple modelling study to ensure the calculation required comparatively short CPU time on a UNIX. The modelling of complex, large-scale systems, is often more difficult than the modelling of simple representative physical systems. To simplify the problem of the balcony spill plume and minimize the number of factors affecting smoke flow under a balcony, the flow generated from a fire compartment was replaced with a layer of flow with an imposed temperature and velocity.

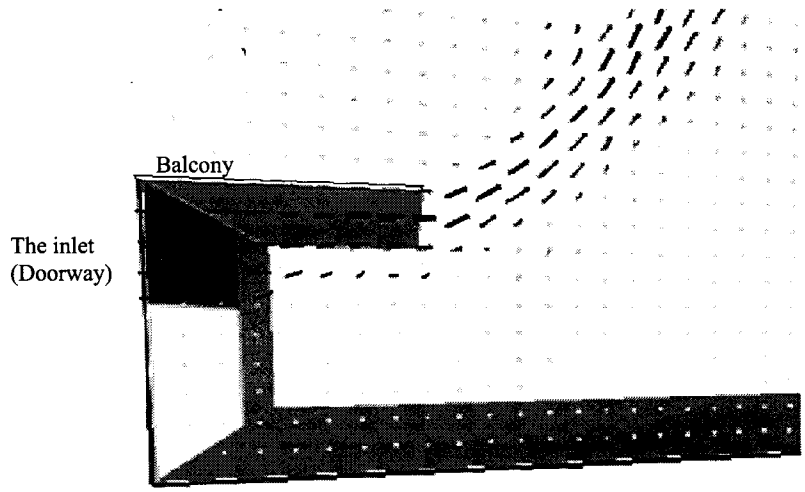

Figure 4.1 The problem of the buoyant jet in the simple modelling study

This layer of hot gas flow was horizontally injected into the large reservoir, and the behaviour of this buoyant jet was investigated. A depiction of the set-up of this buoyant jet system to represent a balcony spill plume is given in Figure 4.1. This simple model using a coarse grid size of 500 mm allowed the examination of fundamental aspects of the problem of balcony spill plumes under various conditions, within a relatively short CPU time. This simulation required 10~30 CPU seconds per simulated second on an SGI Origin350 with 8 R16K CPUs and 8 Gigabytes of RAM running IRIX 6.5.28f. For a fine grid size of 250 mm with room fire modelling, 300~500 CPU seconds per simulated second were required.

4.1.4 Objectives

This coarse grid simple model study aims;

1) to determine the impact of domain size on the balcony spill plume
2) to investigate the impact of temperature and velocity on the balcony spill plume

3) to study the effect of critical components, such as balcony length, draft curtain and fascia, on the flow of the plume

4.2 Domain size testing

4.2.1 Description of modelling

A simple coarse grid (500 m) model was tested with different computational domain sizes to find the optimal domain size. A layer of hot gas flow with a uniform temperature and velocity was injected into different sizes of reservoir, to test the effect of computational domain size on the mass flow rate.

In Table 4.1, six different computational domain sizes with various D (depth of the domain), W (width of the domain), and H (height of the domain) were tested, and a free boundary condition was applied to the computational domain, at all boundaries except the floor of the atrium. .

In each simulation, the inlet condition remains the same. The inlet representing the doorway smoke flow had dimensions of 12 m (width) and 2 m (depth). The injected flow had uniform temperature and velocity of 245°C and 2.22m/s, respectively, which was estimated using FDS from a doorway smoke flow from a room fire model [the size of the room was 13.6 m (depth) × 5 m (width) × 5 m (height), opening width was 12m, and the heat source was 5 MW]. Thus, the mass flow rate at the inlet was about 36 kg/s. For all cases, the breadth of the balcony was 4.2m, and the width of the balcony is extended to the end of the domain width. A thermally inert boundary condition was applied to the balcony.

Table 4.1 Computational domain size test (D, W, and H are depicted in Figure 4.2)

Size ID	D (m)		W (m)		H (m)
Domain Q	12.6	×	16	×	10
Domain P	12.6	×	20	×	6
Domain N	16.8	×	20	×	10
Domain C	21	×	28	×	10
Domain D	25	×	36	×	10
Domain E	40	×	50	×	20

As a convergence criterion, mass flow rates were monitored at 1 m intervals along the entire flow path for each computational domain size. Figure 4.2 shows planes where mass flow rates were measured [at the end of balcony (x = 4.2m), at the edge of the balcony (z = 0m), and at z = 4m].

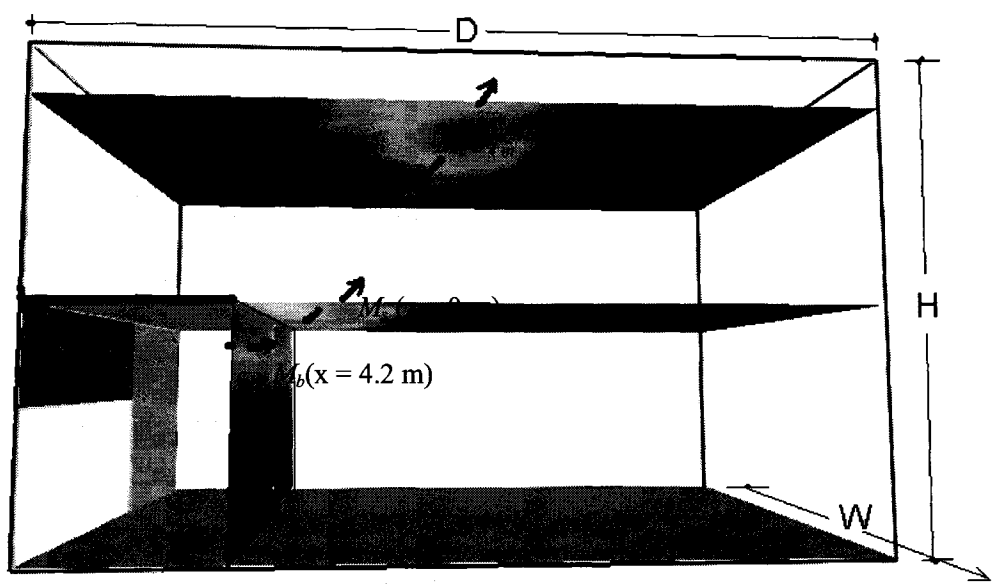

Figure 4.2 Mass flow rate measurements at planes of interest

4.2.2 Results

It was found that mass flow rates over all planes monitored increases as the volume of a computational domain increases. The difference in mass flow rates due to

different computational domain sizes was more significant for greater heights of rise. Figure 4.3 shows the variation of the mass flow rates at z = 4 m with time, which were measured for each domain size. For each domain size, the pattern of variation with time is similar, but the mean value of the mass flow rate prediction is different.

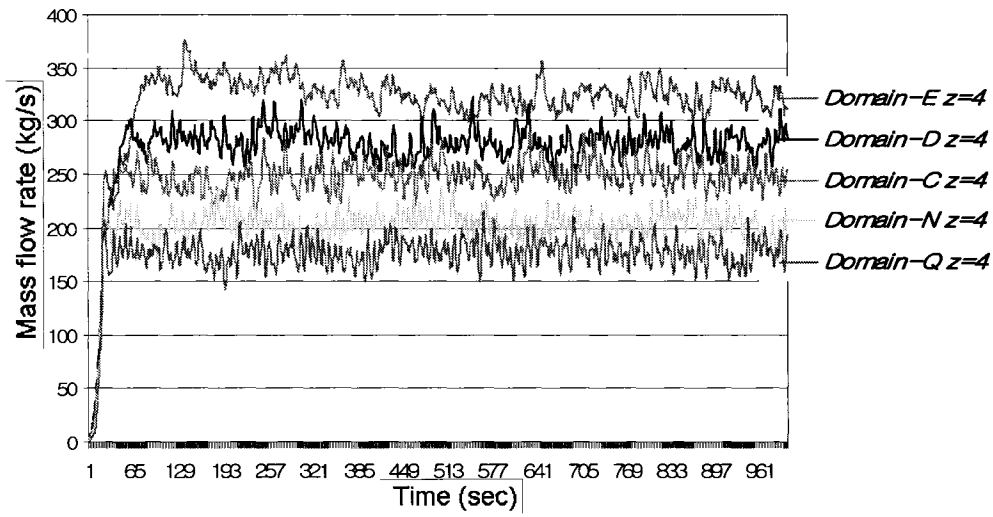

Figure 4.3 Mass flow rates at z = 4 m over time for computational domain size tests

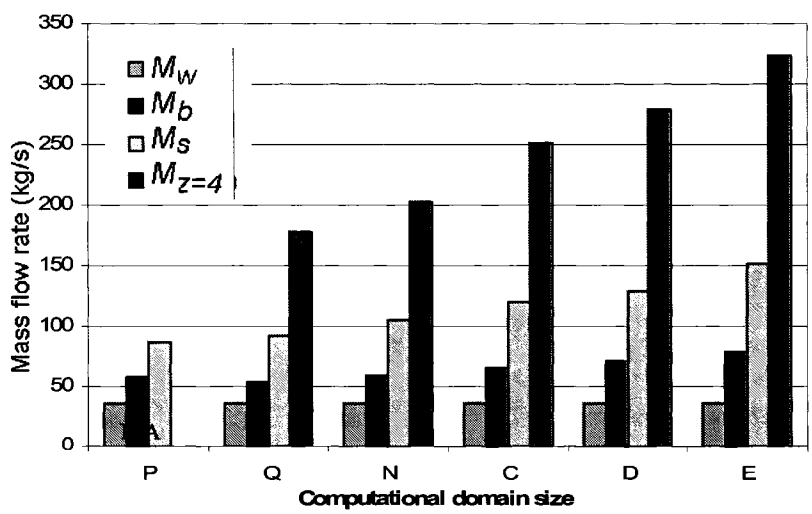

Figure 4.4 Mass flow rate variation with respect to computational domain size

Averaged mass flow rates after the onset of steady-state behaviour are calculated at the door way (M_w), at the end of the balcony (M_b), at the edge of the balcony (M_s), and at z = 4 m ($M_{z=4m}$). In Figure 4.4, the calculated results are compared. The volume of the computational domain affects the mass flow rate of the vertically moving plume, and the width and depth of the domain have a greater effect on the mass flow rate of the horizontally moving flow than the vertical flow. The results indicate a bigger computational domain is required in order to achieve convergence.

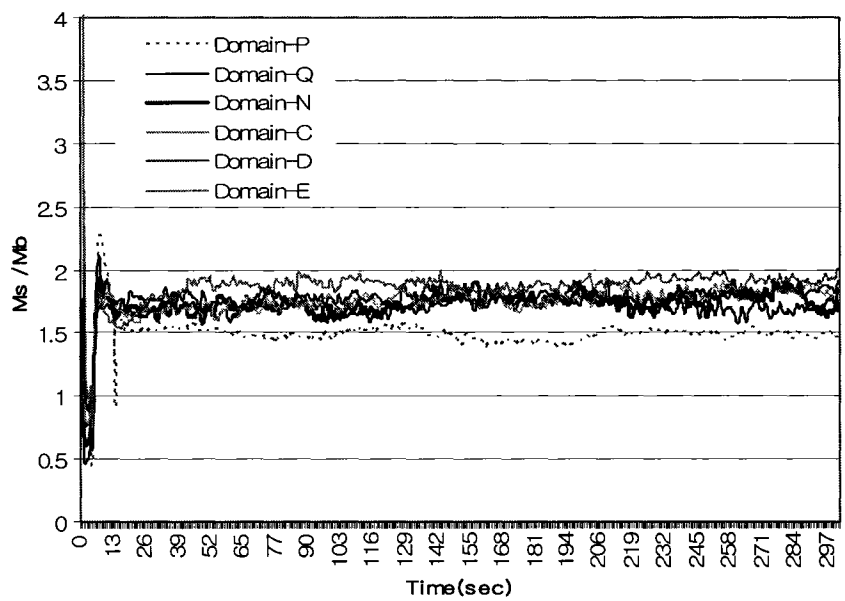

Figure 4.5 The air entrainment rates at the rotating region using various computational domain sizes

Since our interest is centered on the air entrainment of the initial approach flow, air entrainment rates at the rotating region, M_s/M_b, were processed and compared in Figure 4.5. It was found that although a larger volume of a computational domain

predicts the entrainment of more air, the ratio of the mass flow rates, M_s/M_b, converged as long as the height of the computational domain is high enough. As shown in the figure, domains of 20 m high and 10 m high show a similar M_s/M_b ratio (approximately 1.85 in this case), but the case, 'Domain-P', with a height of 6m, a lower ratio is obtained (about 1.43).

Therefore, "Domain-N"[of size 16.8 m (D) × 20 m (W) × 9.97 m (H)], was selected as an optimal computational domain for this study.

The results of this study show that the mass flow rate is sensitive to the computational domain size even though free boundaries were applied. This sensitivity makes it difficult to use Multi-Parallel Processing, which requires less CPU time by breaking up the computational domain into multi-meshes and running a single FDS job with multiple computers [McGrattan and Forney 2004]. From the test runs, it was found that each domain of broken up meshes can affect the mass flow rate of the spill plume. For this reason, a single mesh was used in the computational domain in order to obtain more accurate results.

4.3 Temperature and velocity effects

The subject of the present simulation work is the study of a buoyant jet discharging into a large reservoir of a uniform stationary ambient environment, which represents an atrium. This testing aims to examine the flow behaviour at the rotating region.

4.3.1 Description of modelling

An inlet flow representing the horizontal flow at the end of the balcony was injected into the reservoir. The dimensions of the injected flow were 5 m (width) and 2 m (depth). For each simulation, the initial source flow was defined as a buoyant jet with an assigned uniform temperature and velocity.

Table 4.2 summarizes the conditions of each scenario. Simulations were carried out to examine the effect of temperature and velocity on balcony spill plumes.

Table 4.2 Series of simple simulation : temperature and velocity effects

Simulation ID	Temperature (°C)	U-Velocity (m/s)	Ri
TV1	197	0.1	886.60
TV2	197	1.3	5.20
TV3	197	2.65	1.26
TV4	197	3.98	0.56
VT1	28.9	2.65	0.10
VT2	46.55	2.65	0.28
VT3	108.5	2.65	0.78
VT4	285.3	2.65	1.60
T1V3	176	5.0	0.33
T2V2	91	3.3	0.42
T3V1	203	0.3	100.6

In the first four simulations, TV1 to TV4, the temperature was kept constant at 197°C, and the velocity was varied from 0.1 m/s to 3.98 m/s. In the second series, in VT1 to VT4, the velocity was kept constant at 2.65m/s and the temperature varied from 28.9°C 285.3°C. Additional simulations, T1V3 to T3V1 were also carried out to examine various flow characteristics. The depth of the flow layer was set to be 2 m for all cases, and the width of the flow was 5m.

Since a buoyant jet is driven by both buoyancy and momentum, the Richardson

number (Ri) of each flow, a dimensionless characteristic of the flow, was calculated to determine the ratio of its buoyancy to momentum [Turner 1973].

$$Ri = \frac{g(\rho_0 - \rho)D}{\rho \upsilon^2} \tag{4.1}$$

where
ρ = source fluid density (kg m^{-3})
ρ_o = ambient density (kg m^{-3})
υ = injecting velocity (*U-Vel*) (m s^{-1})
D = layer depth (m)

The mass flow rate was measured at the spill edge, where a horizontally injected flow starts to rotate, and the air entrainment rate, M_s / M_b is calculated. The values of M_s / M_b are compared with Ri to ascertain whether a direct correlation exists.

4.3.2 Results

4.3.2.1 Flow behaviour

Figure 4.6 shows simulated results from TV2 and T2V2. The trajectory of the flow is determined by its buoyancy (B) and jet momentum (M). The entrainment takes place due to the plume motion, and this motion can be represented by the trajectory of the buoyant plume jet. As flow rises up, the trajectory of flow motion is continuously adjusted due to dilution and loss of momentum. Eventually, the buoyant jets will be converted to fully buoyant plumes, which will have only upward momentum due to density differences.

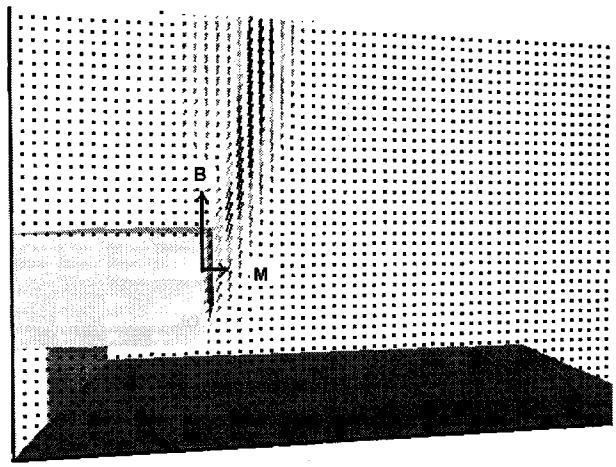

(1) TV2 : T = 197°C. *U-Vel* = 1.3 m/s, Ri = 5.20

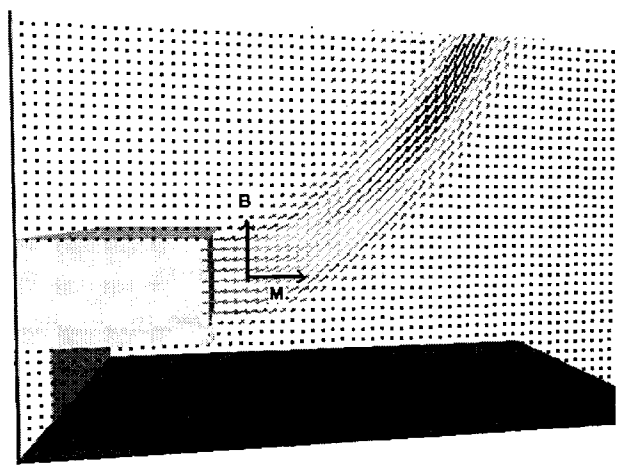

(2) T2V2 : T = 91°C. *U-Vel* = 3.3 m/s, Ri = 0.42

Figure 4.6 Vector slice of simulation TV2 (1) and T2V2 (2)

Flows with a greater Ri, (1) in Figure 4.6, emerge into the large reservoir immediately after being injected, and the entrainment and mixing process rapidly occur in a vertically moving spill plume. On the other hand, for flows with lower Ri, (2) in Figure 4.6, the complete transition from horizontal flow to a fully vertical plume is achieved at greater height of rise.

4.3.2.2 M_s / M_b and Ri

In the rotating region, buoyancy and jet momentum compete, and the flow rotates up only if the density of the flow is less than that of ambient air. The air entrainment rate into rotating flows, M_s / M_b, increases with a rise in temperature and decreases with a rise in U-velocity. In fact, the value of M_s / M_b depends on both temperature and velocity of the initial flow. In Figure 4.7, M_s / M_b is plotted as a function of Richardson number (Ri) on a log scale.

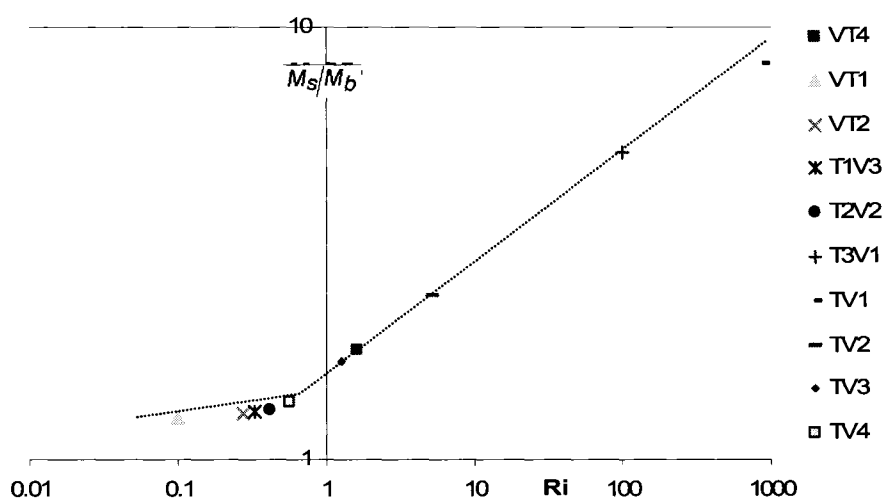

Figure 4.7 Simple model results displayed as a plot of M_s / M_b with respect to Ri

With Ri values higher than 0.7, the flow behaves more like an axisymmetric plume in which buoyancy governs, and M_s / M_b increases in a power-law fashion, the slope of power-law correlation being 1/4.

$$\frac{M_s}{M_b} = 1.6 Ri^{1/4}, \text{ for } Ri > 0.7 \tag{4.2}$$

However, the correlation displays a discontinuity at a Ri value of 0.7. With Ri values lower than 0.7, the flow behaves more like a jet. In Equation 4.2, M_s / M_b is expected to be valid in actual physical experiments only for the same conditions of layer depth and width as in this simple model test. In practice, such a well-defined correlation as in Equation 4.2 is difficult to obtain from flows induced by fires. Nonetheless, the results of this simple model reasonably describe the physics of the buoyant jet in the flows induced by fire. The limiting value of Ri determines whether buoyancy governs the flow or jet momentum governs the flow. For balcony spill plumes, free unbounded spill plumes have jet momentum governing flows, and adhered plumes have buoyancy governing flows.

4.4 Parameter sensitivity testing

Another set of simple modelling simulations was conducted to check the effect of selected parameters on the behaviour of the plume. The parameters studied were those related to a balcony, a draft curtain, and a fascia.

4.4.1 Description of modelling

Representing the door flow, a layer of hot gas at the inlet was injected into the reservoir (the atrium). The properties of the injected flow at the inlet were consistent in all simulations. The layer of the inlet flow was 5 m wide and 2 m deep. The temperature (T_w) and velocity ($U\text{-}Vel_w$) of the injected flow were 197°C and 2.65 m/s respectively. These values were estimated from a room fire of a 5 MW heat source and a compartment opening of 5 m width.

Table 4.3 summarizes the series of simulations carried out and the conditions used. To examine the parameters altering the flow characteristics of the initial inlet doorway flow, a balcony, draft curtains, and fascia were added to the initial model, 'TV0'. The breadth of the balcony was 2 m or 4.2m, and the width of the balcony was extended to the end of the computational domain. The distance between draft curtains was the width of the inlet, that is, the width of the door flow. A thermally inert boundary condition was applied to the balcony and draft curtains.

Table 4.3 Series of simple model used for sensitivity testing

ID	T_w (°C)	$U\text{-}Vel_w$ (m s^{-1})	Fascia (D_f)	Balcony (b)	Draft Curtain (D_c)
TV0	197.0	2.65	No	No	No
B-1	197.0	2.65	No	b = 2m	No
B-2	197.0	2.65	No	b = 4.2m	No
DC	197.0	2.65	No	b = 4.2m	D_c = 3m
F	197.0	2.65	D_f = 1.6m	b = 4.2m	No

4.4.2 Results

4.4.2.1 Parameter effects

Figure 4.8 shows the simulation results of the parameter sensitivity test. The trajectory of the flow at the end of the balcony is determined by the flow characteristics that are affected by parameter conditions: the breadth of the balcony; and the presence of the draft curtain and fascia.

With no balcony (TV0), the horizontal inlet flow immediately rotates up due to its buoyancy. This buoyancy of the horizontal inlet flow results in rapid transition to a vertical flow, which can cause the vertical flow to adhere or bound back to the wall above

the balcony. On the other hand, the buoyancy of flows running under a balcony, shown in (2) and (3) of Figure 4.8, is impeded since the horizontal velocity increases under the balcony. When there is a longer balcony and a draft curtain, shown in (4) of Figure 4.8, the momentum of the buoyant jet becomes stronger. When there is a fascia, as shown in (5) of Figure 4.8, the momentum of the horizontal flow also increases significantly, and the flow appears more turbulent than the flow with no fascia.

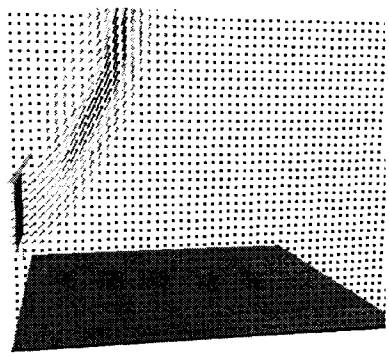

(1) Simulation TV0 (T_w = 197'C, $U\text{-}Vel_w$ 2.65m/s)

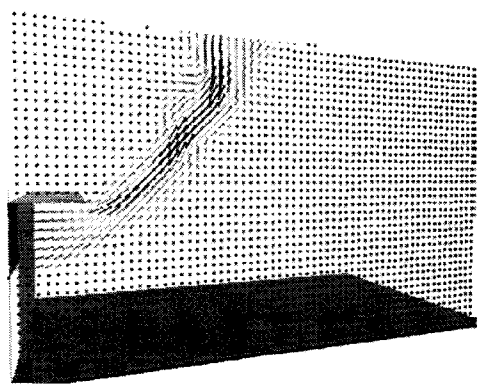

(2) Simulation B-1
under short projecting balcony

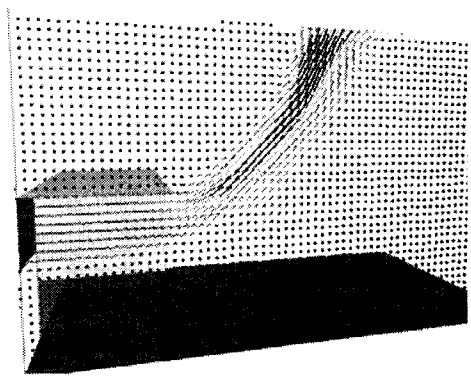

(4) Simulation DC
With draft curtain

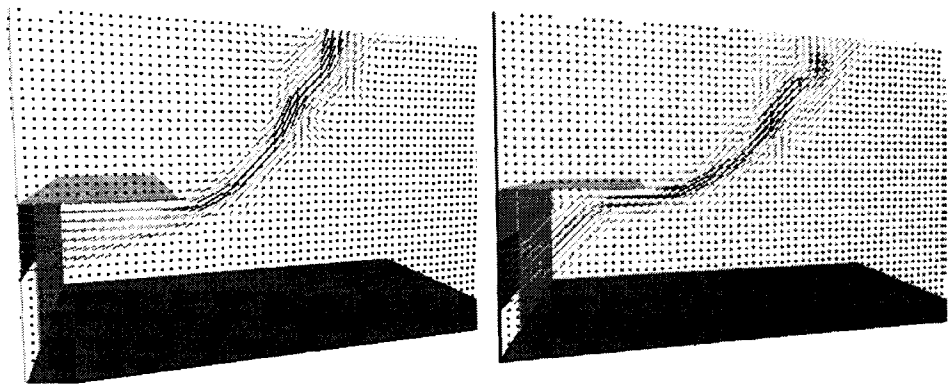

(3) Simulation B-2 under long projecting balcony

(5) Simulation F With fascia

Figure 4.8 Velocity vector slices of simulation of the sensitivity test

4.4.2.2 Parameter effect on flow characteristics and the air entrainment

The maximum temperature and velocity of the horizontal flow, as well as the layer depth were measured at the end of the balcony. The Ri number of the flow at the end of the balcony was then calculated based on these values. Mass flow rates at the end of the balcony and at the spill edge were calculated. Results are presented in Table 4.4.

Table 4.4 Flow characteristics at the end of the balcony and M_s/M_b

ID	T_b (°C)	$U\text{-}Vel_b$ (m s^{-1})	D_b (m)	Ri	M_s/M_b	
TV0	197.0*	2.65*	2*	1.26*	1.70	* initial condition
B-1	196.2	3.62	1.5	0.54	1.18	$b = 2$m
B-2	188.1	3.65	1	0.35	1.16	$b = 4.2$m
DC	194.4	4.28	1.5	0.39	1.07	$D_c = 3$m
F	179.1	4.48	1.55	0.34	1.54	$D_f = 1.6$m

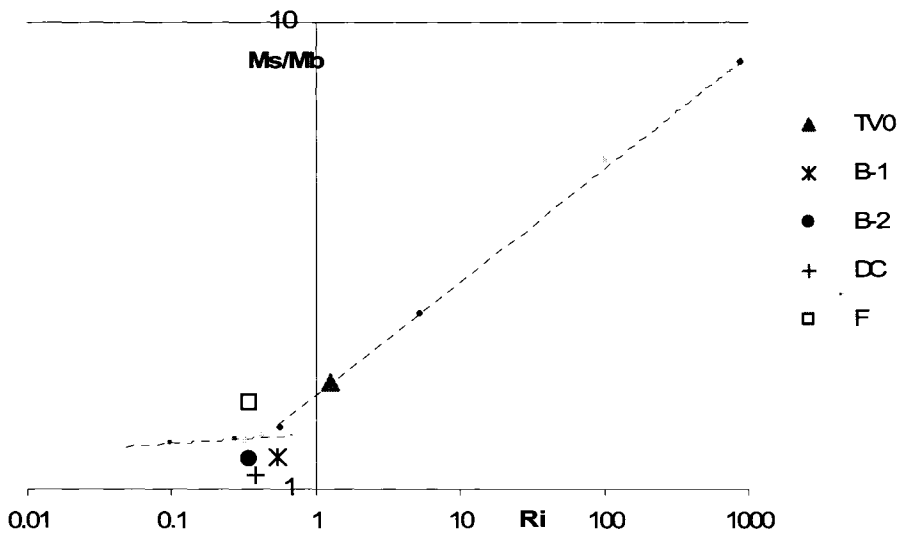

Figure 4.9 A plot of M_s/M_b with respect to Ri : from parameter sensitivity tests

In Figure 4.9, the values of M_s/M_b are plotted with respect to Ri on a log scale, and compared with the correlation obtained from the temperature and velocity effect tests in Section 4.3.2. Figure 4.9 shows that the results from simulations of this sensitivity test appear to obey the general pattern of M_s/M_b correlation with Ri.

Under the initial conditions used (TV0), the doorway flow induced by fire has initially both momentum and buoyancy. This initial condition had Ri = 1.26 with a temperature of 197°C and velocity of 2.65m/s, as shown for Simulation 'TV0' in Table 4.4.

When the balcony is introduced (Simulation 'B-2'), the characteristic of the flow is found to drop from its initial Ri = 1.26 to Ri = 0.35. The critical changes made to the flow due to the presence of a balcony is that the resultant Ri at the end of the balcony dropped below the limiting Ri criteria, 0.7, which was discussed in Section 4.3.2.2. The resulting buoyant jet due to the balcony behaves as a momentum-leading buoyant jet,

which is more appreciably affected by its horizontal momentum, rather than its buoyancy.

For simulation 'B-1', the balcony breadth was set to at 2m, which is at the limiting balcony breadth suggested by Hansell et al. As the resultant Ri was found to be below the limiting Ri, this relatively short projection of the balcony (b = 2m) also causes the horizontal velocity of the flow to increase so the horizontal momentum becomes dominant when the flow spills up.

Compared with Simulation 'B-2', the presence of the draft curtain (Simulation 'DC') results in a reduced value of M_s/M_b despite a slightly greater Ri at the end of the balcony. A possible reason for this is that, for Simulation 'DC', the channelled flow did not spread out under the balcony so that the thick layer depth at the end of the balcony affects air entrainment. Using similar reasoning, greater air entrainments for Simulation 'F' than Simulation 'B-2' resulted from the fascia effect, which causes the layer of the flow to spread and causes the flow to be turbulent.

4.5 Summary of results and Discussion

1. Domain size test: The results of this study show that the mass flow rate is sensitive to the computational domain size. The optimal domain size is obtained by employing M_s/M_b as a convergence criterion.

2. Temperature and velocity effect test: The trajectory of the flow is governed by its buoyancy and jet momentum. These effects can be represented by Ri, which can be calculated from the flow temperature and velocity. Although some variability of M_s/M_b is found depending on parameter conditions, it can be stated with some confidence that the air entrainment depends on the Ri of the flow. More importantly, Ri defines the flow

behaviour, i.e., whether the buoyant plume behaviour is more dominant or not. The limiting Ri criteria is found to be approximately 0.7, below which the horizontal momentum appreciably affects the flow.

3. Parameter sensitivity test: It was found that the presence of a balcony is critical. The Ri value of the flow at the end of the balcony is lowered as the balcony increases the horizontal velocity of the flow. At the end of the balcony, the flow characteristic of the initial flow is found to be below the limiting Ri criteria.

4. The limiting Ri criteria can be used to assess whether the balcony spill plume is free-unbounded, along with the limiting temperature and balcony breadth criteria suggested by Hansell et al [1993].

5. The simple modelling study helps to understand the mechanisms of buoyant jets and in particular the air entrainment into the rotating flow of balcony spill plumes.

5 CFD Modelling: Description and Procedure

In this study, the Fire Dynamics Simulator (FDS) developed at the National Institute of Standards and Technology (NIST) was used to investigate the flow under a balcony and near the balcony area. Results are compared with experimental measurements.

5.1 CFD Modelling Description

5.1.1 Model geometry

The computational domain used in FDS consists of a fire compartment which opens into a reservoir representing an atrium space. As shown in Figure 5.1, the modelled fire compartment is 13.6 m by 5.0 m(in floor area), and 5.0 m high, with an opening facing an atrium. This fire compartment has the same dimensions as the full-scale test facility at the National Research Council of Canada (NRC).

As shown in Figure 5.1, the ceiling of the compartment extends out as a balcony, and the width of the balcony is the same as that of the compartment. For some cases, a 1.6 m deep fascia and /or a 3 m deep channelling draft curtain were added. Thermally inert boundary conditions were applied to the compartment walls, and the free boundary conditions were applied to the computational domain, at all boundaries except the floor of the atrium.

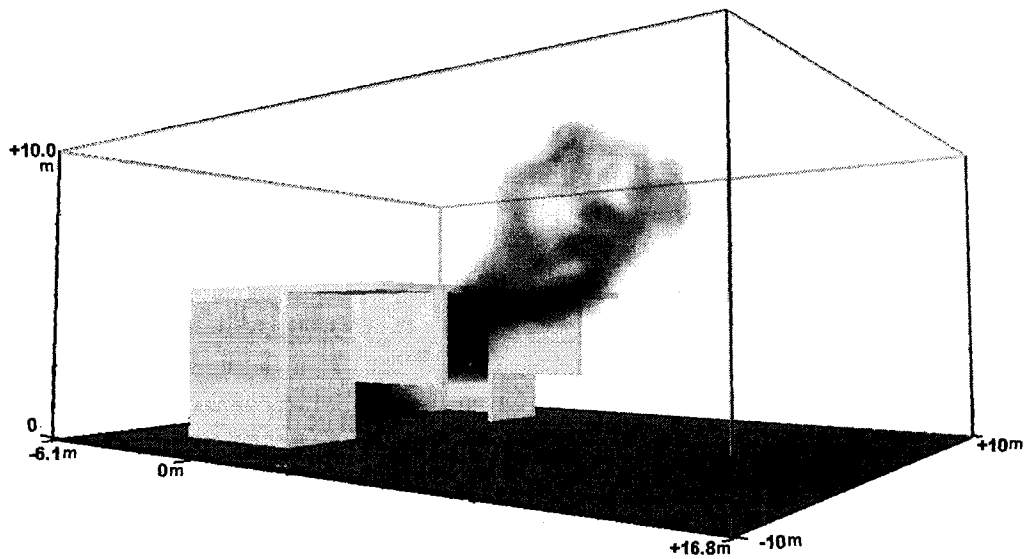

Figure 5.1 Model geometry

5.1.2 Fire simulation and boundary conditions

The goal of the simulations is to estimate the mass flow rate under steady-state conditions. Therefore, the fire source (a rectangular burner) placed at the centre of the fire compartment was defined as a constant heat source which was prescribed by the heat release rate per unit area. The energy flowing out of the domain, (convective/radiative loss to open boundaries) was calculated by the FDS model.

To determine the impact of the boundary conditions used for the room and the burner on heat loss, four simulations were carried out using different boundary conditions as shown in Table 5.1. Two boundary conditions were used for the compartment walls and ceiling: inert and gypsum board, and for the floor: concrete and inert. Two boundary conditions were also used for the burner surface: inert and a constant surface temperature

of 1000°C. The heat release rate of the burner was set to 3 MW. The compartment opening size was 7.5 m, and uniform grid size of 250 mm was used.

Table 5.1 Boundary conditions used for test simulations

ID	Burner	Compartment wall and ceiling	Compartment floor
S1	Inert	Inert	Inert
S2	Inert	Gypsum board	Concrete
S3	Surface temperature 1000°C	Inert	Inert
S4	Surface temperature 1000°C	Gypsum board	Concrete

The heat output results are compared in Figure 5.2. The convective heat output (Q_c) in gypsum board compartments is greater than the compartments with inert walls since there is less conduction loss to the boundary (Q_{con}). Prescribing the burner surface temperature to be 1000°C reduces the conduction loss by about 40 % so that the convective heat output reaches 66 % and 76 % of the total heat release rate (Q) for S3 and S4, respectively.

Consequently, the maximum temperature of smoke flow in S3 and S4 is found to be higher than S1 and S2. Figure 5.3 compares the temperature profiles of the flow at the end of the balcony from test simulations.

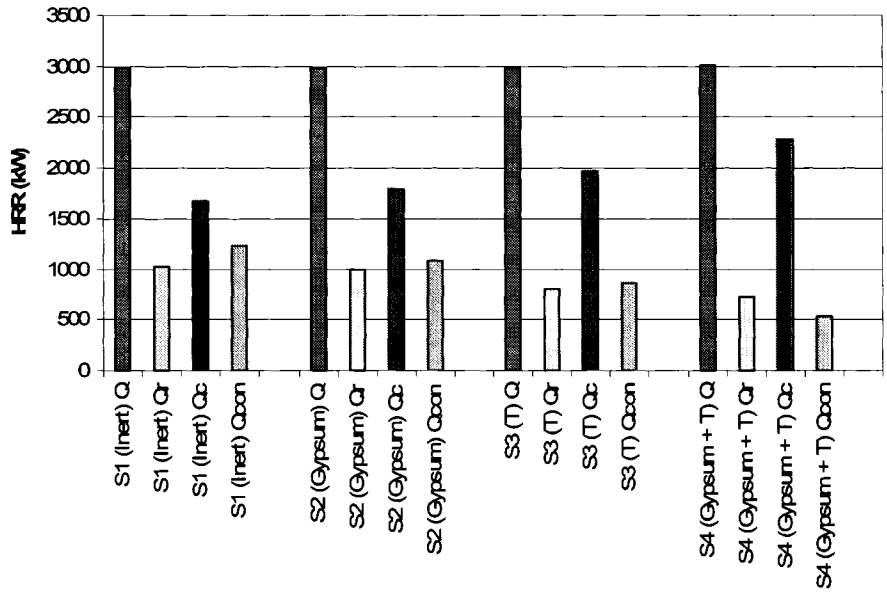

Figure 5.2 The heat output results from test simulations

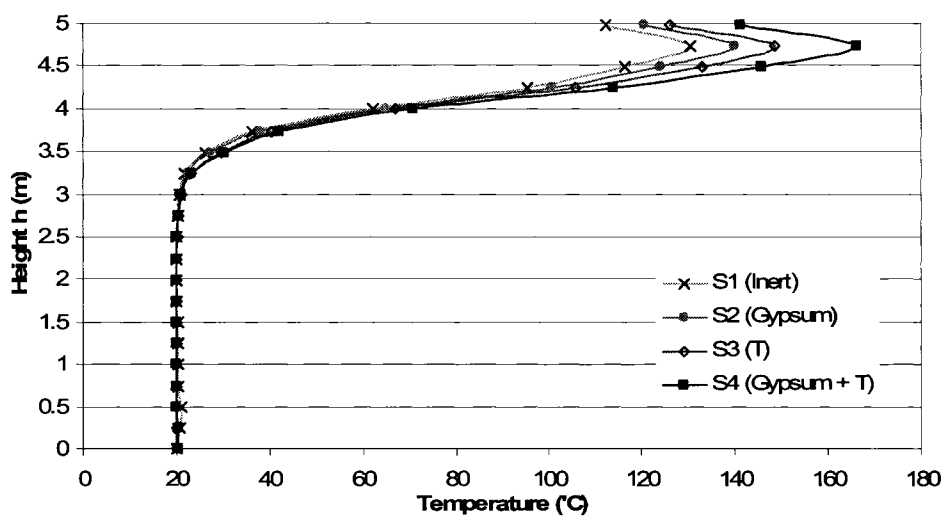

Figure 5.3 Temperature profiles at the end of the balocny resulted from test simulations

5.1.3 Computational domain and grid size

As discussed earlier in the simple modelling study, smoke-movement simulations are very sensitive to the computational domain size and spatial resolution. Domain size and grid convergence tests were conducted by monitoring the mass flow rate at selected planes. From these tests, the selected computational domain size was set at 23 m (D) × 20 m (W) × 10 m (H), and free boundary conditions were assigned at all boundaries except the floor of the atrium.

Figure 5.4 shows the results of the grid convergence tests, in which 4 MW heat source, 12 m opening width were used, and there was fascia but not draft curtain. Mass flow rates were monitored (1) at the end of the balcony, (2) at the balcony edge, and (3) at the top of the model domain. A spatial dimension of 250 m was selected, and applied to the entire computational domain, excluding the area under the balcony and near the balcony. By adopting the non-uniform grid method used by FDS, a finer grid size of 125 mm was used under the balcony and the near balcony areas, where steep variable gradients are expected. This enabled the detailed monitoring of the boundary layer under the balcony and of the rotating flow.

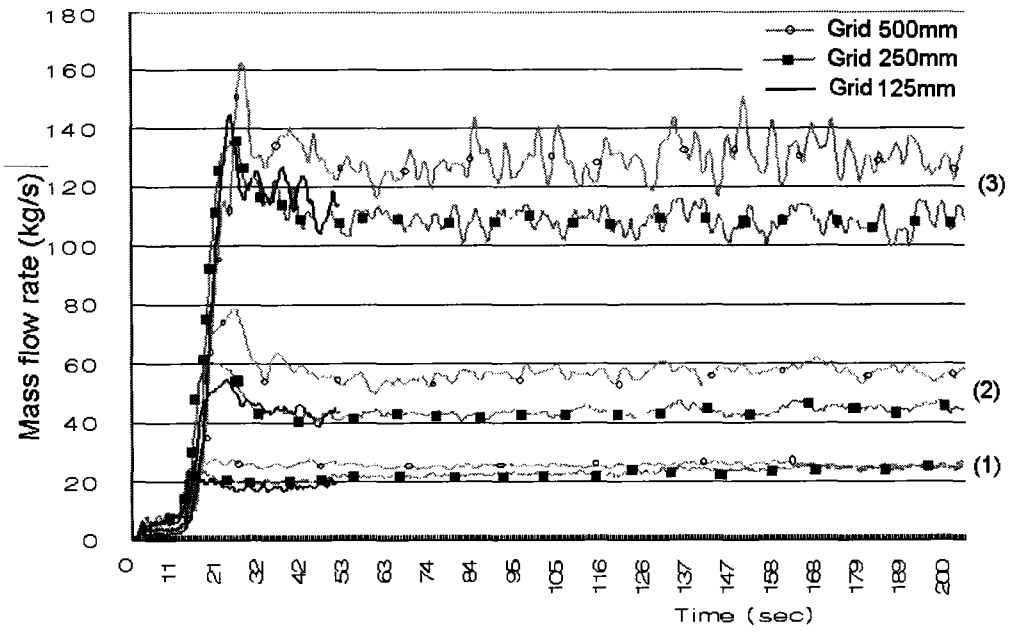

Figure 5.4 Plot of results of grid convergence test

Figure 5.5 shows the modelling geometry and grid meshing, consisting of the fire compartment and the large open reservoir.

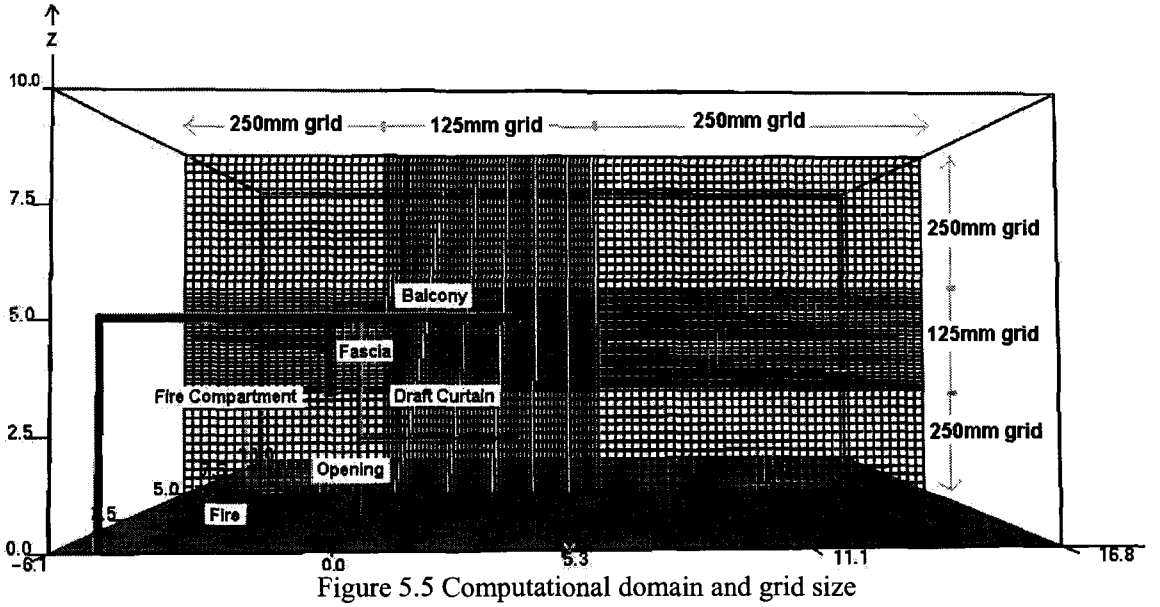

Figure 5.5 Computational domain and grid size

5.2 *Simulations*

5.2.1 Parameters of interest and variations

For the purpose of investigating variations of the air entrainment rate, and in an attempt to quantify the effect of each parameter under the balcony area, the following parameters and variations, collected in Table 5.2, were investigated.

Table 5.2 Parameters of interest and variations

Parameters	Variation
Fire source (Q)	1, 2, 3, 4, or 5 MW total heat release rate
Width of opening (W)	5, 7.5, or 12 m
Depth of the fascia (D_f)	0 or 1.6 m
Breadth of balcony (b)	4.2 m fixed
Depth of draft curtain(D_c)	0 or 3 m

The air entrainment rate is expected to depend mainly on the condition of the source flow. As a result of the variations of the above parameters, the initial gas flow, which is generated from the fire compartment, is expected to have a broad range of flow characteristics, such as mass flow rate, temperature, velocity, and layer depth. These variations give four parameter conditions, as in Table 5.3.

Table 5.3 Parameter conditions used in the modelling

Parameters Conditions	Fascia	Draft curtains	Description
Case-YN	Y	N	unchanneled flow with fascia
Case-NN	N	N	unchanneled flow with no fascia
Case-YY	Y	Y	channelled flow with fascia
Case-NY	N	Y	channelled flow with no fascia

Table 5.4 lists the simulations performed; with each simulation's heat release rate used (Q), the opening width (W) and the presence of fascia and draft curtain. A total of 52 simulations were carried out to cover all variations of the parameters shown in Table 5.2.

Table 5.4 The series of FDS simulations

	ID	Q(MW)	W(m)	Fascia	Draft curtain
1	S1M5NN	1	5	N	N
2	S2M5NN	2	5	N	N
3	S3M5NN	3	5	N	N
4	S4M5NN	4	5	N	N
5	S1M75NN	1	7.5	N	N
6	S2M75NN	2	7.5	N	N
7	S3M75NN	3	7.5	N	N
8	S4M75NN	4	7.5	N	N
9	S1M12NN	1	12	N	N
10	S2M12NN	2	12	N	N
11	S3M12NN	3	12	N	N
12	S4M12NN	4	12	N	N
13	S1M5YN	1	5	Y	N
14	S2M5YN	2	5	Y	N
15	S3M5YN	3	5	Y	N
16	S4M5YN	4	5	Y	N
17	S1M75YN	1	7.5	Y	N
18	S2M75YN	2	7.5	Y	N
19	S3M75YN	3	7.5	Y	N
20	S4M75YN	4	7.5	Y	N
21	S1M12YN	1	12	Y	N
22	S2M12YN	2	12	Y	N
23	S3M12YN	3	12	Y	N
24	S4M12YN	4	12	Y	N
25	S1M5NY	1	5	N	Y
26	S2M5NY	2	5	N	Y
27	S3M5NY	3	5	N	Y
28	S4M5NY	4	5	N	Y
29	S1M75NY	1	7.5	N	Y
30	S2M75NY	2	7.5	N	Y
31	S3M75NY	3	7.5	N	Y
32	S4M75NY	4	7.5	N	Y
33	S1M12NY	1	12	N	Y
34	S2M12NY	2	12	N	Y
35	S3M12NY	3	12	N	Y
36	S4M12NY	4	12	N	Y
37	S1M5YY	1	5	Y	Y
38	S2M5YY	2	5	Y	Y
39	S3M5YY	3	5	Y	Y
40	S4M5YY	4	5	Y	Y
41	S1M75YY	1	7.5	Y	Y
42	S2M75YY	2	7.5	Y	Y
43	S3M75YY	3	7.5	Y	Y
44	S4M75YY	4	7.5	Y	Y
45	S1M12YY	1	12	Y	Y
46	S2M12YY	2	12	Y	Y
47	S3M12YY	3	12	Y	Y
48	S4M12YY	4	12	Y	Y
49	R5M5NN	5	5	N	N
50	R5M5YN	5	5	Y	N
51	R5M5NY	5	5	N	Y
52	R5M5YY	5	5	Y	Y

*A simulation ID is formed as following,
Example:

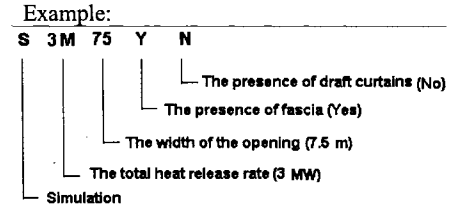

5.3 *Output data*

5.3.1 Calculation of the mass flow rate of gases

5.3.1.1 FDS code modification

Mass flow rate is calculated by the FDS model, on a specified plane of interest. In the FDS calculation, the mean value of the mass flow rate is calculated using the integral $\int \rho\, v_n \cdot dS$, regardless of the flow direction. The FDS model was modified so that the mass flow rate is computed using the flow crossing the plane in one direction only, neglecting the flow in the opposite direction.

Figure 5.6 compares mass flow rates at the doorway calculated by the modified FDS and by the original FDS. At the doorway, the modified FDS calculates outflows of smoke only, excluding the counter flow of incoming fresh air, while the FDS model shows zero net mass flow rates, summing both positive and negative directions of flow.

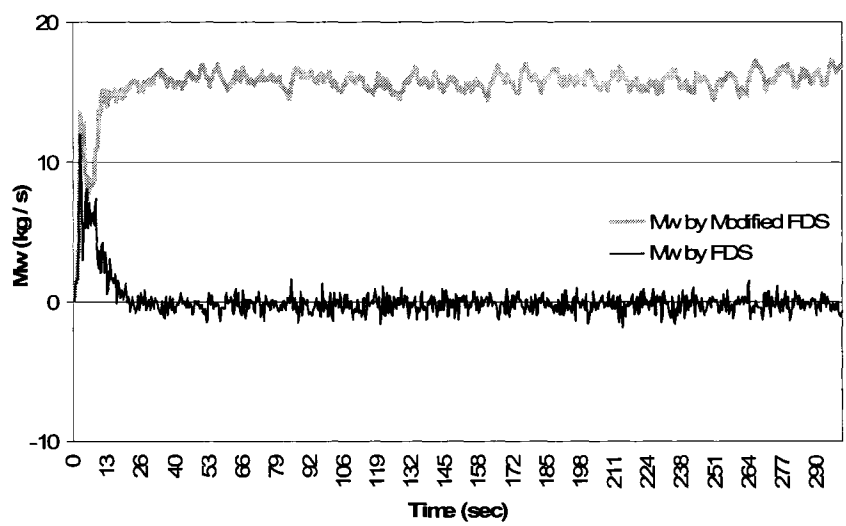

Figure 5.6 Comparison of calculations of mass flow rate between the modified FDS and the FDS model. (M_w from HRR = 4 MW, W = 5m)

The modified version of the program was validated by comparing the mass flow rate prediction to the mass flow rate calculated using temperature and velocity profiles. This modification enables the monitoring of the variation of mass flow rate with time. The modified code is given in Appendix A.

5.3.1.2 Planes of interest

The modified FDS program calculates the mass flow rate of smoke by integrating quantities over a specified plane.

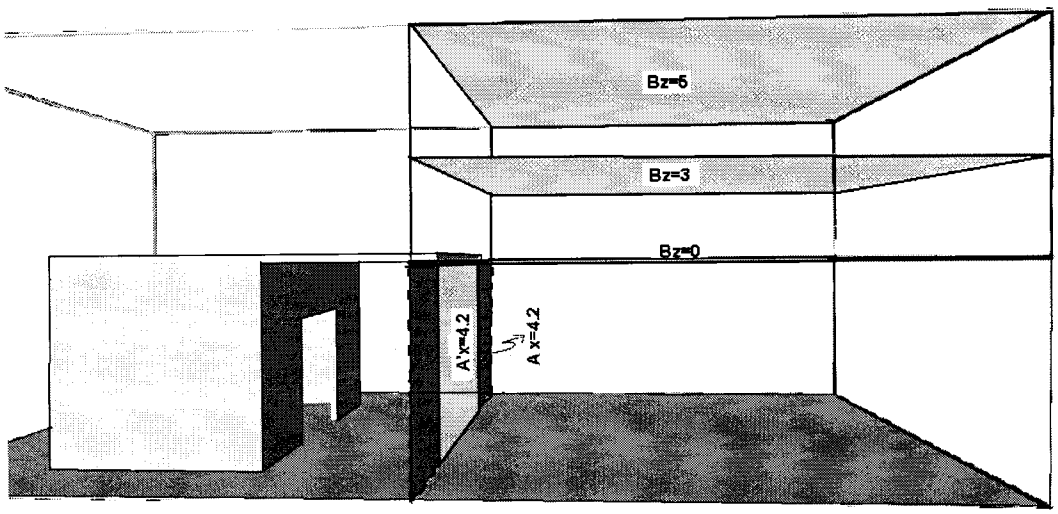

Figure 5.7 Definition of planes of interest to calculate mass flows

Figure 5.7 illustrates horizontal planes and vertical planes of interest that were used to calculate mass flow rates.

Mass flow rates of spill plumes were calculated taking into account any vertically moving gases through the defined planes 'B'. In that way, since the free spill

plumes are expected to move vertically through the B planes, any possible mass loss from the sides of the balcony is excluded, while fresh air entrainment into the free spill plumes is allowed.

The mass flow rate of the initial approach flow was calculated taking into account any horizontally moving gases through the planes defined as (A′), located under the balcony area. For example, for any unchanneled flows, the width of plane (A′) is the width of the balcony, while for channelled flows, the width of plane A' is the width of the opening. In addition, to detect any mass loss from the sides of the balcony, mass flows moving through a plane (A) were also monitored. The width of the plane A is the width of the computational domain.

5.3.2 Calculation of the layer depth

The layer depth at the end of the balcony was calculated from temperature profiles by integrating the temperature-height curve. The equation below is given by Thomas et al [1963].

$$D = \frac{\max T_b}{\max \Delta T_b} \int_0^{h_b} \frac{\Delta T_b}{T_b} dh \tag{5.1}$$

where
D = layer depth
h_b = the height of the balcony (5 m)
h = height above the floor
T_b = temperature of the flow at the end of the balcony
ΔT_b = temperature rise at the end of balcony

5.3.3 Error Analysis

There are various sources of error inherent in CFD modelling, due to the effects

of computational domain size and grid resolution, and fluctuations in mass flow rate measurements in the sampling period.

The simulated results are presented with a standard deviation which is calculated based on sample variations only. Therefore, the results represent the air entrainment rate more accurately than the actual amount of mass flow rate.

6 Full-scale Experiments: The Test Facility

For CFD validation purposes, full-scale experiments examining the area under the balcony have been conducted at the National Research Council as part of a research project on balcony spill plumes. Details of the experiments, the experimental facility, and the instrumentation are provided and discussed in the following sections.

6.1.1 Model geometry: Fire compartment

A fire compartment, shown in Figure 6.1, was constructed in the NRC Burn Hall. The dimensions of the fire compartment were 13.6 m (W) × 5.0 m (D) × 5.0 m (H).

Figure 6.1 Full-scale test facility at the NRC: the fire compartment

Figure 6.2 Fire simulation in the fire compartment

6.1.2 Fire simulation

A rectangular propane gas burner was placed at the center of the fire compartment, as shown in Figure 6.2. This fire source was used to provide a steady Heat Release Rate (HRR).

6.1.3 Instrumentation

The temperature and pressure were measured using thermocouples and pitot tubes respectively, and data were converted to temperature rise and velocity. A sketch of the instrumentation map in the area under the balcony is shown in Figure 6.3, and Figure 6.4 shows the detailed instrumentation map under the balcony area.

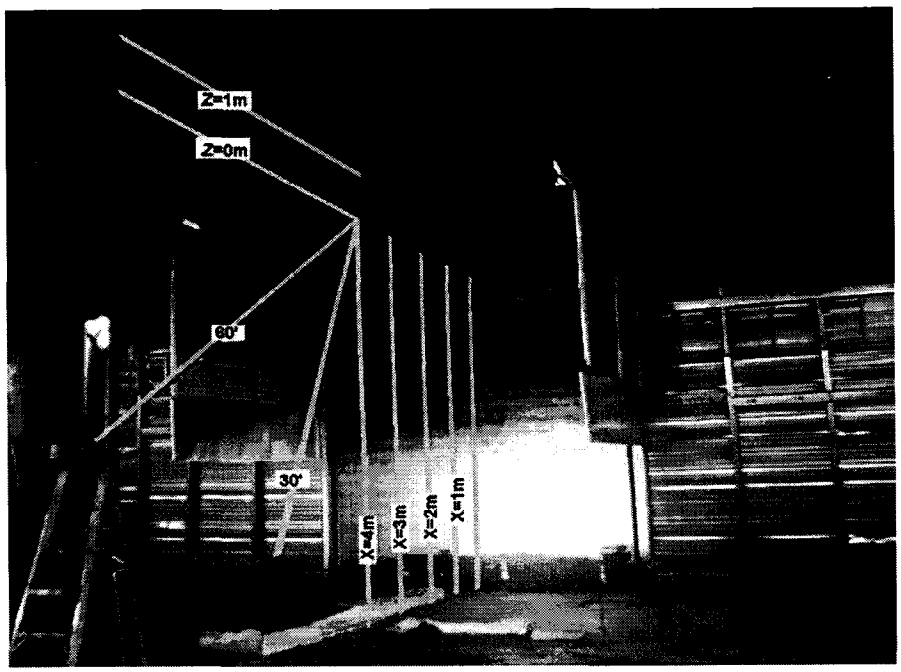

Figure 6.3 A sketch of locations of the instrumentaion trees

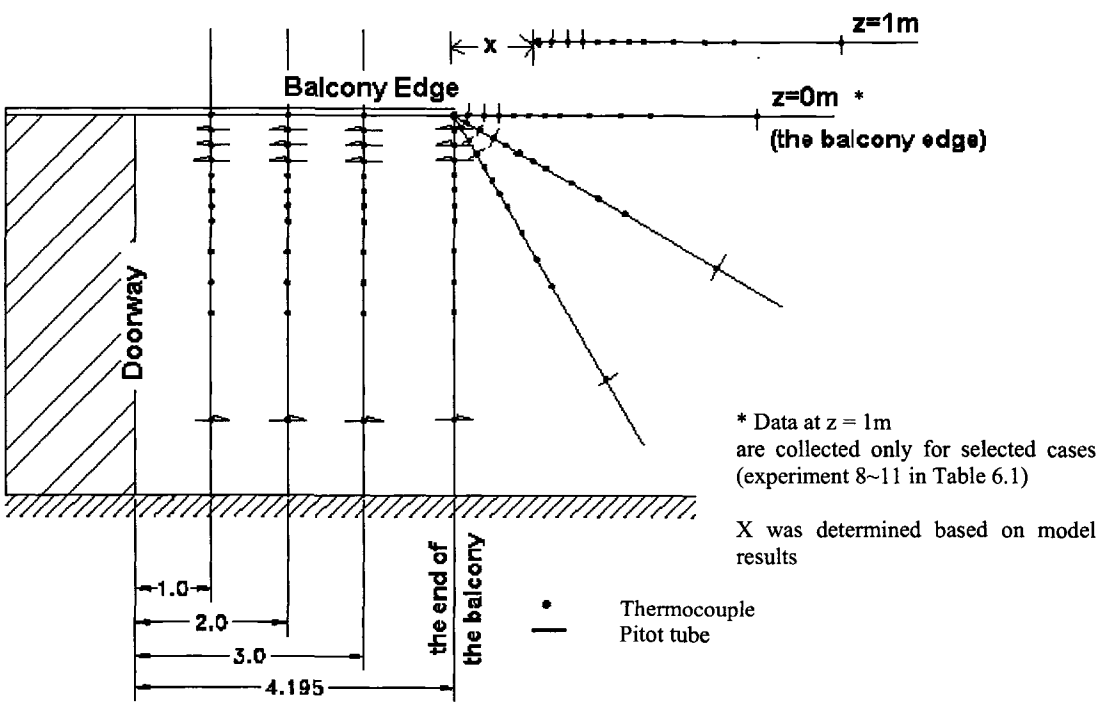

Figure 6.4 Side view of the instrumentation map under the balcony area

Figure 6.5 Side view of instrumentation tree at the balcony edge tilted through 90 degrees to the perpendicular

Figure 6.6 Tilting down the measuring tree

A moveable instrumentation tree containing thermocouples and pitot tubes was

built to obtain temperatures and velocities along a perpendicular line passing the middle of the balcony edge to the ground. This instrumentation tree, which could move along a railway underneath the balcony, collected temperature and velocity data at designated points. For measurements at the rotating region, the instrumentation tree was rotated upwards so that data could be collected at 30, 60 and 90 degrees angles to the perpendicular, as shown in Figure 6.5 and Figure 6.6.

6.1.4 The series of experiments

Table 6.1 shows the experiments conducted at the NRC. For experiments 8~11, data were collected only at z = 1m, which is 1 m above the balcony edge, and compared with CFD simulations 49~52 in Table 5.4.

Table 6.1 Experiments conducted at the NRC

Experiment	Test ID	Q(MW)	W(m)	Fascia	Draft Curtain
1	T1M5NY	1	5	N	Y
2	T3M5NY	3	5	N	Y
3	T1M5YY	1	5	Y	Y
4	T3M5YY	3	5	Y	Y
5	T5M5YY	5	5	Y	Y
6	T5M5NN	5	5	N	N
7	T5M5YN	5	5	Y	N
8	RT5M5NY	5	5	N	Y
9	RT5M5YY	5	5	Y	Y
10	RT5M5NN	5	5	N	N
11	RT5M5YN	5	5	Y	N

7 Results

In this chapter, the results from both CFD modelling and actual physical experiments are given. The results are presented in three parts:

1) The general flow behaviour observed with CFD modelling
2) CFD results compared with experimental data
3) CFD results of mass flow rates analyzed and compared with existing methods

7.1 General

7.1.1 Flow behaviour

The output from the FDS simulations is monitored by using the Smokeview 3.1, a visualization tool, developed by NIST.

7.1.1.1 Typical flow behaviour

Figure 7.1 and Figure 7.2 shows the typical behaviour of the balcony spill plume as it travels from a compartment into a large reservoir.

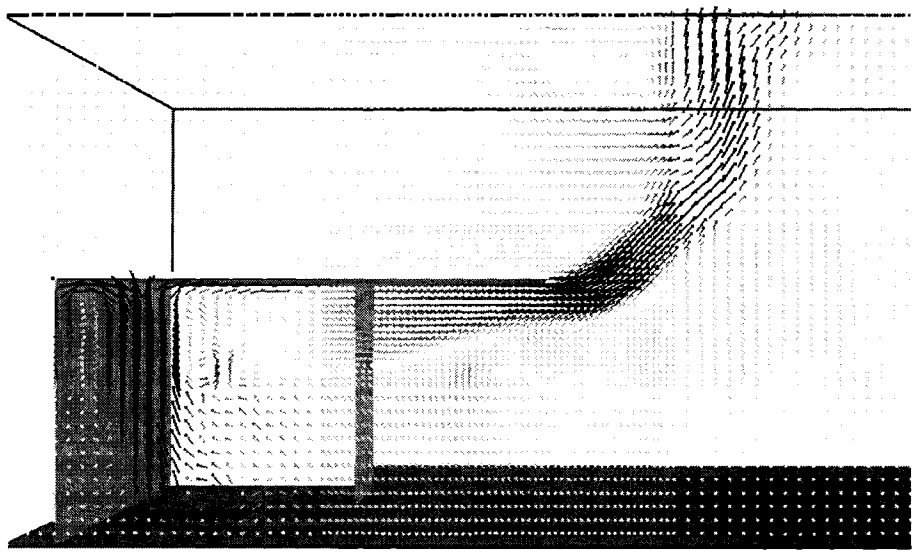

Figure 7.1 Velocity vectors of the flow under the balcony (from Simulation S2M75NN)

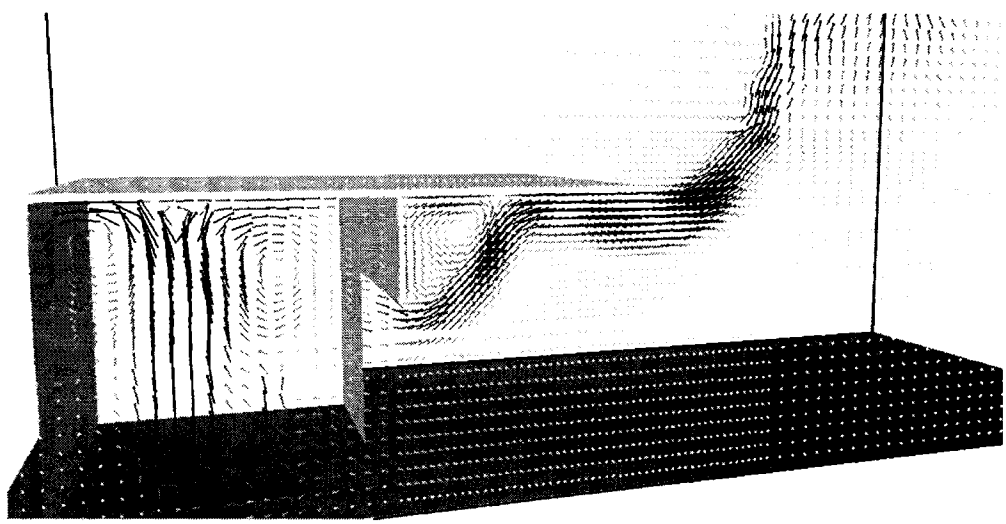

Figure 7.2 Velocity vector of the flow under the balcony S2M75YN

Figure 7.1 shows the velocity vectors obtained from simulation 'S2M75NN' . The ceiling jet in the fire compartment enters the area under the balcony through the opening and its horizontal velocity (U-Velocity) increases while flowing horizontally

under the balcony. The increased momentum of the flow affects the trajectory at the spill edge, which is similar to the result observed from the simple modelling study in Section 4.4.

Figure 7.2 shows the typical flow behaviour in the presence of fascia, obtained in simulation S2M75YN. The figure shows the detailed flow motion from the compartment opening to the spill edge. It can be seen that the door flow projects up beyond the opening and impinges on the underside of the balcony. At the edge of the balcony, the flow shows a buoyant jet behaviour. However, it was found that the emerging flow from the opening tends to circulate due to the fascia.

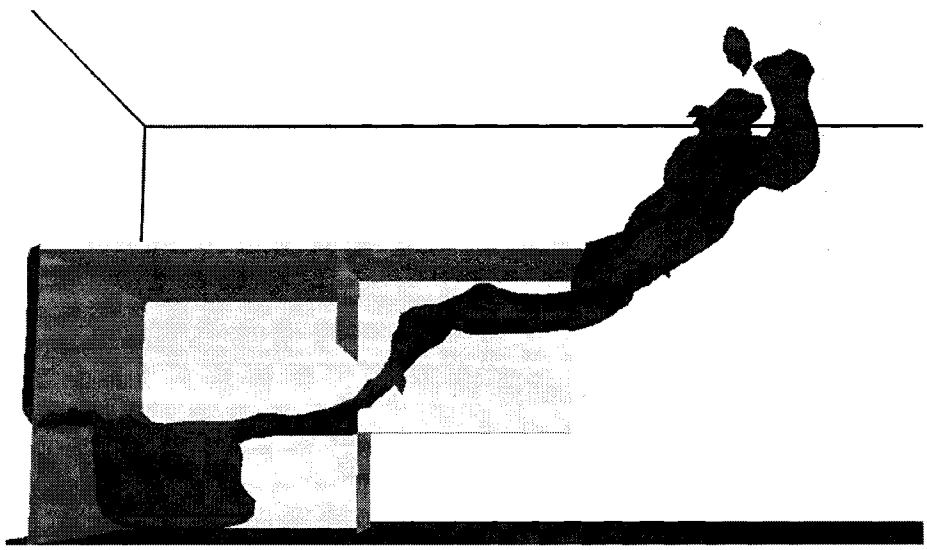

Figure 7.3 Flow behaviour for channelled flow with fascia and draft curtains (from simulation S2M75YY)

Figure 7.3 shows the behaviour of channelled gas flows in the presence of fascia, obtained from simulation S2M75YY.

7.1.1.2 Turbulent motion at the balcony area

Figure 7.4 shows velocity contours plotted on a vertical plane at the end of the

balcony and on a horizontal plane at z = 0m. As can be seen, the spill plume at the balcony edge undergoes extra upward movement in the ambient environment. This somewhat irregular, random flow motion is also observed in the horizontal flow under the balcony area.

This flow behaviour is a result of the effects of the balcony edge and yields a relatively high local value of mass flow rate under the balcony area as well as at the rotating region. Consequently, this finding casts doubt on the reliability of the spill plume correlation, $M_a \propto \left(Q_c L^2\right)^{1/3} z$, near the balcony [Morgan and Marshall. 1975].

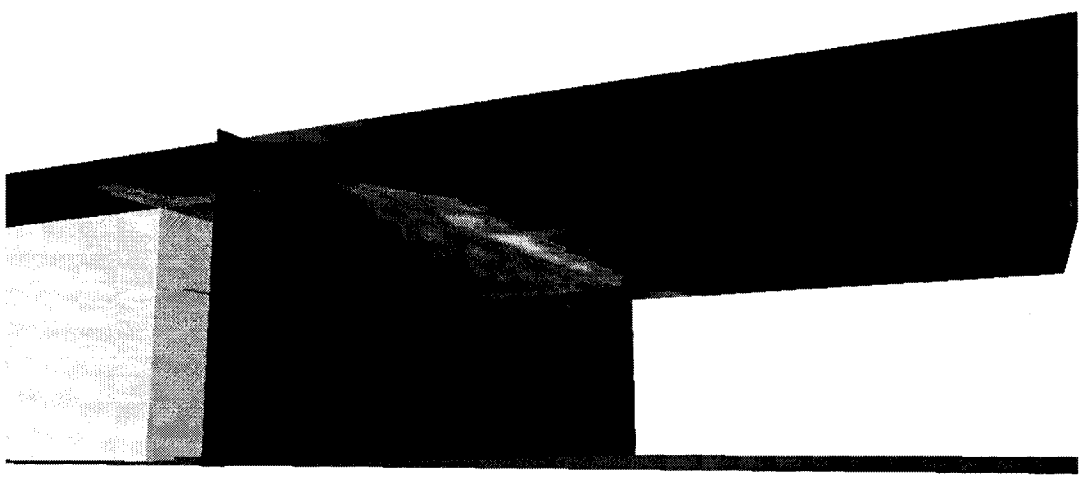

Figure 7.4 Turbulent motion in the balcony area

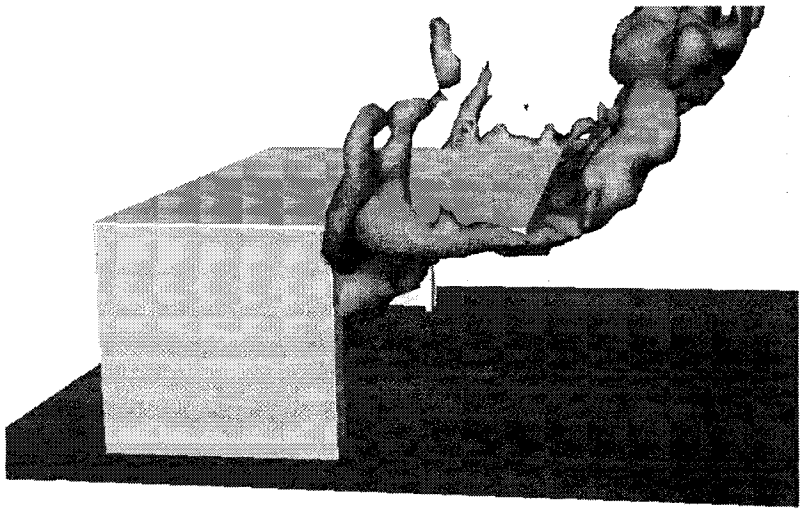

Figure 7.5 Mass loss through both sides of the balcony

7.1.1.3 Mass loss for unchanneled flows

An issue with the simulation for the area under the balcony without a draft curtain is that there is mass loss from both sides of the balcony (This is discussed in Section 5.3.1.2). Figure 7.5 and Figure 7.6 show that the flow out from the doorway spreads out to the sides of the balcony, in addition to moving into the reservoir.

Figure 7.7 shows velocity vectors on a vertical plane at the end of the balcony and at a horizontal plane (z = 2m), for simulation S1M75YN. In the simulation, mass flows from the sides of the balcony were ignored since they were dissipated into the large reservoir and assumed to be part of the ambient air. Mass flow rates under the balcony region as well as at the spill plume region were measured by taking into account only the flow through the planes of interests depicted in Figure 7.7.

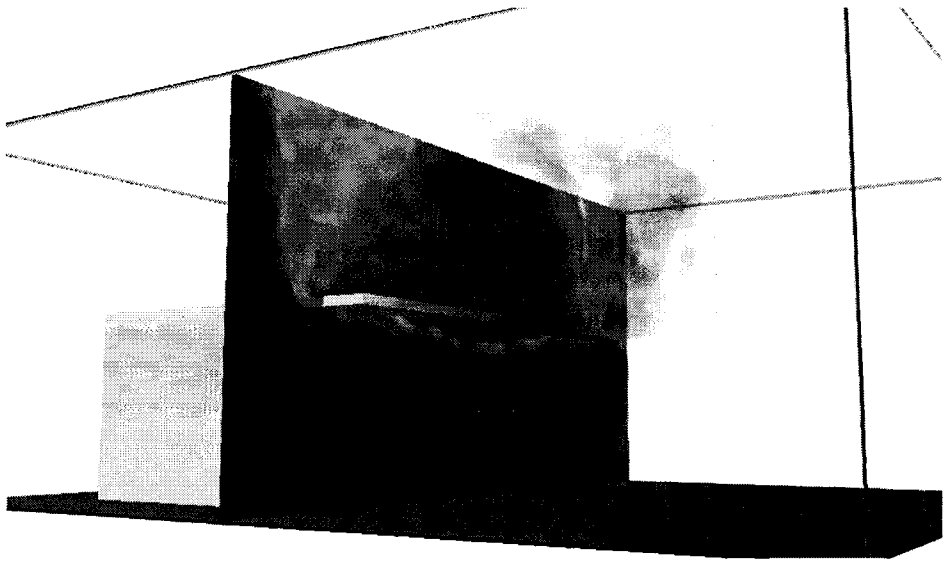

Figure 7.6 Mass loss observed for unchanneled flows (from simulation S3M75YN)

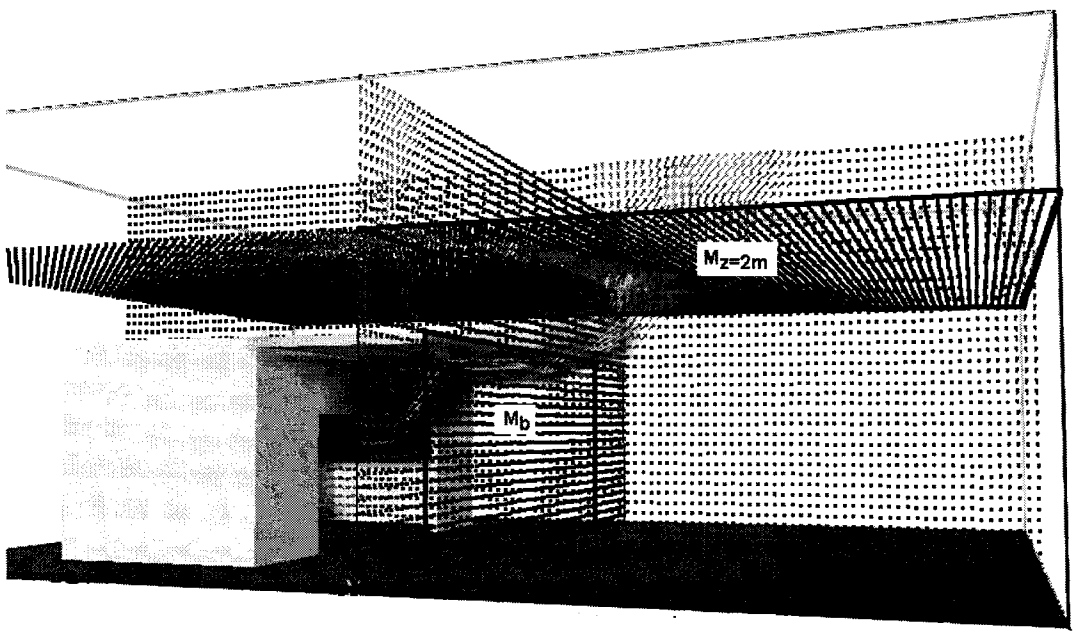

Figure 7.7 Mass loss observed in S1M75YN and areas to calculate the mass flow rate

7.1.2 The onset of steady-state conditions

Mass flow rates were monitored at four selected planes: one across the compartment opening, one at the end of the balcony, another at the edge of the balcony,

and a horizontal plane at a height of 9 m from the floor (the height of rise, z = 4m).

Figure 7.8 and Figure 7.9 show the mass flow rate as a function of time for simulation S4M5NY and S1M12NY respectively. For simulation S4M5NY, the mass flow rate at all four monitored planes is steady after about 60 seconds. For most simulations, steady-state is reached rapidly, as a steady heat release rate was used from the beginning.

Time-averaged data between 200 seconds and 300 seconds is used for data analysis, except for special cases, in which the onset of steady-state is delayed.

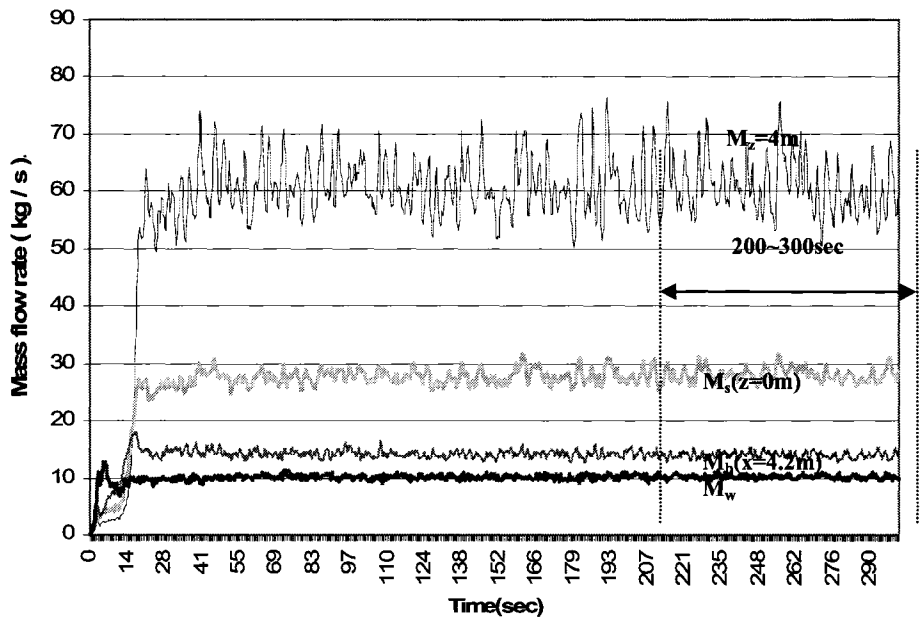

Figure 7.8 Mass flow rate over time (Simulation S4M5NY)

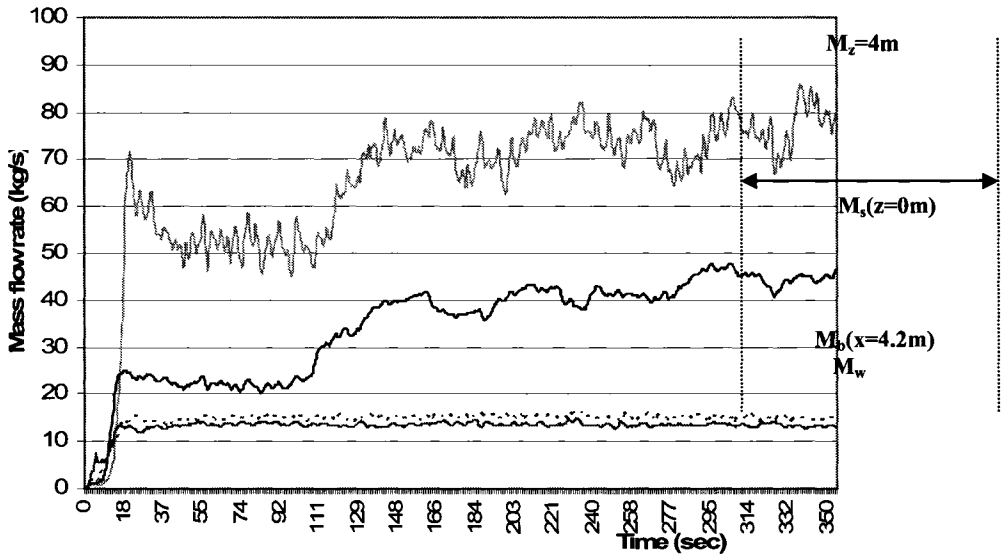

Figure 7.9 Mass flow rate over time (Simulation-S1M12NY)

Figure 7.9 shows the mass flow rate as a function of time for simulation S1M12NY. In this simulation, the mass flow rate shows an initial steady behaviour followed by increase after 130 seconds (for z = 4 m and z = 0 m only). The reason for this behaviour could not be identified. Therefore, for cases with a small fire size and a wide opening, the mass flow rate was carefully monitored, and the results were averaged after the time when steady-state was reached.

7.2 Comparison of FDS results with experimental results

The time-averaged mean values of temperature and velocity were obtained from both FDS modelling and actual experiments. In order to verify the validity of the FDS modelling results, the simulated predictions were compared with experimental data. Figure 7.10 shows the planes where temperature and velocity profiles were obtained (at the end of the balcony and at the balcony edge, as well as 1 m above the balcony (z = 1m)

for selected cases).

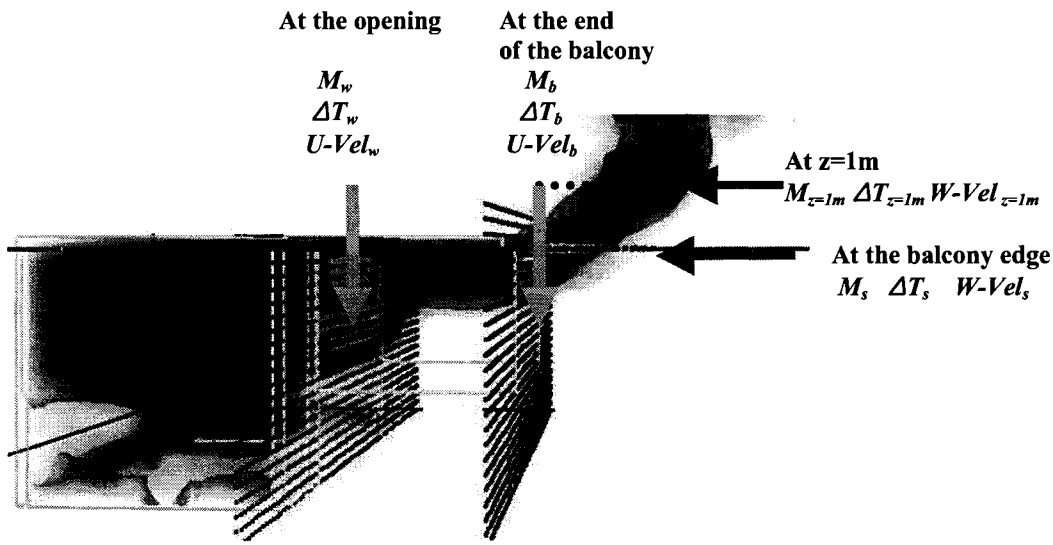

Figure 7.10 Temperature and velocity measurements at the opening, at the end of the balcony and at the balcony edge

7.2.1.1 Temperature and velocity profiles at the doorway

Figure 7.11 shows the temperature profiles at the doorway from simulation-S3M5YY and experiment T3M5YY. Since in the experiment, velocities and temperatures were measured at positions 1 m away from the doorway to the end of the balcony (Figure 6.4), the comparison between the simulated and experimentally obtained results was made initially at x = 1 m instead of at the opening. As shown in the figure, for a given height, FDS predicts a smaller temperature rise than is actually measured experimentally. FDS under predicts the maximum temperature rise of the flow, for all experiments used for comparison. As discussed in Section 5.1.2, this is partially due to definition of the boundary condition of the room and the burner.

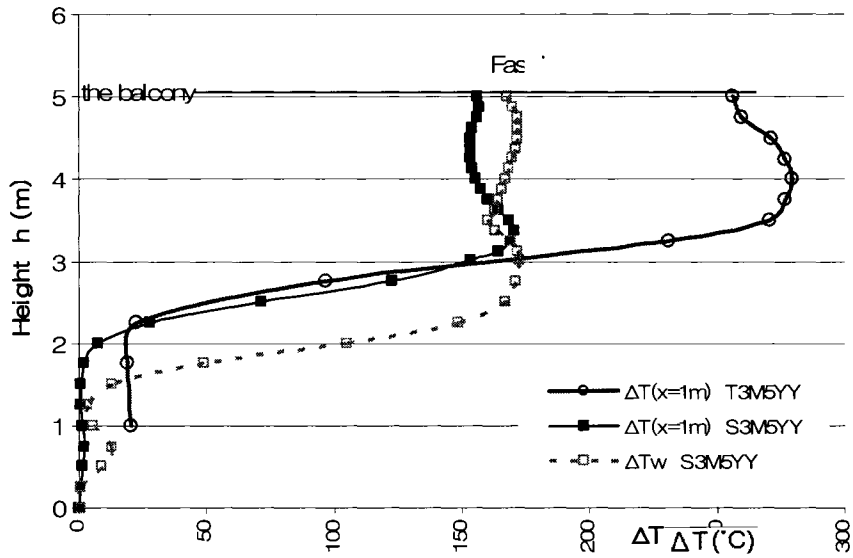

Figure 7.11 Temperature rise profiles at the opening (S3M5YY and T3M5YY)

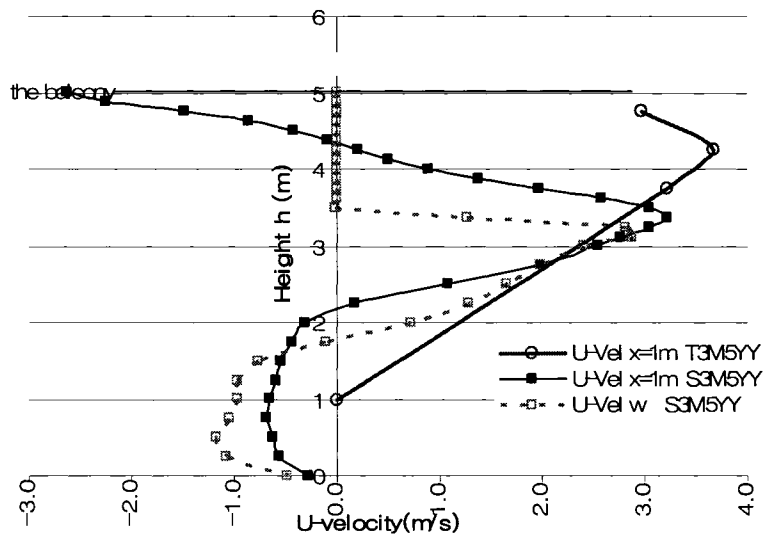

Figure 7.12 U-Velocity profiles at the compartment opening (S3M5YY and T3M5YY)

Figure 7.12 shows U-Velocity profiles near the opening. Through the lower part of the opening, counter flow is observed with negative velocities. In general, velocity profiles at x = 1 m from both FDS and experiments result in similar patterns of velocity profiles.

7.2.1.2 Temperature and velocity profiles at the end of the balcony

Figure 7.13 and Figure 7.14 show temperature rise and velocity profiles at the balcony end.

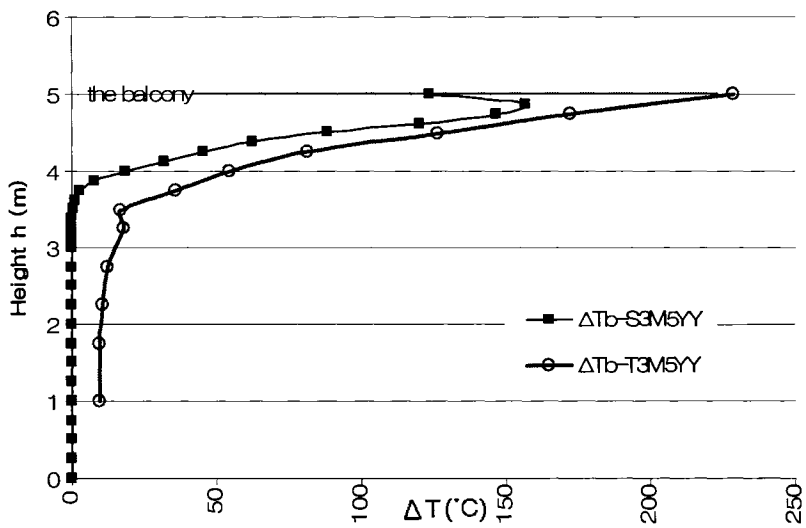

Figure 7.13 Temperature rise profile at the balcony end (S3M5YY and T3M5YY)

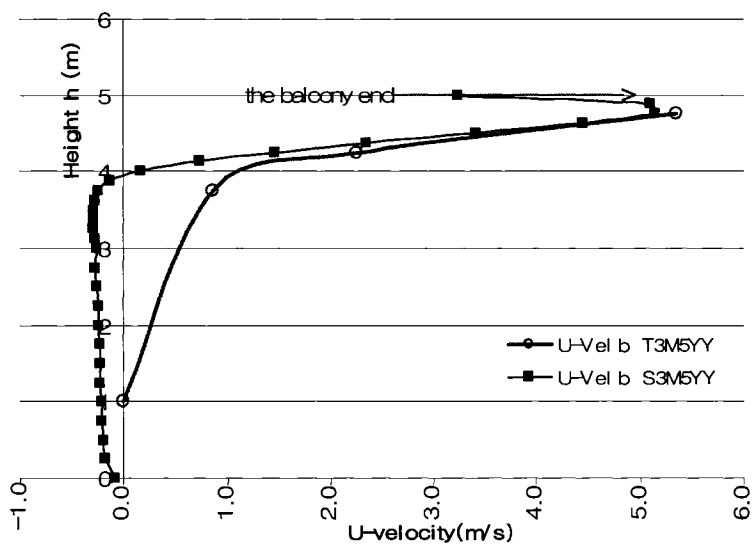

Figure 7.14 U-Velocity profile at the balcony end (S3M5YY and T3M5YY)

There is very good agreement between the modelled profile and the experimentally determined profile for the temperature rise, a similar result being found

for the velocity profile. This indicates that FDS modelling accurately predicts the flow characteristics of the approach flow at the end of the balcony. The layer depth from FDS modelling velocity profiles agrees well with the experimental measurement.

7.2.1.3 Temperature and velocity profiles at the balcony edge

Figure 7.15 and Figure 7.16 show comparisons between the FDS prediction and the experimental data for the temperature rise profile and the velocity profile of the horizontal gas flow at the spill edge (at z = 0m). 'X' represents the distance to the opening, so the origin on the x-axis is set at 4m, which is the edge of the balcony.

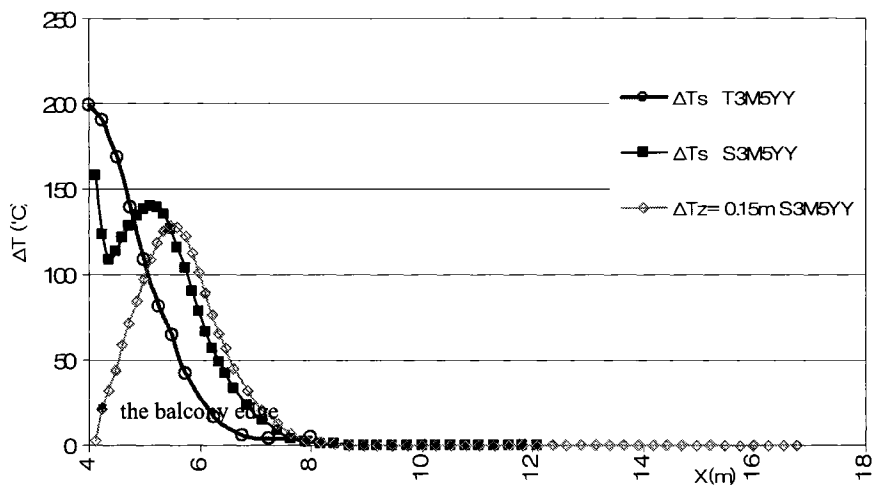

Figure 7.15 Temperature rise profile at the balcony edge (S3M5YY and T3M5YY)

Figure 7.15 shows that the predicted profile of ΔT_s at z = 0 m has two peaks, however, ΔT at z = 0.15 m has a single peak consistent with the experimented data. The two peaks are probably caused by the transition turbulence.

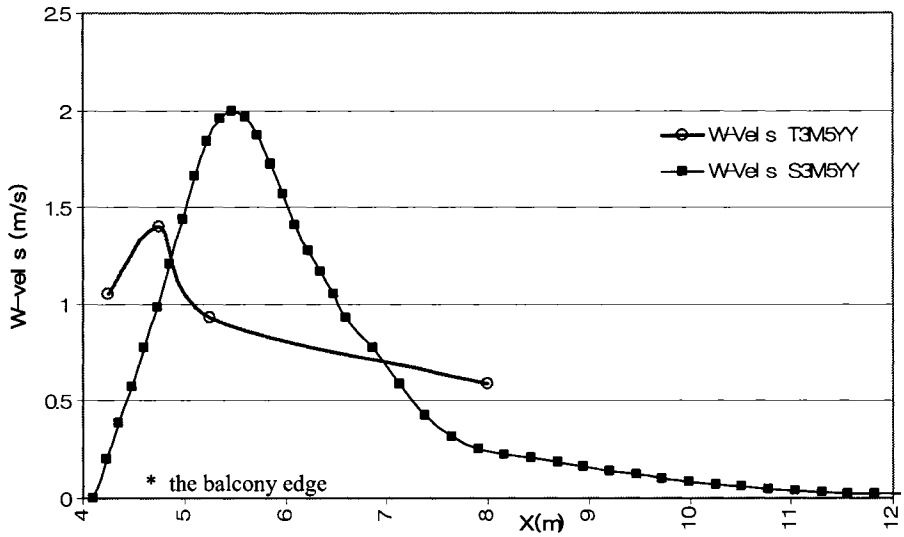

Figure 7.16 W-Velocity profile of the vertical spill plume at the balcony edge (z = 0m)

While the FDS simulation predicts a lower maximum temperature rise at the spill edge, FDS overestimates the maximum W-Velocity values in this region, shown in Figure 7.16. Pitot tube measurements, however, were too sparse to satisfactorily monitor the whole velocity profile and to capture the maximum velocity.

7.2.1.4 Temperature and velocity profile 1 m above the balcony

Figure 7.17 and Figure 7.18 show the temperature rise and velocity profiles respectively, at points 1 m above the balcony and at points with varying distance from the doorway, obtained from simulation R5M5YY and experiment RT5M5YY. The figures show that the FDS simulation under predicts the maximum temperature rise and the maximum W-Velocity compared to those found in actual experiments; however, similar shapes of profiles are obtained.

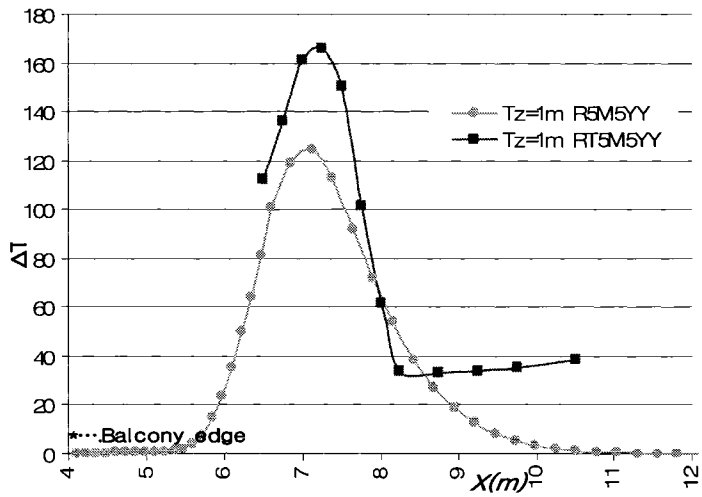

Figure 7.17 Temperature rise profile at z = 1 m (R5M5YY and RT5M5YY)

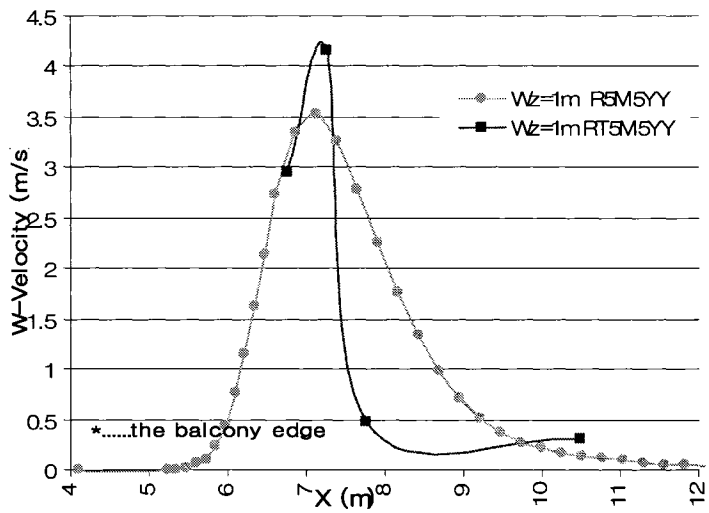

Figure 7.18 W-Velocity profile at z = 1 m (R5M5YY and RT5M5YY)

7.2.1.5 Discussion

The comparisons between prediction of FDS and the experimental data show good agreement. For the majority of cases, the simulated maximum temperature and velocity values were 10~20% lower than the experimental data. Considering the

uncertainties in the experimental data and discrepancies of the domain boundaries, these variations can be considered reasonable. In general, there was good agreement between the FDS prediction and the experimental data for all comparisons. All of the comparisons between the FDS prediction and the experimental results are given in Appendix C.

The agreement between the model results and experimental results gave confidence in using mass flow rates generated by FDS to develop an empirical correlation to predict the mass flow rate at the spill edge. FDS–generated mass flow rates are further studied in the next section.

7.3 Mass flow rate results

7.3.1 Summary of the results from CFD modelling

The time-averaged mass flow rates were calculated every 1 m interval over the flow path after the onset of steady-state. A summary of results is given in Table 7-1. Mass flow rates measured at the doorway, at the end of the balcony, at the balcony edge, and at a point 4 m away from the doorway (z = 4m) are given in columns (6), (9), (10), and (11) respectively in Table 7-1. The standard deviation of the mean value of the mass flow rate was associated and was calculated based on sample variations, by using a function in the EXCEL spreadsheet. The air entrainment rates under the balcony (M_b/ M_w) and at the rotating region (M_s/ M_b) are presented in column (12) and (13) respectively.

In addition, the total heat release rate and the opening width are shown in

column (3) and (5) respectively. Column (4) is the convective heat release rate from the FDS analysis, which is used as one of the factors governing spill plume. The maximum temperature rise and the layer depth of the initial approach flow at the end of the balcony are also given in columns (7) and (8) respectively.

Table 7.1 Summary of results from CFD modelling (a)

(1) NO	(2) ID	(3) Q(MW)	(4) Q_c(kW)	(5) W(m)	(6) M_w (kg/s)			(7) $\Delta T_{b\,max}$	(8) D_b (m)
1	S1M5NN	1	532	5	9.37	+/-	0.21	58.91	0.99
2	S2M5NN	2	1088	5	11.05	+/-	0.36	103.86	1.08
3	S3M5NN	3	1665	5	14.67	+/-	0.46	117.88	1.29
4	S4M5NN	4	2244	5	15.64	+/-	0.60	150.74	1.29
5	S1M75NN	1	573	7.5	11.21	+/-	0.20	55.29	1.32
6	S2M75NN	2	1124	7.5	12.68	+/-	0.30	96.84	1.26
7	S3M75NN	3	1689	7.5	16.82	+/-	0.44	110.51	1.33
8	S4M75NN	4	2292	7.5	17.42	+/-	0.49	142.59	1.32
9	S1M12NN	1	593	12	14.27	+/-	0.33	44.15	1.12
10	S2M12NN	2	1164	12	15.53	+/-	0.43	75.03	1.07
11	S3M12NN	3	1773	12	21.94	+/-	0.46	83.18	1.43
12	S4M12NN	4	2400	12	22.78	+/-	0.65	107.23	1.41
13	S1M5YN	1	462	5	6.60	+/-	0.13	59.32	0.73
14	S2M5YN	2	928	5	7.66	+/-	0.24	104.33	0.80
15	S3M5YN	3	1443	5	9.72	+/-	0.26	157.17	0.94
16	S4M5YN	4	1888	5	10.16	+/-	0.40	195.76	0.97
17	S1M75YN	1	506.6	7.5	7.93	+/-	0.20	53.95	1.08
18	S2M75YN	2	964	7.5	8.67	+/-	0.24	96.21	1.26
19	S3M75YN	3	1527	7.5	11.37	+/-	0.35	106.89	1.33
20	S4M75YN	4	2004	7.5	11.53	+/-	0.34	141.31	1.09
21	S1M12YN	1	535	12	9.89	+/-	0.27	44.96	1.05
22	S2M12YN	2	1028	12	10.47	+/-	0.32	76.37	1.07
23	S3M12YN	3	1638	12	14.97	+/-	0.36	84.12	1.28
24	S4M12YN	4	2136	12	14.98	+/-	0.49	109.14	1.25
25	S1M5NY	1	538	5	9.56	+/-	0.21	67.17	1.27
26	S2M5NY	2	1096	5	11.01	+/-	0.33	114.19	1.31
27	S3M5NY	3	1455	5	9.69	+/-	0.27	147.24	1.05
28	S4M5NY	4	1904	5	10.22	+/-	0.36	184.22	1.09
29	S1M75NY	1	576	7.5	11.20	+/-	0.31	63.34	1.48
30	S2M75NY	2	1132	7.5	12.62	+/-	0.31	96.84	1.30
31	S3M75NY	3	1695	7.5	16.93	+/-	0.49	110.51	1.52
32	S4M75NY	4	2280	7.5	17.41	+/-	0.55	169.95	1.51
33	S1M12NY	1	590	12	13.60	+/-	0.36	44.17	1.13
34	S2M12NY	2	1156	12	15.19	+/-	0.50	75.03	1.08
35	S3M12NY	3	1770	12	21.65	+/-	0.52	98.14	1.49
36	S4M12NY	4	2360	12	22.07	+/-	0.68	124.25	1.48
37	S1M5YY	1	472	5	6.70	+/-	0.14	71.25	0.86
38	S2M5YY	2	934	5	7.65	+/-	0.33	124.41	0.93
39	S3M5YY	3	1461	5	9.70	+/-	0.26	156.73	1.05
40	S4M5YY	4	1912	5	10.19	+/-	0.36	197.15	1.09
41	S1M75YY	1	510	7.5	7.94	+/-	0.22	64.70	1.18
42	S2M75YY	2	968	7.5	8.78	+/-	0.28	109.73	1.05
43	S3M75YY	3	1539	7.5	11.50	+/-	0.32	138.77	1.10
44	S4M75YY	4	2020	7.5	11.71	+/-	0.40	174.78	1.14
45	S1M12YY	1	536	12	9.82	+/-	0.24	45.77	0.98
46	S2M12YY	2	1012	12	10.33	+/-	0.37	78.46	0.99
47	S3M12YY	3	1635	12	15.31	+/-	0.41	102.22	1.27
48	S4M12YY	4	2116	12	15.08	+/-	0.43	124.20	1.23
49	R5M5NN	5	2805	5	16.07	+/-	0.70	182.99	1.30
50	R5M5YN	5	2300	5	15.07	+/-	0.49	196.03	0.99
51	R5M5NY	5	2770	5	10.44	+/-	0.69	215.98	1.47
52	R5M5YY	5	2300	5	10.45	+/-	0.47	228.14	1.12

Table 7.1 Summary of results from CFD modelling (b)

NO	(9) M_b(kg/s)			(10) M_s(kg/s)			(11) $M_{z=A}$(kg/s)			(12) M_b/M_w	(13) M_s/M_b
1	11.62	+/-	0.61	24.04	+/-	0.90	66.20	+/-	2.94	1.24	2.07
2	13.77	+/-	0.69	30.25	+/-	1.43	81.46	+/-	3.89	1.25	2.20
3	18.35	+/-	1.15	40.13	+/-	2.11	105.14	+/-	4.88	1.25	2.19
4	19.53	+/-	1.04	44.44	+/-	1.81	116.14	+/-	6.21	1.25	2.28
5	13.24	+/-	0.90	34.86	+/-	1.81	79.28	+/-	3.70	1.18	2.63
6	15.10	+/-	0.88	37.81	+/-	1.84	89.80	+/-	3.58	1.19	2.50
7	19.69	+/-	0.85	40.24	+/-	1.74	103.70	+/-	5.27	1.17	2.04
8	20.62	+/-	0.97	43.60	+/-	2.18	113.73	+/-	5.33	1.18	2.11
9	15.53	+/-	0.71	41.67	+/-	1.25	81.34	+/-	3.75	1.09	2.68
10	15.88	+/-	0.81	39.99	+/-	2.11	92.76	+/-	4.09	1.02	2.52
11	23.28	+/-	2.36	50.24	+/-	3.31	115.91	+/-	6.18	1.06	2.16
12	23.80	+/-	1.23	49.27	+/-	2.46	121.00	+/-	5.71	1.04	2.07
13	9.81	+/-	0.70	22.15	+/-	1.34	63.63	+/-	2.99	1.49	2.26
14	11.82	+/-	0.86	27.56	+/-	1.03	80.04	+/-	3.67	1.54	2.33
15	14.40	+/-	0.83	35.81	+/-	1.89	97.41	+/-	4.15	1.48	2.49
16	15.22	+/-	0.88	38.07	+/-	1.56	104.06	+/-	4.36	1.50	2.50
17	12.32	+/-	0.72	32.96	+/-	1.88	74.59	+/-	3.35	1.55	2.68
18	12.86	+/-	0.59	29.49	+/-	1.96	82.27	+/-	3.32	1.48	2.29
19	17.19	+/-	1.21	37.57	+/-	1.73	99.53	+/-	4.05	1.51	2.19
20	17.96	+/-	1.09	39.65	+/-	1.66	109.50	+/-	4.75	1.56	2.21
21	14.40	+/-	0.96	42.43	+/-	2.30	77.09	+/-	4.06	1.46	2.95
22	15.55	+/-	0.81	41.68	+/-	2.67	87.13	+/-	4.69	1.49	2.68
23	19.97	+/-	1.04	44.86	+/-	1.85	101.18	+/-	5.09	1.33	2.25
24	20.91	+/-	1.61	47.13	+/-	2.06	109.52	+/-	5.71	1.40	2.25
25	10.94	+/-	0.39	17.81	+/-	0.70	35.71	+/-	2.72	1.14	1.63
26	12.66	+/-	0.49	21.33	+/-	0.86	43.40	+/-	3.36	1.15	1.68
27	13.63	+/-	0.73	26.13	+/-	1.34	56.08	+/-	4.18	1.41	1.92
28	14.08	+/-	0.62	28.10	+/-	1.24	60.90	+/-	4.91	1.38	2.00
29	12.87	+/-	0.82	34.18	+/-	1.97	61.20	+/-	3.18	1.15	2.66
30	14.21	+/-	0.63	33.08	+/-	1.22	68.11	+/-	3.87	1.13	2.33
31	19.20	+/-	0.73	32.26	+/-	1.38	67.71	+/-	5.07	1.13	1.68
32	19.87	+/-	0.68	34.66	+/-	1.45	71.78	+/-	5.51	1.14	1.74
33	15.19	+/-	0.58	42.08	+/-	2.16	73.89	+/-	3.84	1.12	2.77
34	17.11	+/-	0.85	42.91	+/-	2.30	81.06	+/-	4.16	1.13	2.51
35	24.58	+/-	0.83	49.97	+/-	1.61	103.10	+/-	4.70	1.14	2.03
36	24.99	+/-	1.21	47.46	+/-	2.58	104.18	+/-	4.91	1.13	1.90
37	9.47	+/-	0.42	18.14	+/-	0.77	38.28	+/-	2.98	1.41	1.92
38	11.00	+/-	0.57	22.14	+/-	0.96	46.98	+/-	3.10	1.44	2.01
39	13.60	+/-	0.71	25.99	+/-	1.20	55.71	+/-	4.04	1.40	1.91
40	14.06	+/-	0.62	28.00	+/-	1.24	61.10	+/-	4.91	1.38	1.99
41	11.81	+/-	1.09	32.21	+/-	2.42	62.85	+/-	2.62	1.49	2.73
42	13.20	+/-	0.90	27.08	+/-	2.23	55.82	+/-	3.73	1.50	2.05
43	17.73	+/-	0.99	33.42	+/-	1.47	69.16	+/-	4.49	1.54	1.88
44	18.57	+/-	1.33	35.11	+/-	1.86	75.17	+/-	5.09	1.59	1.89
45	14.98	+/-	0.92	41.64	+/-	2.27	73.23	+/-	3.69	1.53	2.78
46	16.84	+/-	0.79	41.52	+/-	1.91	81.33	+/-	3.62	1.63	2.47
47	22.71	+/-	1.16	47.67	+/-	1.74	97.39	+/-	4.76	1.48	2.10
48	22.95	+/-	1.15	47.29	+/-	2.01	93.69	+/-	5.77	1.52	2.06
49	20.18	+/-	1.05	46.83	+/-	2.02	125.29	+/-	6.03	1.26	2.32
50	17.16	+/-	1.04	31.22	+/-	2.19	62.40	+/-	4.99	1.14	1.82
51	14.50	+/-	0.72	29.85	+/-	1.66	64.22	+/-	4.82	1.39	2.06
52	15.86	+/-	0.72	41.06	+/-	1.47	112.27	+/-	5.18	1.52	2.59

7.3.2 Mass flow rates over the flow path

For selected cases, results are presented in graphical form to enable visualization of mass flow rate increments over the flow path, and to compare the impact of various parameters on mass flow rates. Figure 7.19 and Figure 7.20 show the mass flow rate results over the flow path of the simulations with a 3 MW HRR and a 7.5 m opening size; and a 4 MW HRR and 12 m opening size, respectively. The mass flow rate M_w is the flow rate at the door of the compartment, and the mass flow rate at $UB_{X=4}$ is the mass flow rate at the end of the balcony. The mass flow rate at z = 0 is the vertical flow rate on the same plane as the balcony edge.

Under the balcony area, mass flow rates of unchanneled flows were shown in two cases. For instance, S3M75NN and S3M75YN in Figure 7.19 have a dotted line and a solid line to present the mass flow rate under the balcony. The dotted line shows the mass flow rate through a vertical plane A in Figure 5.7, which covers the whole width of the computational domain. The solid line shows the flow rate through a vertical plane A' in Figure 5.7, with a width equal to the balcony width. The differences between these two curves represent mass loss at the sides of the balcony. This mass loss was excluded in mass flow rate calculations and the mass flow rate presented by the solid line is used for further analysis.

Overall, for all parameter conditions, vertical spill plumes in the reservoir entrain more air than horizontal flows under the balcony. The mass flow rate of the vertical flow in the reservoir exhibits a linear behaviour with respect to height. At the top of the modelling domain, boundary effects interfere with the linear relation, so these data

were not used in the analysis.

The results show that mass flow rates depend on parameter conditions, whether draft curtains and fascia are present or not. In general, for the same size of fire source and door width, the absence of draft curtains results in greater entrainment, while the presence of fascia appears to have little impact on entrainment rates.

The mass flow rate variation due to draft curtains is found to be less significant in cases with wider openings since the ratio of the balcony width to the opening width (l_b/W) is relatively small. As shown in Figure 7.20, in those cases with an opening of width 12m, the layer width (L) in the absence of draft curtains (S4M12NN and S4M12YN) is not much greater than that in the presence of draft curtains (S4M12NY and S4M12YY), since the layer of flow spreads beyond the width of balcony. This indicates that the width of the spill plume layer (L) is the key factor governing entrainment of line plumes.

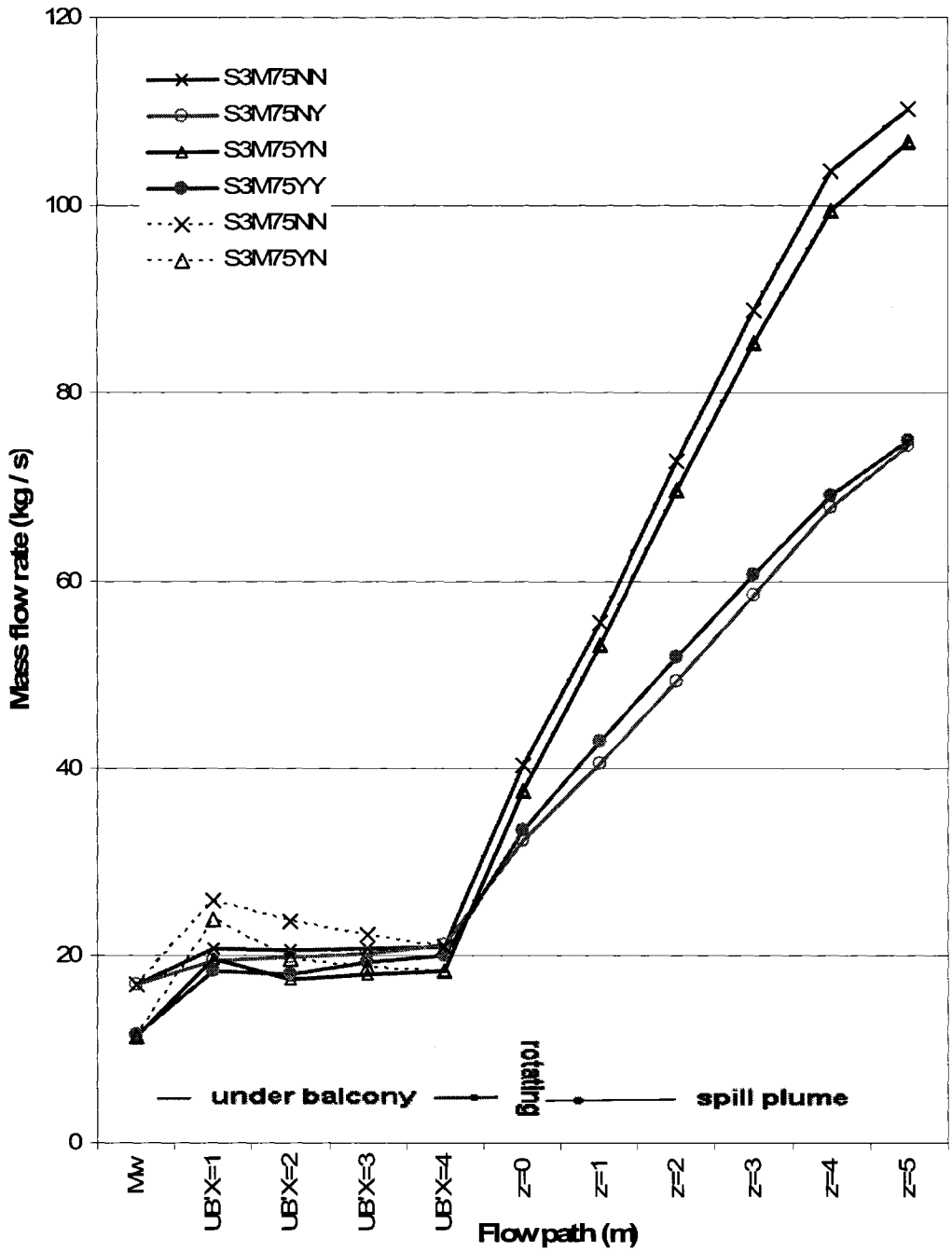

Figure 7.19 Mass flow rates over the flow path (Q = 3 MW, W = 7.5m)

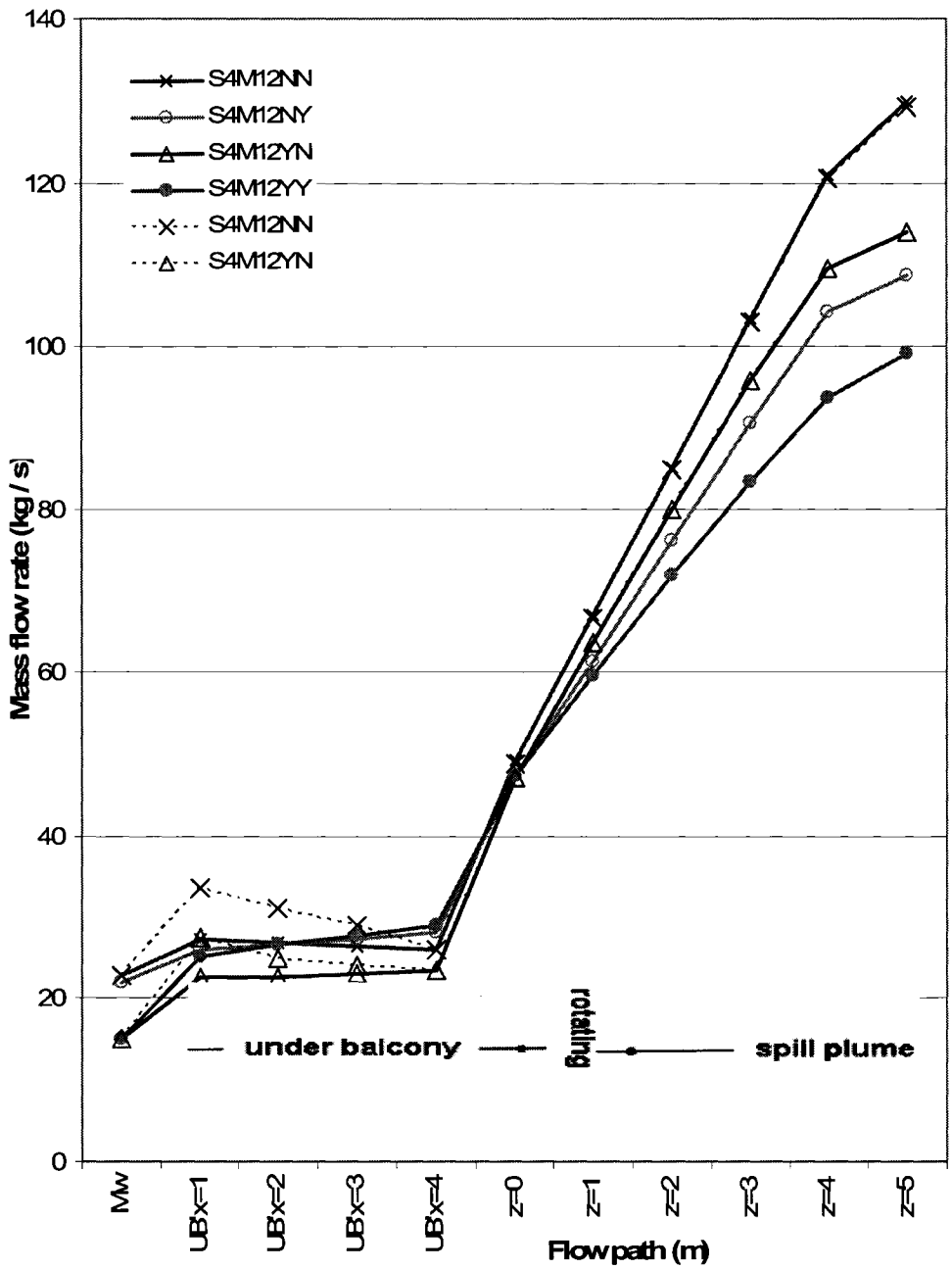

Figure 7.20 Mass flow rate over the flow path (Q = 4 MW, W = 12m)

7.4 Initial analysis of results

Observations and initial analysis of air entrainment rates over the entire flow path from the compartment opening to the top of the atrium have been made in order to:

1) understand overall behaviour of the flow
2) find the limiting height of rise under which the spill plume formula is not valid (to clarify the area of interest in this study), and
3) compare simulated results with the existing methods used to estimate the air entrainment at the rotating region.

7.4.1 Overview of the mass flow rate of the balcony spill plume

Figure 7.21 shows mass flow rates normalized to the mass flow rate at the doorway, every 1 m interval from the opening to the top of the atrium.

Mass flow rates were studied in four regions:

1) Door flow

At the doorway, there is mass gain if the flow is disturbed by fascia or the flow from the fire compartment opening experiences a sudden expansion in the absence of a channelling draft curtain.

2) Flow under balcony

As Figure 7.21 shows, the flow under the balcony does not entrain a great amount of air compared to the vertical spill plume in the large reservoir. The flow under the balcony does not mix with a lot of air when draft curtains are present because the curtains contain the flow. There is linear growth of mass flow for channelled flows under

the balcony, and a decrease for flows without draft curtain. This decrease is due to mass loss at the sides of the balcony. The general pattern of flow under the balcony shows more or less similar mass flow rates throughout the horizontal path.

3) Rotating flow

At the end of the balcony, the flow starts to rotate, as it changes from a horizontal flow to a vertical flow. This rotation entrains a significant amount of air (indicated by the rapid rise in the mass flow rate).

4) Spill plume

The mass flow rate of the vertical flow in the large reservoir exhibits a linear relationship with height. At the top of the computational domain, a boundary effect interferes with the linear relation, so this data will be excluded from further analysis.

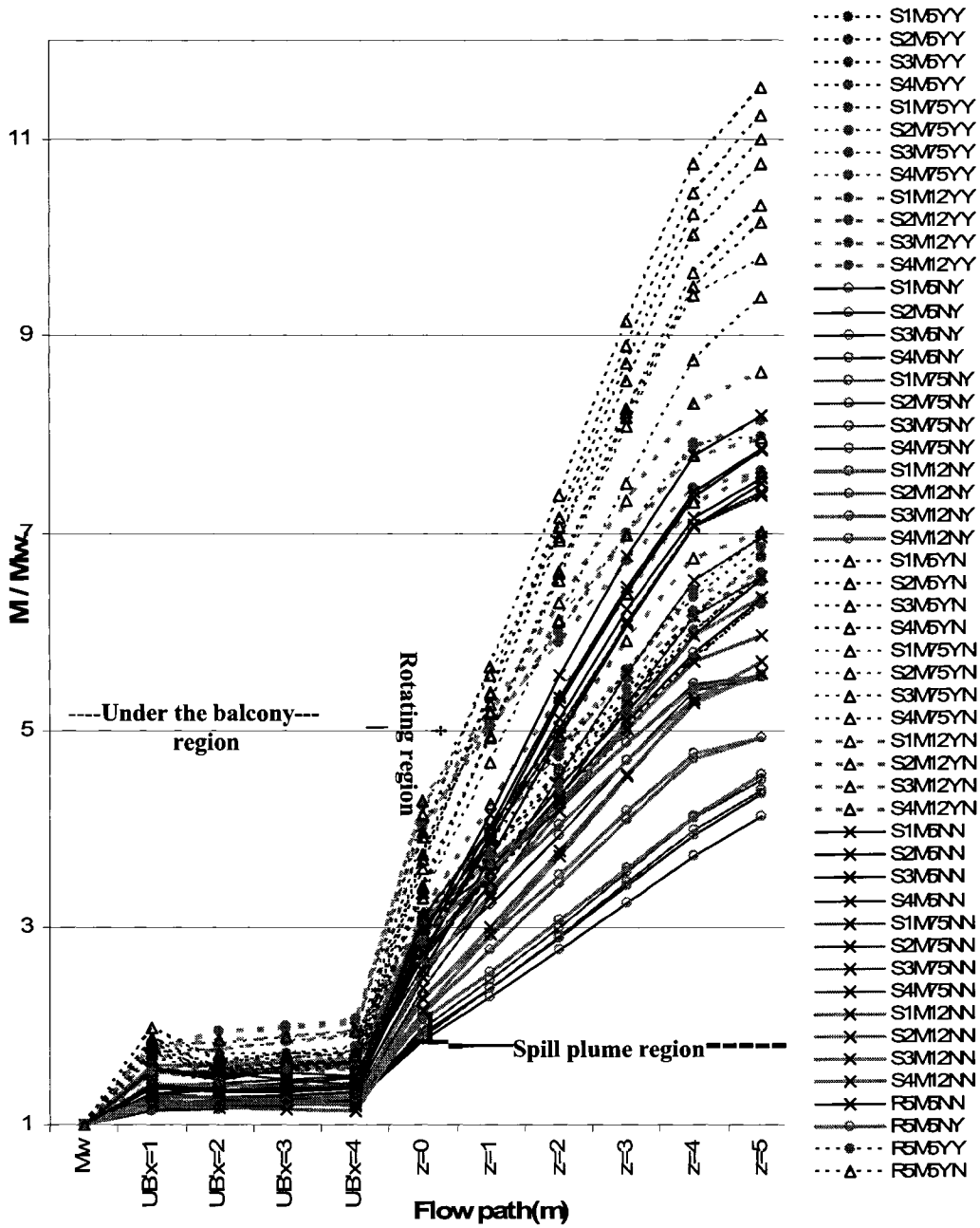

Figure 7.21 Variations of mass flow rates normalized to mass flow rate at the opening over the flow path (m)

7.4.2 The limiting height of rise of the spill plume correlation

As seen in Figure 7.21, the mass flow rate changes in the spill plume region show a clear linear growth over the height of rise which starts from the very edge of the balcony (z = 0). However, it is worth exploring the rotation point problem further since previous studies have raised concerns about the limiting height of the spill plume formula (Thomas 1987, Thomas et al 1998). In addition, we have observed irregular flow motion near the balcony area, which invokes speculation over the applicability of the spill plume correlation near the balcony area.

Using the conventional spill plume factor $(Q_c L^2)^{1/3}$, where L is the layer width at the end of the balcony, mass flow rates per unit spill plume factor, $M/(Q_c L^2)^{1/3}$, are plotted in Figure 7.22, from the top of the domain down to the area under the balcony area, in order to examine how close to the balcony the spill plume method is valid. The layer width L was equal to W for channelled flows, and for unchanneled cases, the layer width L was determined by Equation 2.31, the effective layer width (L_e) proposed by Law [1995]. For the case with a 12 m door width, the flow extended fully out to both sides of the balcony. Thus, the total width of the balcony (l_b) was used for the layer width L in $(Q_c L^2)^{1/3}$ since the calculated effective layer width L_e (12 m + 4.2 m) is greater than l_b (13.6 m). For the cases with draft curtains, L is the distance between the curtains. Figure 7.22 indicates clearly that the mass flow rate near the balcony is governed by the plume correlation.

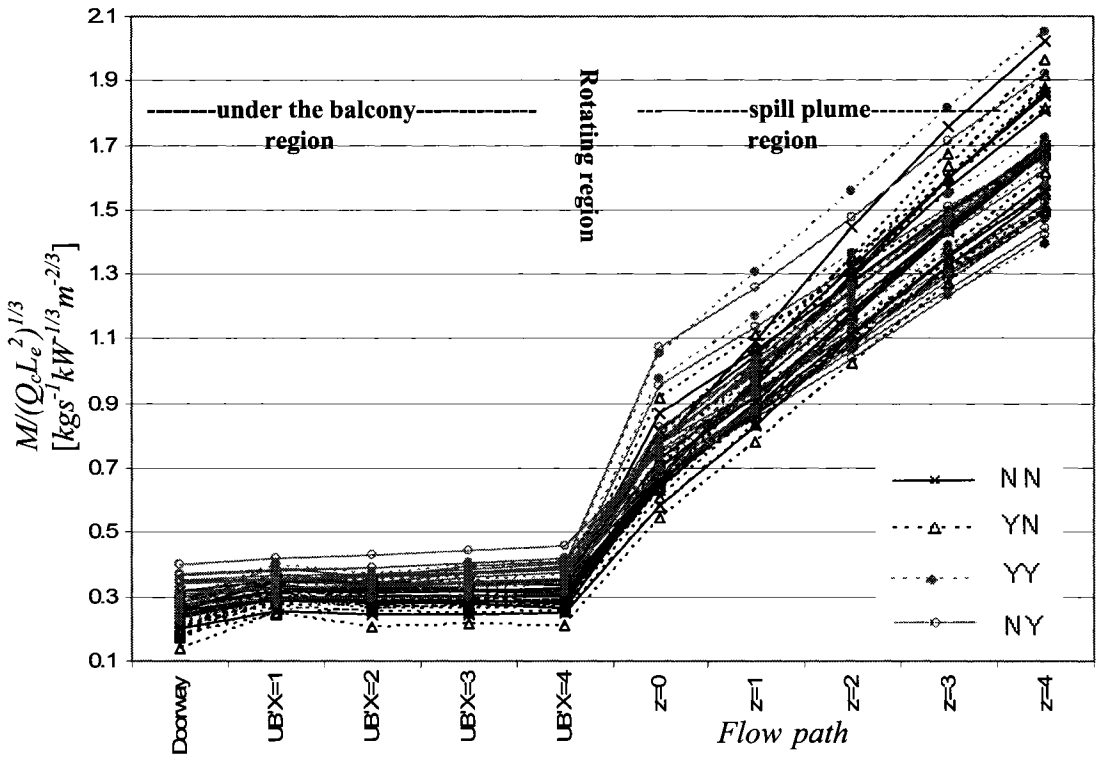

Figure 7.22 Variation of mass flow rate normalized to $(Q_cL_e^2)^{1/3}$ against flow path

To directly test the spill plume correlation near the balcony, FDS temperature results at different heights above the balcony were collected. In Figure 7.23, the maximum temperature values obtained at z = 0, 1, 2, and 3 m from all simulations with draft curtain are plotted on a log-scale against (Q_c / L).

As the plume rises, the temperature decreases, but the same correlation of $(Q_c / L)^{2/3}$ applies. Applying the principle of conservation of heat energy, and assuming that the temperature distribution is uniform across the width of the plume, the mass flow rate correlates with $(Q_cL^2)^{1/3}$ from the temperature correlation with $(Q_c / L)^{2/3}$ [Law 1986].

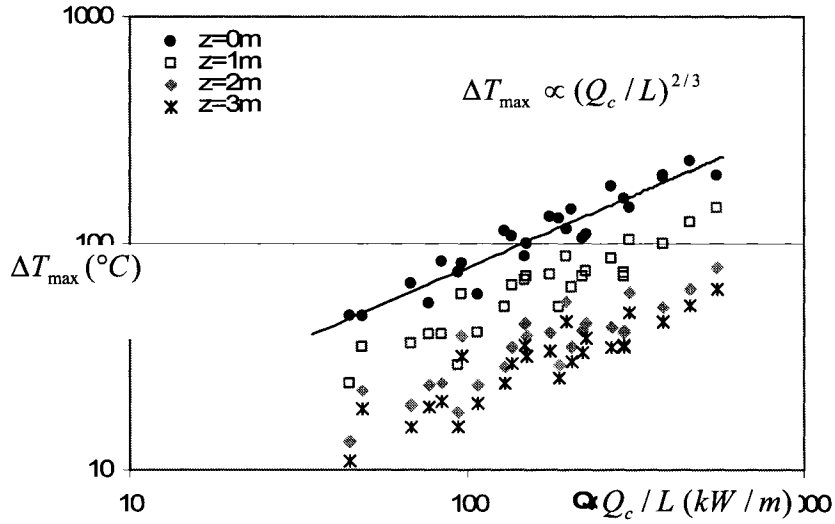

Figure 7.23 Maximum temperature rise at every 1 m above the balcony, plotted with respect to (Q_c/L) , (Simulation with draft curtain)

$$Q_c = C_p M_{z=0} \Delta T_{z=0} = C_p M_{z=1} \Delta T_{z=1} = C_p M_{z=2} \Delta T_{z=2}$$

$$\Delta T_{z=0}\ , \Delta T_{z=1}\ , \Delta T_{z=2} \propto (Q_c / L)^{2/3} \tag{7.1}$$

$$\rightarrow M_{z=0}\ , M_{z=1}\ , M_{z=2} \propto (Q_c L^2)^{1/3}$$

This analysis confirms that the spill plume formula is valid near the balcony, down to the edge (z = 0m).

To verify these results with experimental data, the temperatures measured at z = 0 m and z = 1 m are compared with the CFD predictions. Experimental results also follow the same temperature correlation. In Figure 7.24, experimental results found for cases with draft curtains are compared with temperature predictions obtained from CFD modelling. Considering the fact that the simulated temperature and velocity results are found to be 10~20 % lower than the experimental results (Section 7.2), there is very good agreement between them. Similar results are found for cases without a draft curtain (Figures are given in Appendix D). Thus, these results demonstrate that the spill plume

correlation is valid above the limiting height of rise, which is found to be at z = 0 m for all cases. Therefore, the mass flow rate under this marginal height should be further analyzed to find a method to predict the initial mass flow rate at the spill edge.

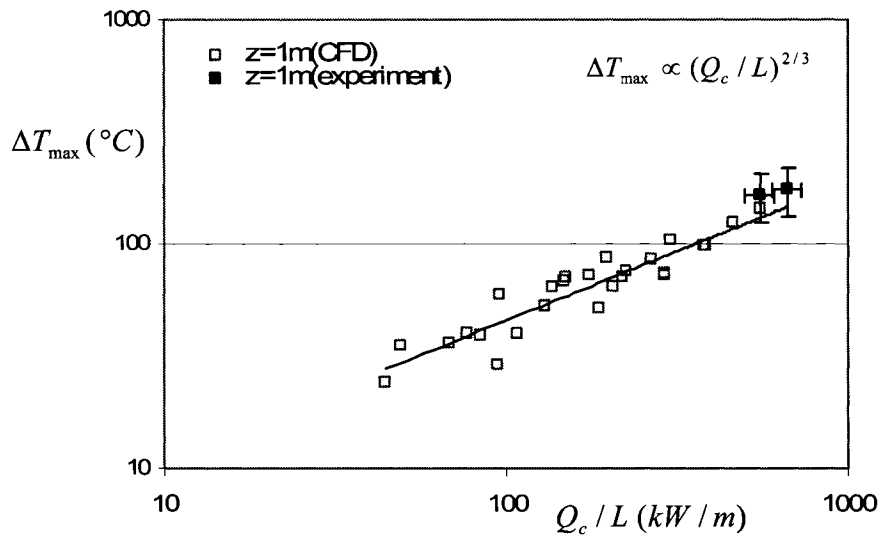

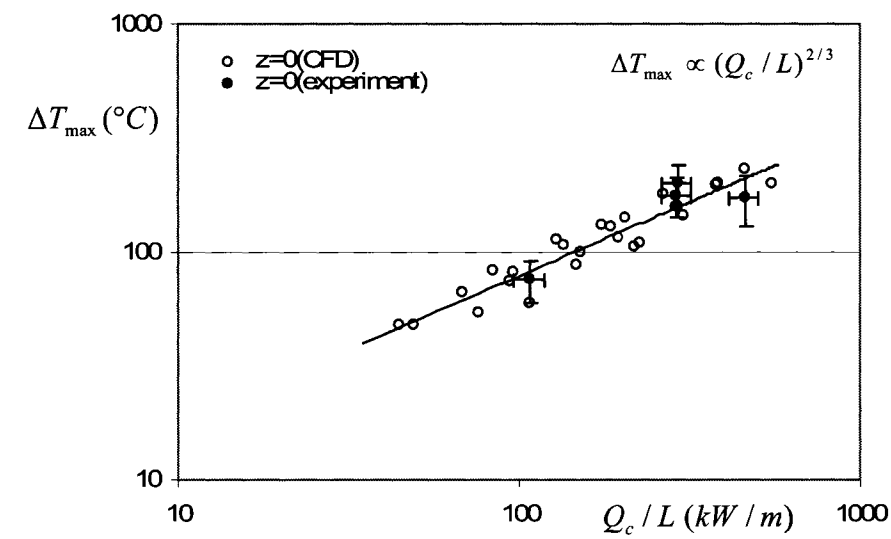

Figure 7.24 Comparison of ΔT (at z = 0 m and 1m) between experiment and simulation (cases with draft curtain)

7.4.3 Comparison with existing methods

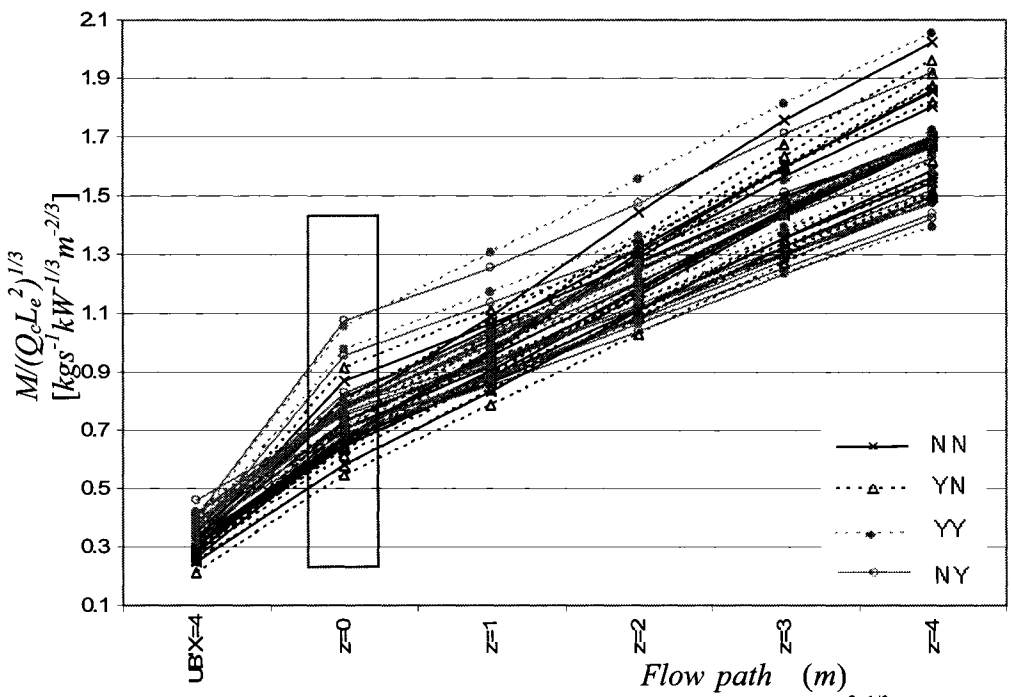

Figure 7.25 Mass flow rate of the spill plume normalized to $(Q_cL^2)^{1/3}$

Figure 7.25 shows a plot of $M/(Q_cL^2)^{1/3}$ of the vertical spill plume with respect to the flow path, from the end of the balcony to the height of rise of z = 4m. In this spill plume region, where $z \geq 0$, mass flow rates near the balcony follow the plume correlation, as most cases have a similar slope. The slope, which is a spill plume constant (B), is found to be 0.19~0.25, regardless of parameter conditions. This is similar to the slope of 0.2 found in the most recent study by Harrison [2004]. For cases with narrow openings, the slope can reach a value of 0.32. This compares well with the slope (0.36) of the NFPA 92B [2000]. Further analysis on the mass flow rate of the spill plume is not pursued in the current study since our focus is in estimating the mass flow rate at the limiting height of rise, which we found to be z = 0.

From Figure 7.25, the computed air entrainment at the spill edge from all FDS simulations in this study are found to be governed by the following equation:

$$\frac{M_s}{\left(Q_c L^2\right)^{1/3}} = 0.55 \sim 1.05 \tag{7.2}$$

A crude estimate can be made based on the above equation; however, knowing the exact amount of the initial mass flow rate at the spill edge would give a more accurate exhaust rate. Simulated results of mass flow rate at the spill edge M_s are compared with existing methods, to examine the accuracy of the predictions. Results from channelled flows are used for comparisons. Most methods predict a lower M_s value than is found in the FDS generated results, so some methods are modified to give a better fit with the FDS results.

7.4.3.1 Method 1: Amount of air entrainment, δm

The following equations are used to calculate the value of M_s, and the results are compared with FDS predictions in Figure 7.26.

Morgan and Marshall [1975]

$$M_s = M_w + \delta m = M_w + \frac{2}{3}\alpha' L \rho_0 \left(\frac{2g\Delta T}{T_0}\right)^{1/2} D^{3/2} \tag{2.13}$$

Thomas [1987]

$$M_s = \beta \rho D \left(\frac{g Q_c}{\rho C_p T_0 L}\right)^{1/3}$$

(2.16)

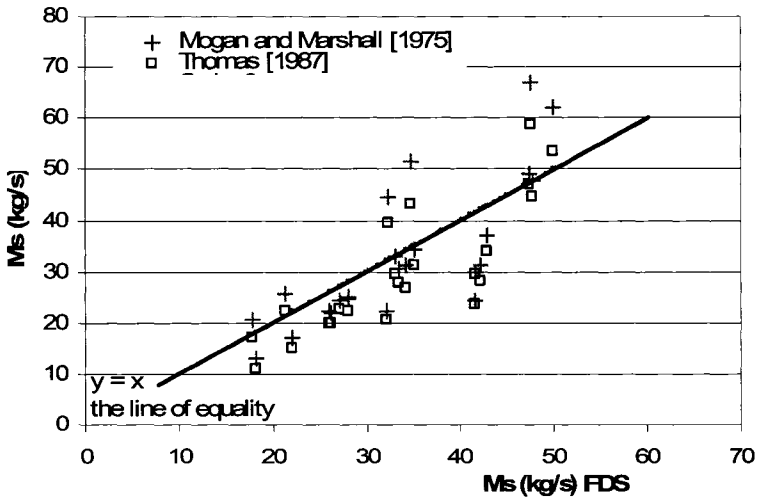

Figure 7.26 Comparison between FDS results with method by Morgan and Marshall [1975], Thomas [1987]

Simulated results for M_w are used in the method of Morgan and Marshall, and in the method of Thomas, a value of 1.56 is assigned to β. Estimations of δm by Thomas are slightly lower than those of Morgan and Marshall, but both methods estimate appreciably greater amounts of entrainment into rotating flow than other methods.

These methods attempt to estimate the actual amount of mass flow by engaging uncertain details of the flow and flow coefficients, which raises questions about their applicability.

7.4.3.2 Method 2: Layer depth

The simulated results of M_s are compared with predictions found using methods based on layer depths, and the results are shown in Figure 7.27. Layer depths computed using Equation 5.1 are applied into the following equations.

Poreh et al [1998]

$$M_s = M_b + 0.16 Q_c^{1/3} L^{2/3} D_b \tag{2.18}$$

Harrison [2004]

$$M_s = 0.2 Q_c^{1/3} L^{2/3} D_b + 0.89 \left(\frac{h_{comp} M_w}{h_w} \right)$$

(2.29)

Thomas et al [1998]

$$M_s = 1.4 M_b + 0.0014 Q_c \tag{2.22}$$

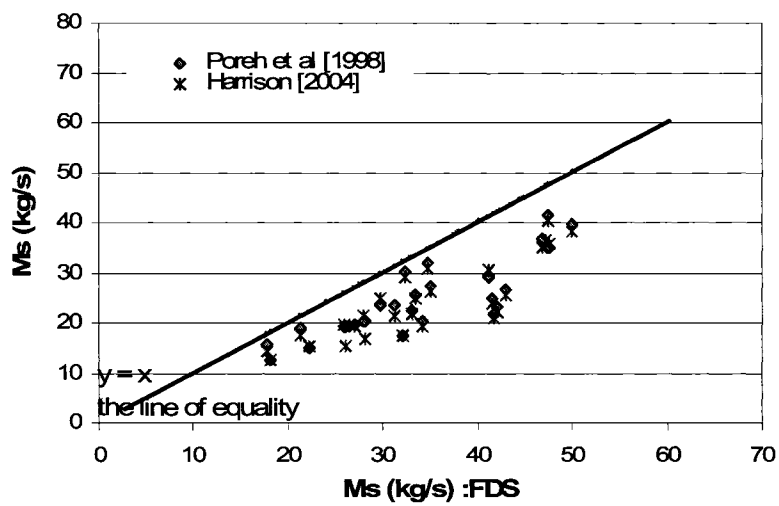

Figure 7.27 Comparison between FDS results from current study and methods by Poreh et al [1998], Harrison [2004]

The method used by Harrison appears to predict lower values than that of Poreh, although the spill plume coefficient of Harrison is greater than that of Poreh et al. This is because the value of M_b found by Harrison's method is low. In Figure 7.28, simulated results from this study are compared with results obtained using the method of Harrison,

plotting $\left(\frac{M_b W}{M_w h_{comp}}\right)$ with respect to $\left(\frac{h_w}{W}\right)$. Despite the fact that both Harrison's correlation and the predicted results are obtained from FDS simulations, there are differences. The possible reasons are a) results of the Harrison's study were obtained from a 1/10th physical scale model; b) the majority of Harrison's simulations used one nominal total heat source.

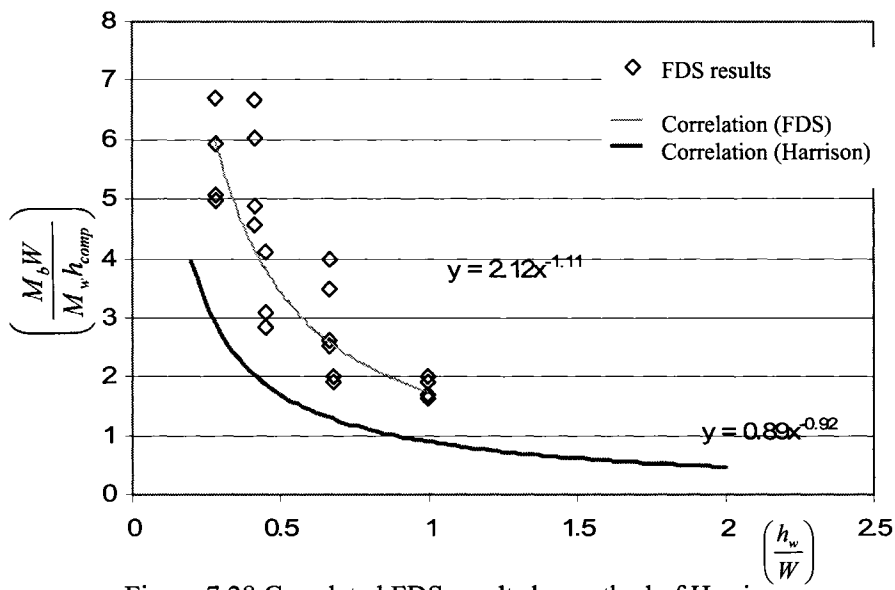

Figure 7.28 Correlated FDS results by method of Harrison

Overall, the methods used by Poreh et al and Harrison based on layer depth underestimate M_s by approximately 20% as shown in Figure 7.27. Considering the fact that the method by Thomas was developed based on the method of Poreh, the former was modified. Using a constant of 1.8 instead of 1.4, the simulated results compare well with the method as shown in Figure 7.29

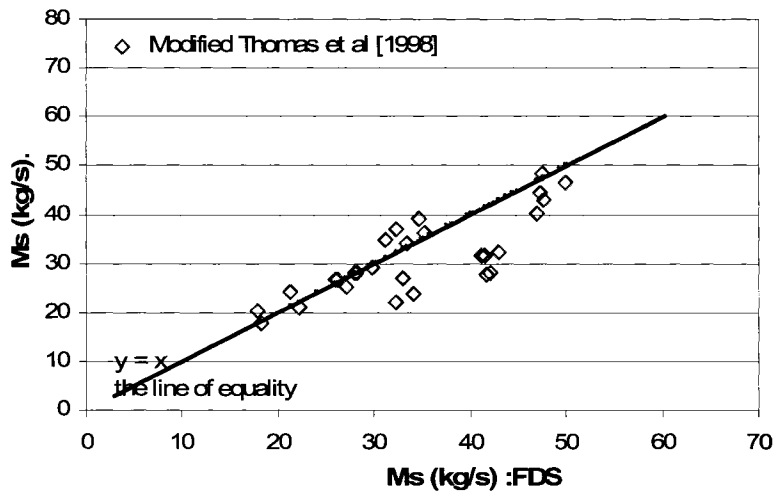

Figure 7.29 Comparison between FDS results from current study with those from method used by Thomas et al [1998] (modified)

7.4.3.3 Method 3: The virtual origin

The following two methods based on the virtual origin concept are used for comparison.

Law [1986]

$$M_a = 0.31 Q^{1/3} L_e^{2/3} (z + \Delta) \tag{2.6}$$

NFPA 92B [2000]

$$M_a = 0.36 Q_c^{1/3} L^{2/3} (z + \Delta) \tag{2.8}$$

In Figure 7.30, FDS-generated predictions of M_s are compared with the results obtained using methods using the virtual origin. The suggested virtual origin of $\Delta = 0.25 h_{comp}$ underestimates M_s significantly. Considering the fact that Thomas [1987] presented a number of possible estimates for the position of the virtual origin, ranging

from $0.3h_{comp}$ to $0.8h_{comp}$, we modified Equation 2.6 and Equation 2.8 so that the virtual origin is located at $\Delta = 0.4h_{comp}$ for the methods of Law and the NFPA 92B analysis.

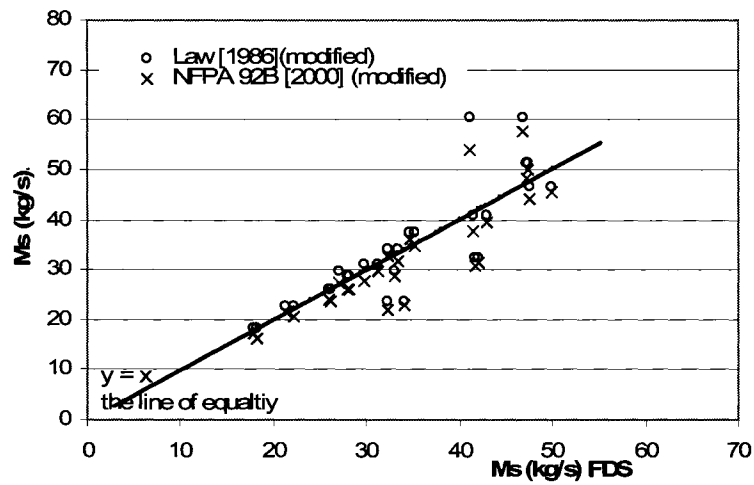

Figure 7.30 Comparison of FDS results with methods of Law [1986] (modified), NFPA 92B [2000] (modified)

This comparison shows that simple methods based on the virtual origin perform relatively well. However, spill plume constants in both Law and NFPA methods are high since they are empirically obtained based on data obtained near the balcony, where additional entrainments are observed. Thus, it should be further examined.

7.4.3.4 Discussion

Comparisons with existing methods highlight interesting aspects of the behaviour of rotating flows. The methods based on the virtual origin assume that M_s is a function of $(Q_c L^2)^{1/3}$. The method of Thomas correlated M_s with M_b and an additional function of Q_c. However, the comparison with CFD predictions indicates that there must

be an unknown function governing the entrainments. Therefore, detailed analysis of the air entrainment rate at the rotating region is necessary. In an attempt to find a new method, other than methods using δm, D_b or Δ, the temperature and velocity transition under the balcony area was further analysed in the next chapter.

8 Analysis and Discussion

The initial analysis that is presented in the previous chapter provided insights into the relationship between horizontal gas flow under the balcony and the vertical spill plume. In the previous chapter, it has also been clarified that the area of interest in this study is below the balcony edge (z = 0m). Therefore, this chapter focuses on the flow from the doorway to the limiting height, which is at the edge of the balcony, and conducts further analysis in an attempt to develop a new method to predict the mass flow rate of the balcony spill plume at the spill edge. This chapter consists of three parts of analyses:

1) temperature and velocity transition under the balcony area
2) air entrainment rate into the rotating flow
3) air entrainment rate into the flow under the balcony

Finally, an empirical correlation to calculate the mass flow rate at the spill edge is obtained based on these analyses.

8.1 Temperature and velocity transition under the balcony area

The transition of the temperature and velocity of the flow at the balcony is investigated to determine the effect of various parameters on entrainment rates. The maximum temperature and velocity are the properties of the flow, which greatly influence the trajectory at the spill edge and consequent air entrainment. Thus, analyzing the maximum temperature and velocity should assist in determining the impact of various parameters.

Along the centreline of the flow, the maximum temperature rise and maximum

velocity were collected at the doorway, at the end of the balcony, and at the edge of the balcony, using results from all simulations and experiments. These data are plotted with (Q/W) instead of (Q_c/L) in order to have data scattered. Data from the doorway area are correlated with (Q/W), the total heat release rate per unit width of opening. At the balcony end and spill edge, the same factor (Q/W) is used for the analysis in order to evaluate changes in temperature rise and velocity from the initial state.

8.1.1 Behaviour at the door opening

Figure 8.1 shows a plot of $\Delta T_{w\,\max}$ against Q/W, on a log scale. Both simulated results and experimental results fall on a line of slope 2/3, which agrees with the correlation of $(Q/W)^{2/3}$ that Law has established, based on Yokoi's [1960] correlation of a plume from an opening.

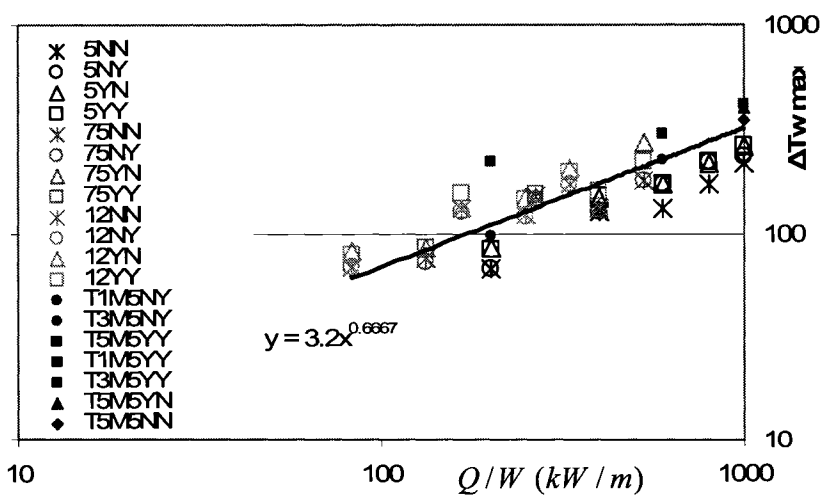

Figure 8.1 The maximum temperature rise at the doorway

The maximum U-Velocity, $U-Vel_{w\,\max}$ is plotted on a log scale against Q/W in

Figure 8.2, for all simulations.

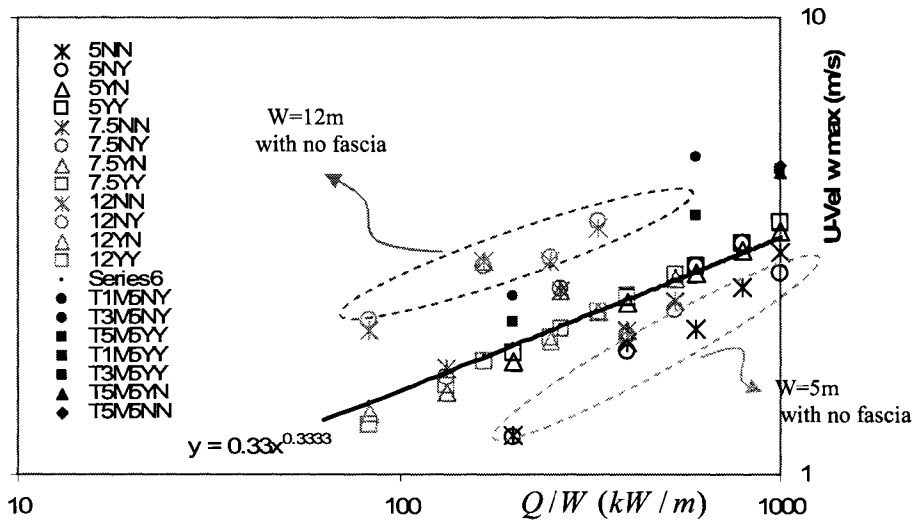

Figure 8.2 The maximum U-Velocity at the doorway

As seen from the figure, $U-Vel_{w\,\max}$ in most cases with fascia (marked with Δ and □) can be correlated with Q/W by a 1/3 power law, which is consistent with the doorway velocity equation developed by Morgan and Hansell [1987].

Results from cases without fascia, [which are marked with an asterisk (*) or a circle (o)], reveal an interesting effect of the absence of fascia on $U-Vel_{w\,\max}$. A group of results from cases with a wide opening (W = 12m), with no fascia present, exhibit a greater $U-Vel_{w\,\max}$ value than the correlation. This is presumably caused by the momentum of the ceiling jet. On the other hand, another group of results from cases with a narrow opening (W = 5m), with no fascia present, shows a lower doorway velocity than the correlation. This implies that the fascia effect on the velocity of the door flow entering into the balcony area is associated with opening sizes.

The figure also shows that experimental results exhibit relatively good

agreement with $\Delta T_{w\,\max}$; however, velocity data from experiments have greater values of $U-Vel_{w\,\max}$ than simulated results. This is because $U-Vel_{w\,\max}$ values were actually measured at 1 m away from the doorway in all experiments.

To sum up, the fascia effect on the temperature rise is minor, regardless of opening size, yet the fascia effect on the velocity is relatively great and diverse, depending on the opening size.

8.1.2 The end of the balcony

As flow moves under the balcony, the temperature decreases whereas U-Velocity increases due to the balcony and draft curtain effects.

In most cases, the draft curtain effect on the temperature rise is weak, except for cases with narrow openings. In Figure 8.3, which includes results of cases with a 5 m opening width, without fascia and draft curtains (5NN), it can be seen that the temperature drops in the absence of a draft curtain, which indicates that the draft curtain effect is connected to the ratio of the balcony width to the opening width (l_b/W).

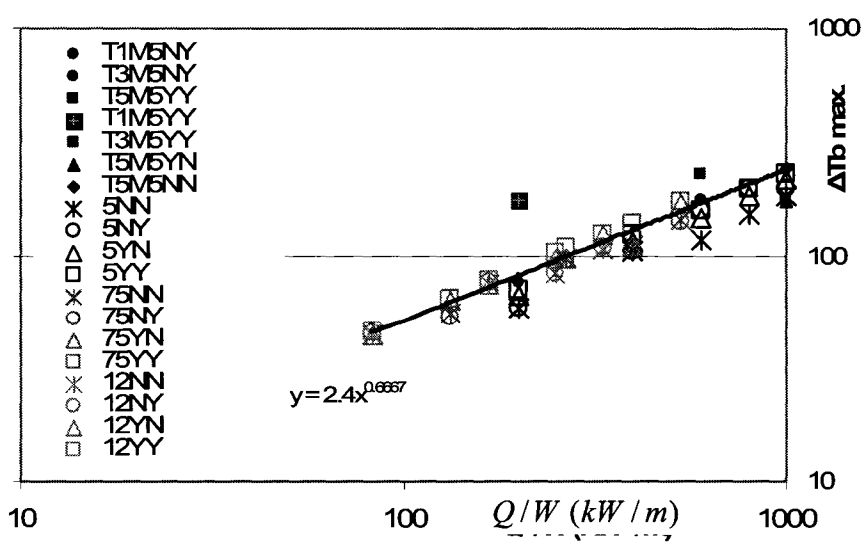

Figure 8.3 The maximum temperature rise at the balcony end

Figure 8.4 shows that the effect of draft curtains on velocity is minor, compared with the effect of fascia. Noticeable U-Velocity increases are found for cases with fascia (marked with Δ and □) , which are correlated to Q/W by a 0.4 power law, characterized by a greater constant (0.4) than the correlation for cases without fascia (0.32). As discussed earlier, the fascia impedes the velocity at the doorway for cases with W = 12m, but in these cases, the velocity at the end of the balcony still increases to the level of the velocity observed in cases with no fascia. This implies that velocity is the combined outcome of flow temperature, fascia depth, balcony breadth, and draft curtains.

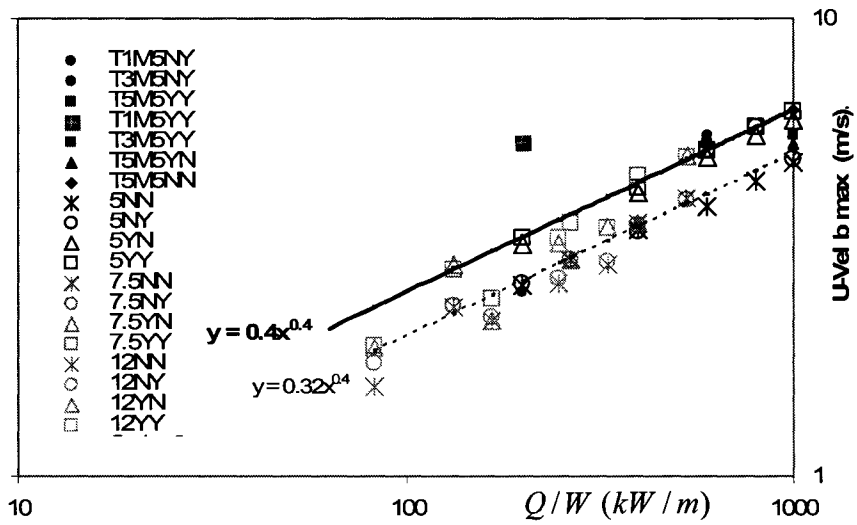

Figure 8.4 The maximum velocity at the balcony end

For both $\Delta T_{b\ \max}$ and $U-Vel_{b\ \max}$, reasonable agreement between simulated results and experimental results is found. Both simulated results and experimental results generally agree with the power correlation of 2/3 with Q/W for max. ΔT_b and 2/5 for $U-Vel_{b\ \max}$.

8.1.3 At the balcony edge

Figure 8.5, and Figure 8.6 show plots of $\Delta T_{s\,\max}$ and $W-Vel_{s\,\max}$ against Q/W respectively. When flow emerges up into the large reservoir, the maximum temperature remains the same, but the W-Velocity of the vertically moving spill plume, decreases significantly compared to U-Velocity at the end of the balcony.

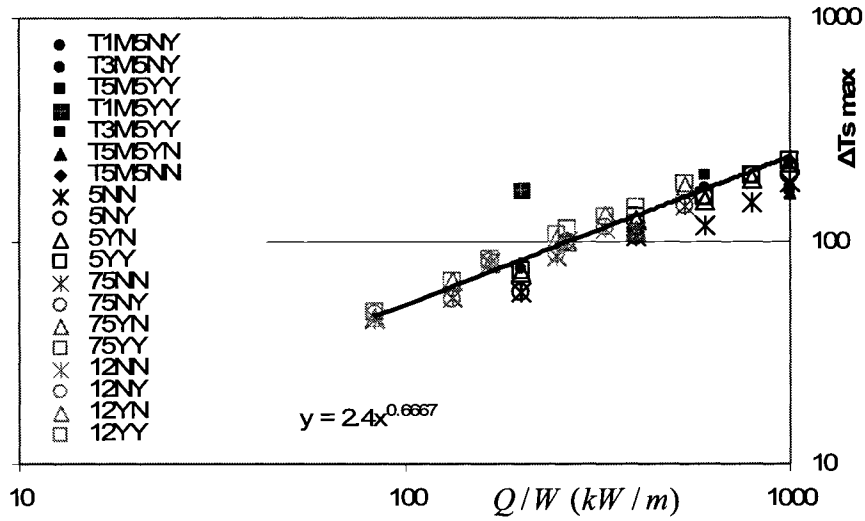

Figure 8.5 The maximum temperature rise at the spill edge

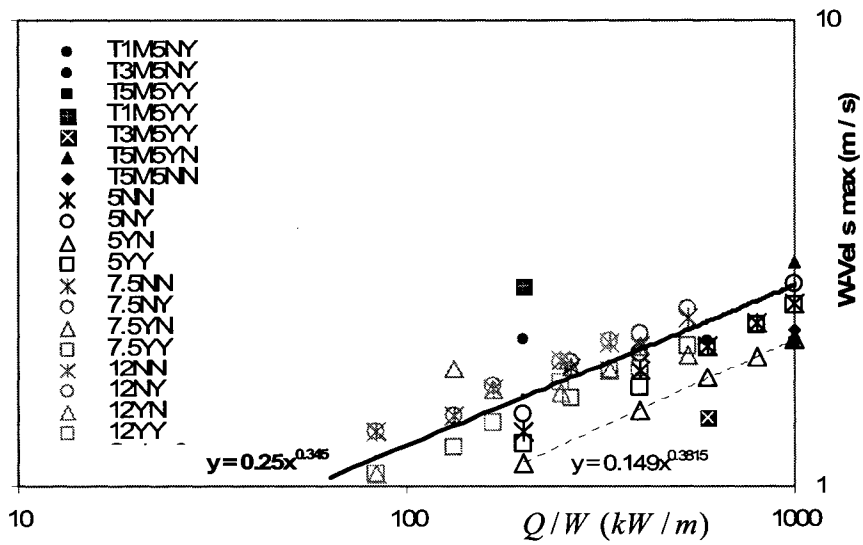

Figure 8.6 The maximum W-Velocity at the balcony edge

As shown in Figure 8.6, the velocity is correlated to Q/W by an approximately 0.35 power relation, despite there being a significant dependence on the opening size. One possible reason for this is the different layer depth of the flow caused by the opening size. Under the same temperature and velocity conditions at the end of the balcony, a thinner layer is likely to have a higher W-Velocity component. Thus, cases with wider openings, (which would give thinner layers), have a slightly higher W-Velocity.

Another interesting observation from Figure 8.6 is that in the case of 'NY' [marked with a circle (o)], the value of W-Velocity shows a marked increase, even though it had a lower U-Velocity than other cases at the end of the balcony. This confirms that the trajectory at the balcony edge is defined by both the temperature and U-Velocity of the flow.

Experimental results show good agreement of $\Delta T_{s\,\max}$ with Q, but some of the velocity data do not lie on the line of correlation. Presumably, this is because of the sparse distribution of manometers on the instrumentation tree, which resulted in failure to catch adequately the maximum velocity of the spill plume.

8.1.4 Characteristics of approach flow

Using selected parameters of the approach flow ($\Delta T_{b\,\max}$, $U-Vel_{b\,\max}$ and D_b), the Richardson number, Ri, was calculated using Equation 4.1. The ratio M_s/M_b is plotted as a function of Ri at the end of the balcony in Figure 8.7. Calculated Ri values are in the range 0.14-0.7, which are equal to or below the limiting Ri criteria (0.7),

discussed earlier in Chapter 4.

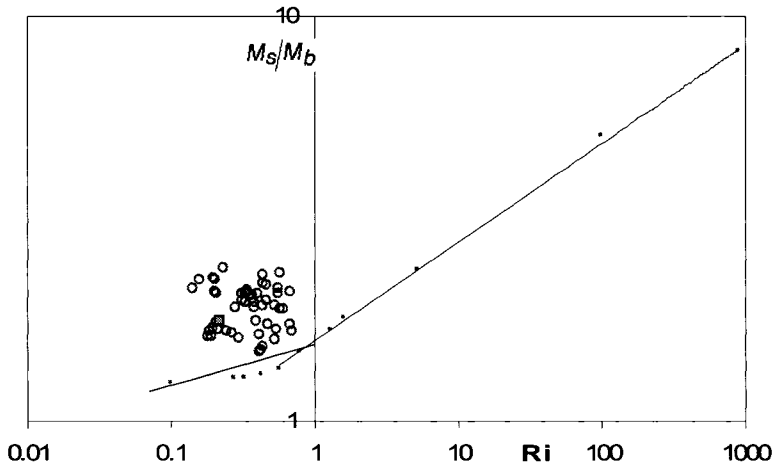

Figure 8.7 Variation of air entrainment rate at the rotating region with Ri of the initial flow

The maximum temperatures at the end of the balcony in all simulations are in the range 64-248°C. The temperature value of 248°C resulted from simulation-R5M5YY, and almost reached the limiting temperature criteria in Table 2.1 (250°C for a 5 m opening size suggested by Hansell et al [1993]). The corresponding Ri is 0.22, [marked with (□) in Figure 8.7], and mass flow rates at the spill plume region behave as expected with this Ri number.

8.2 Air entrainment rate into the rotating flow

8.2.1 Overview of air entrainment into rotating flow

To find the factors governing the air entrainment at the rotating region and the effect of parameters on the entrainment rate, mass flow rates normalized to the mass flow rate at the end of the balcony are plotted in Figure 8.8.

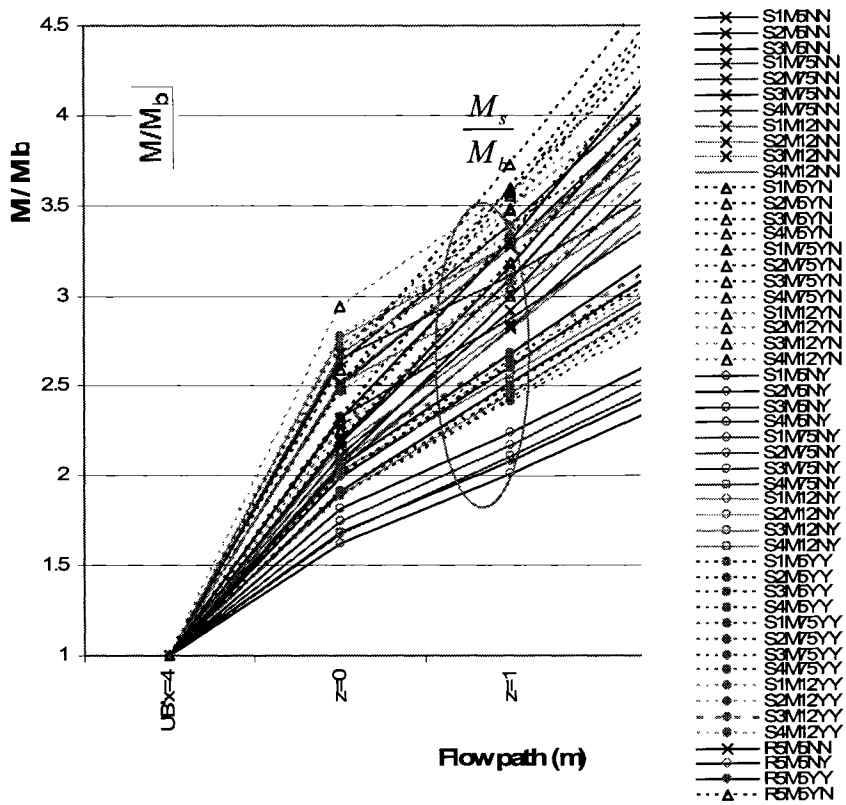

Figure 8.8 Air entrainment rate at rotation region

The figure provides some insight into the behaviour of the spill plume when it leaves the area under the balcony and rotates up into the atrium. It is clear from the figure that air entrainment rates of the spill plume are less in the presence of draft curtains (marked with ○ and ●).

Most of the cases without draft curtains (marked with Δ and ×) seem to have a higher air entrainment value, which varies from 1.8 to 2.9 (estimated from Figure 8.8) The large fire size seems to result in small rates of air entrainment, but this trend is not consistent for cases with opening sizes of 5m. This suggests that the air entrainment rate

of the rotating flow is affected by the characteristics of the approach flow. Assuming that the characteristics of the source flow can be described in the form, $\Psi = function\{Q, W\}$, one can assume that the mass flow rate of the rotating flow is described as

$$\frac{M_s}{M_b} \propto [\Psi \times Parameter\ effects] \quad (8.1)$$

The following analysis of the air entrainment rate of the rotating flow is made based on insights gained from the initial analysis on the overall air entrainment rates, and analysis on transitions of temperature and velocity under the balcony area. These considerations showed that:

1) The air entrainment rate is dependent on the source strength and is characterized by temperature, velocity, and layer depth, which forms the flow trajectory of the buoyant jet at the end the balcony.
2) The presence of fascia decreases the velocity and temperature of the flow, causing additional air entrainment.
3) Unchanneled flows are likely to entrain more air than channelled flows.
4) As the flow moves under the balcony, its U-Velocity increases, which results in possible reduction in the air entrainment, since it is difficult for the buoyancy to counteract the momentum of the flow.
5) Parameter effects act in conjunction with source strength, such that their impacts are proportional to the characteristic source strength.

Thus, a simple correlation can be constructed in the following format;

$$\frac{M_s}{M_b} \propto \Psi,\ P_{fascia},\ P_{draftcurtain},\ \frac{1}{P_{balcony}},\ \frac{1}{F_{layer}}$$

$$\frac{M_s}{M_b} \times F_{layer} = function\left\{\Psi \times P_{fascia} \times P_{draftcurtain} \times \frac{1}{P_{balcony}}\right\} \qquad (8.2)$$

where
M_s = the mass flow rate at the spill edge
M_b = the mass flow rate at the end of the balcony
Ψ = characteristic source strength
F_{layer} = initial layer width-depth factor
P_{fascia} = the fascia effect
$P_{draftcurtain}$ = the draft curtain effect
$P_{balcony}$ = the balcony effect

Simple expressions representing the relative effects of these factors are sought, rather than adopting complicated theories to explain the results obtained.

8.2.2 Initial source conditions

Temperature, velocity, and layer depth describe the initial condition of the approach flow.

8.2.2.1 Characteristic source strength

The initial temperature and velocity conditions define the potential strength of the source flow, which controls the air entrainment rate of rotating flow. The optimum balance of thermal and mechanical energy of the source results in a maximum air entrainment rate. These two competing parameters can be expressed in terms of the convective heat release rate (Q_c) and the effective layer width (L_e). However, we have seen that the dynamics of air entrainment into a rotating flow involve more factors than

just the trajectory. Characteristics of the source flow will be described as an unknown function of Q_c and L_e, and an expression to describe the system will be sought, by correlating data from simulations.

$$\textit{Characteristic source strength} \quad \Psi = \textit{function}\{Q_c, L_e\} \tag{8.3}$$

8.2.2.2 Layer width –depth effect

The initial layer width and depth effect is considered as a primary factor affecting the air entrainment rate. The width of approach flow governs the mass flow rate of the balcony spill plume since it makes the plume behave as a line plume [Lee and Emmons 1961]. In the relation, the effective width of the balcony spill plume, L_e, is employed along with the fascia effect h_{comp} / h_w , since the layer depth depends on them.

$$F_{layer} \propto \left\{ \frac{1}{L_e}, \frac{h_{comp}}{h_w} \right\} \tag{8.4}$$

8.2.3 Parameter effects

8.2.3.1 Fascia and Draft curtain effect

A more deeply-placed fascia decreases a greater extent of the momentum of flow (it neutralizes a great portion of the momentum), because it impedes the increase in velocity of the source flow and causes a temperature drop. This fascia effect is strengthened if it is coupled with a sudden expansion (of the smoke) due to the absence of a draft curtain. The draft curtain effect can be written in the form, $\left(P_{fascia}\right)^{1+P_{draft\ curtain}}$.

$$\textit{Fascia effect} \quad P_{fascia} = \left\{ \frac{h_{comp}}{h_w} \right\} \tag{8.5}$$

$$\textit{Draft curtain effect} \quad P_{draftcurtain} = \frac{l_b}{W} \tag{8.6}$$

8.2.3.2 Balcony effect

The horizontal velocity (U-Velocity) increases under the balcony, depending on whether there is fascia/ curtain or not, and the effect of the balcony is proportional to the effective breadth of the balcony, b / h_{comp}. As observed in the analysis of temperature and velocity transition in Section 8.1, the presence of fascia also has an influence on the velocity increase. The balcony effect can be described as follows:

$$\textit{Balcony effect} \quad P_{balcony} \propto \left\{ \frac{b}{h_{comp}} \times \left(\frac{h_{comp}}{h_w} \right) \right\} \tag{8.7}$$

8.2.4 Empirical correlation of air entrainment rate of rotating flow

CFD results from all simulations are used for the analysis, in an attempt to develop a simple correlation that can describe all four parameter conditions (i.e., case-YN, NN, YY, and NY). The characteristic source strength term is empirically found.

$$\Psi = \left\{ Q_c^{1/5} \, L_e^{3} \right\} \tag{8.8}$$

Simple expressions (from Equation 8.4 to Equation 8.8) are placed into the form of Equation 8.2. $\frac{M_s}{M_b} \times \left(\frac{h_{comp}}{L_e \, h_w} \right)^2$ is plotted on a log scale with respect to

$\left[\left(Q_c^{1/5} L_e^{3} \right) \times \frac{1}{\left(\frac{h_{comp}}{h_w} \right)^{1+K_c}} \times \left(\frac{1}{\frac{b}{h_{comp}} \times \left(\frac{h_{comp}}{h_b} \right)} \right) \right]$ in Figure 8.9.

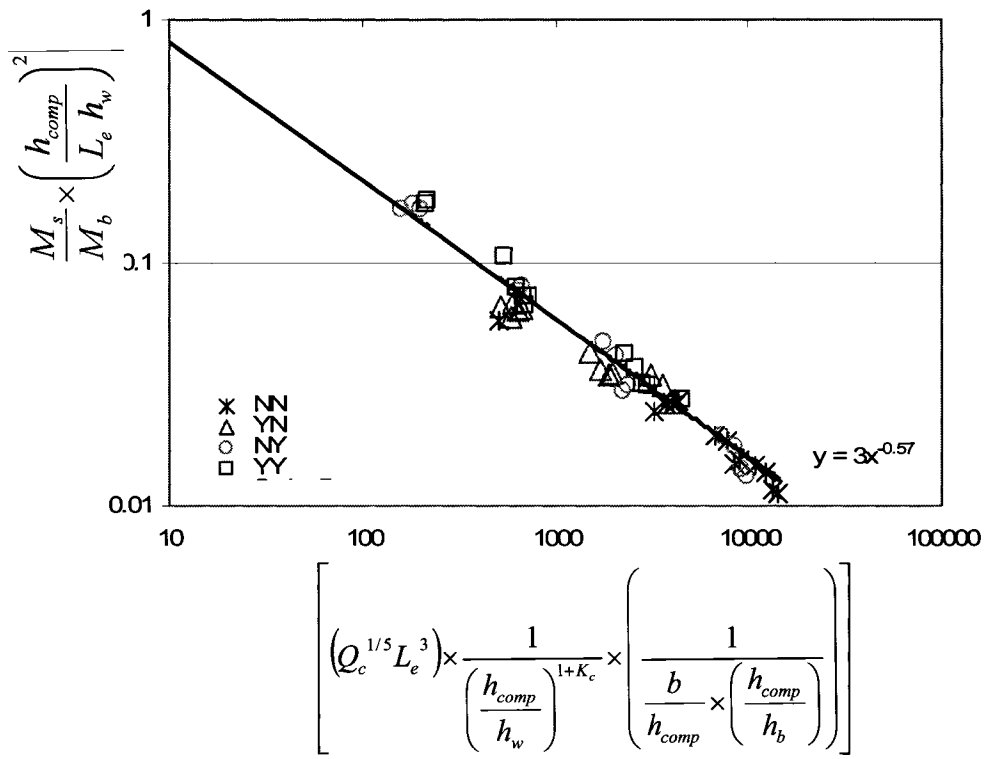

Figure 8.9 Correlated FDS predictions

The best-fit correlation is found in the form of the following power law.

$$\frac{M_s}{M_b} \times \left(\frac{h_{comp}}{L_e\, h_w}\right)^2 = 3.0 \left[\left(Q_c^{1/5} L_e^{3}\right) \times \frac{1}{\left(\frac{h_{comp}}{h_w}\right)^{1+K_c}} \times \left(\frac{1}{\frac{b}{h_{comp}} \times \left(\frac{h_{comp}}{h_w}\right)}\right)\right]^{-0.57}$$

$$where \quad K_c = \frac{l_b}{W} \tag{8.9}$$

8.3 Air entrainment rate under the balcony

8.3.1 Overview of air entrainment rate under the balcony area

Due to mass loss from under both sides of the balcony, the air entrainment rate under the balcony area is estimated by a simple approximation, and the correlation of the air entrainment rate under the balcony area is obtained only for the case with draft curtains. Earlier, this mass loss from the sides was ignored for the analysis of air entrainment at the rotating region. However, to estimate the air entrainment rate under the balcony, the amount of loss is approximately estimated.

Figure 8.10 shows the mass flow rate normalized with respect to the mass flow rate at the doorway, which is measured through vertical planes right under the balcony (plane A′ in Figure 5.7). From Figure 8.10, the air entrainment rate at the end of the balcony was predicted, including mass loss.

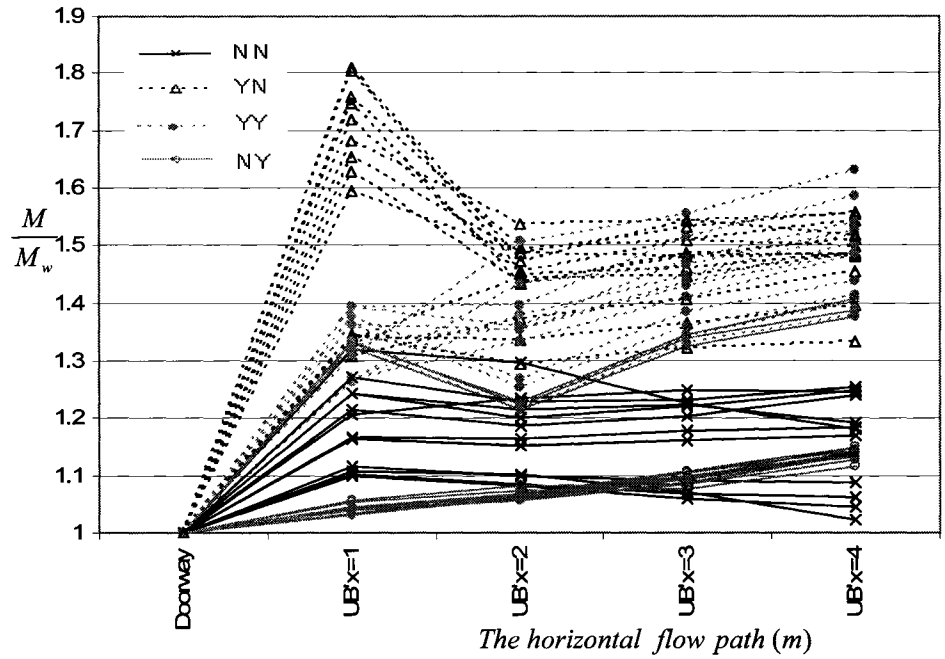

Figure 8.10 The mass flow rate normalized to the mass flow rate at the door way

$$\frac{M_b}{M_w} \cong 1.15 \quad , Case-NY \qquad \frac{M_b}{M_w} \cong 1.2 \sim 1.4 \quad , Case-NN$$
$$\frac{M_b}{M_w} \cong 1.5 \sim 1.6 \quad , Case-YY \qquad \frac{M_b}{M_w} \cong 1.8 \sim 2.0 \quad , Case-YN \tag{8.10}$$

Equation 8.10 is consistent with empirical results given by Morgan et al [1999].

As shown in Figure 8.10, the fascia effect is greater than the effect of draft curtains for flows under the balcony. For these channelled flows, there is a linear mass gain along the horizontal path under the balcony. A broad range of behaviours dependent on the parameters can be characterized, such as the dimensions of fascia, draft curtains, and the balcony. However, here we will limit the analysis to cases with a draft curtain.

8.3.2 Empirical correlation of air entrainment rate under the balcony area for case with draft curtains

In Figure 8.11, $1.2\times\left(\frac{h_{comp}}{h_w}\right)^{0.5}\times\frac{M_s}{M_b}$ is plotted with respect to $\left(\frac{M_s}{M_w}\right)$.

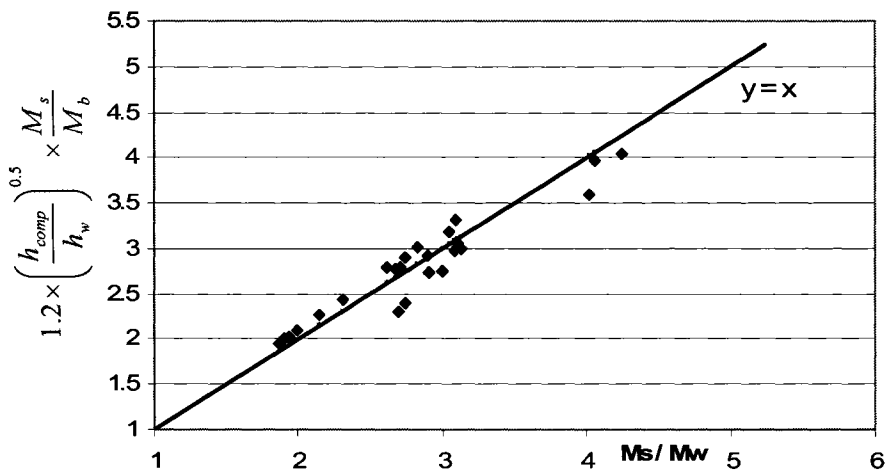

Figure 8.11 Correlated air entrainment rate under the balcony (for channelled flows)

The simple correlation is obtained as below.

$$\frac{M_s}{M_w}=1.2\times\left(\frac{h_{comp}}{h_w}\right)^{0.5}\times\frac{M_s}{M_b} \qquad 8.11$$

where
M_b = the mass flow rate at the end of balcony
M_w = the mass flow rate at the doorway
h_{comp} = the height of the fire compartment
h_w = the door height

8.4 Validation of empirical correlation

8.4.1 Comparison of experimental and simulated results

In order to evaluate the use of the empirical correlation obtained from CFD modelling, a comparison has been made with experimental results using mass flow rates.

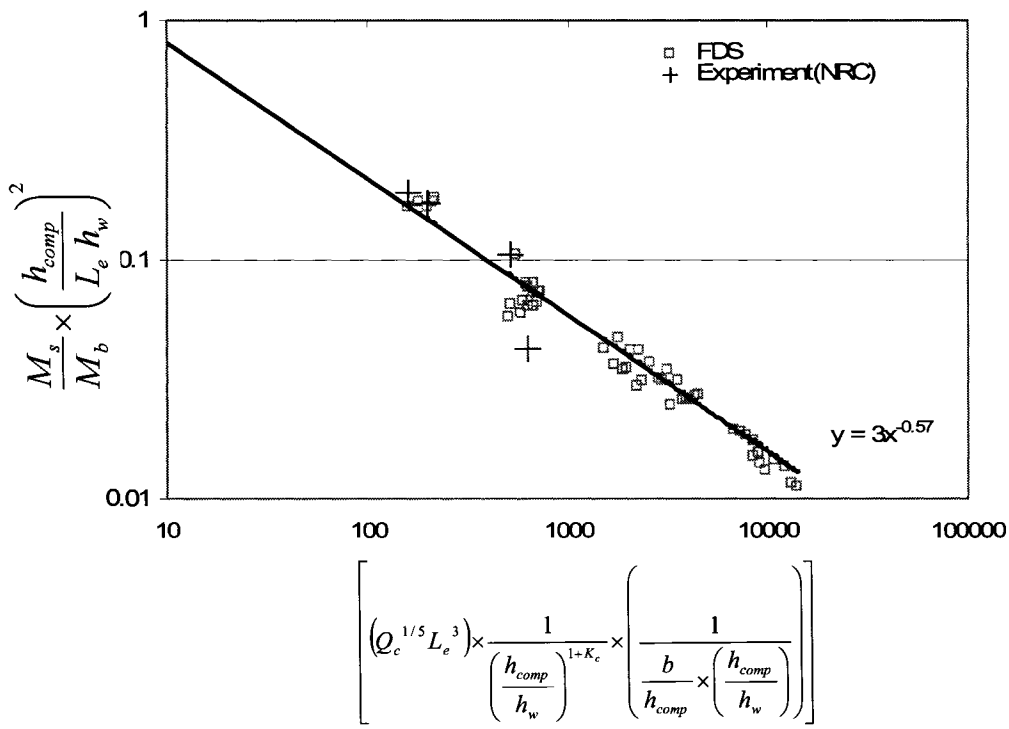

Figure 8.12 Comparison of correlated experimental results with FDS results

Although there was a limitation in calculating the mass flow rate because of insufficient experimental data (collected only along the centreline of the flow), the experimental results agree relatively well with FDS predictions. However, the correlation should be fully validated with full-scale data.

8.4.2 Comparison with previous studies

In addition to the comparison with experimental results, published experimental data from previous studies were employed in order to examine the applicability of the empirical correlation to various atrium sizes, compartment sizes, and balcony breadths, as well as cases with downstand at the spill edge.

Harrison [2004] conducted 1/10th physical scale experiments, in which mass flow rates of balcony spill plumes generated from a fire compartment [of dimensions 1.0 m (D) × 1.0 m (W) × 1.0 m (H)] were measured at various heights of rise in the relatively tall atrium [of dimensions 2.0 m (D) × 1.0 m (W) × 2.5 m (H)]. In the series of tests, mass flow rates at the spill edge (the height of rise of plume = 0 m) were measured under various conditions. The geometry of models and results of each test in this study are given in Table 8.1. The study examined various sizes of downstand at the spill edge (ID #58~#63), which are treated here as fascia.

Data from the 1/10th physical scale experiments of Marshall and Harrison [1996] are also included for validation purposes. The air entrainment rates at the rotating region, M_s / M_b were taken from Series II-3 in Table 8.1 [atrium: 2.0 m (D) × 0.91 m (W) × 2.0 m (H)], and Series III-8 [atrium: 1.0 m (D) × 0.91m (W) × 2.0 m (H)]. Detailed descriptions of these models have been presented in the literature review.

Table 8.1 Parameter variation of small scale experiments by Harrison, Marshall and Harrison

ID	Q (kW)	Q_c (kW)	W (m)	h_{comp} (m)	D_f (m)	D_d (m)	l_b (m)	b (m)	b/h_{comp}	M_s/M_b
Harrison [2004]										
55	6	4.89	0.6	0.5	0	0	0.6	0.3	0.6	1.52
56	9	7.4	0.6	0.5	0	0	0.6	0.3	0.6	1.36
57	12	10.37	0.6	0.5	0	0	0.6	0.3	0.6	1.46
58	6	4.33	0.6	0.5	0	0.1	0.6	0.3	0.6	1.67
59	9	6.33	0.6	0.5	0	0.1	0.6	0.3	0.6	1.69
60	12	9.1	0.6	0.5	0	0.1	0.6	0.3	0.6	1.63
61	6	4.11	0.6	0.5	0	0.2	0.6	0.3	0.6	1.72
62	9	6.34	0.6	0.5	0	0.2	0.6	0.3	0.6	1.66
63	12	8.74	0.6	0.5	0	0.2	0.6	0.3	0.6	1.74
Marshall and Harrison [1996]										
II-3	21.1	16.3	0.91	0.59	0	0	0.91	0.2	0.508	1.4
III-8	10.1	8.09	0.91	0.59	0	0	0.91	0.2	0.508	1.4

where
W = the width of the opening
D_f = the depth of a fascia
D_d = the depth of downstand
l_b = the width of the balcony
b = the breadth of the balcony

Applying the empirical correlation developed in this study, results are plotted in Figure 8.13. Both results from Harrison and Marshall and Harrison appear to follow the empirical correlation.

The empirical correlation appears to predict the air entrainment rate of the flow emerging from the spill edge with a deep downstand, because the effect of the downstand is similar to that of the fascia, both reducing the momentum of the horizontal approach flow. This is consistent with the finding of Harrison [2004] that results from cases with downstand were correlated as a single data series with results from a flat ceiling.

The data of both Marshall and Harrison are found to be better correlated if the effective balcony breadths are properly considered, since the relatively lengthy flat

ceiling of the compartment can contribute to the velocity increase (Figure 2.6 Experimental configuration [Marshall and Harrison 1996])

In general, the empirical correlation is valid for a range of parameters (i.e., the balcony, downstand and door width, as well as compartment and atrium sizes).

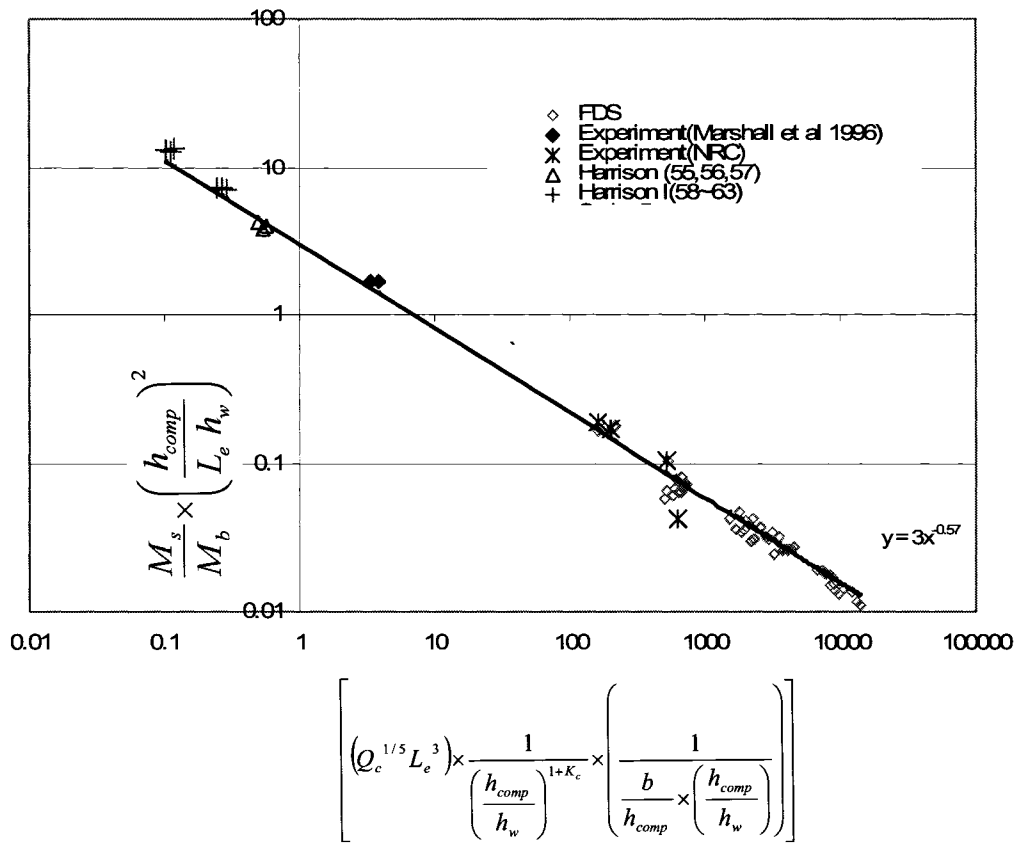

Figure 8.13 Validation of empirical correlation to parameter variation

8.5 *Empirical correlation of the mass flow rate at the spill edge*

An empirical correlation to estimate the mass flow rate at the spill edge is given below:

$$M_s = 3.0\left[\left(Q_c^{1/5} L_e^{3}\right) \times \frac{1}{\left(\frac{h_{comp}}{h_w}\right)^{1+K_c}} \times \left(\frac{1}{\left(\frac{b}{h_w}\right)}\right)\right]^{-0.57} \times \left(\frac{h_{comp}}{L_e\, h_w}\right)^{-2} \times M_b$$

$$, where \quad K_c = \frac{l_b}{W} \qquad (8.12)$$

M_b can be estimated by using the approximated constants from the upper limits of the constants in Equation 8.10.

$$\begin{aligned} M_b &\cong 1.15 M_w && , Case - NY \\ M_b &\cong 1.6 M_w && , Case - YY \\ M_b &\cong 1.4 M_w && , Case - NN \\ M_b &\cong 2.0 M_w && , Case - YN \end{aligned}$$

(8.13)

For channelled flow, Equation 8.11 can be used to calculate the mass flow rate at the end of the balcony, so the mass flow at the end of the balcony can be written as below:

$$M_b = 1.2 \times \left(\frac{h_{comp}}{h_w}\right)^{0.5} \times M_w \qquad (8.14)$$

The mass flow rate at the doorway (M_w) can be calculated using existing methods either by Morgan et al [1999], Thomas et al [1963] or Quintiere et al [1981].

8.5.1 Model limitations

This model predicts the air entrainment rate of the balcony spill plume at the spill edge. The model is not applicable to adhered plumes, and was originally developed only for entrainment rates of a buoyant jet, whose Ri is in the range of 0.14 to 0.7. The

model was developed for plumes that are not influenced by the boundaries of the atria.

9 Conclusion and Recommendation

The general agreement found for temperature as well as velocity profiles between FDS simulated results and experimental data allows the confident use of FDS simulation for the prediction of air entrainment rates under the balcony and in the rotating region.

Overall, for all parameter conditions, vertical spill plumes in the reservoir entrain a large amount of air compared to flows under the balcony. In general, for the same size of fire source and door width, the absence of draft curtains results in greater entrainment while a fascia appears to have little impact on entrainment rates.

In the rotating region, FDS simulated results show a large degree of air entrainment into the rotating flow, suggesting that there is additional entrainment due to irregular flow turbulent motion.

Simulated results of temperature were used to test the spill plume equation near the balcony area, which prove that the general spill plume correlation is valid near the balcony area. The results also show that the limiting height is at z = 0m, above which a linear spill plume function is valid up to the height of the domain used for the simulations. Thus, the initial mass flow rate of the spill plume should be measured at the edge of the balcony.

Existing models underestimate the air entrainment under the balcony and at the rotating region, while early methods of Morgan and Marshall al to calculate the amount of air entrainment estimate appreciably greater amounts of entrainments into the rotating flow.

Existing methods based on the layer depth and the virtual origin perform relatively well and can be used as engineering tools, if modified to consider additional entrainment at the rotating region.

This study sought a simple expression to estimate the initial mass flow rate at the balcony edge, based on evaluations of parameter effects, and attempts to avoid uncertain parameters of flow, such as temperature, velocity and layer depth at the end of the balcony. The simple correlation provides a general fit and succeeds in predicting entrainment rates under the balcony and in the rotating region. The correlation should be further validated using full-scale mass flow rate data, and an alternative form of the correlation can be sought by using existing spill plu well-established spill plume correlation

Recommendations for future work

In order to have a complete calculation method and an engineering guide for dealing with balcony spill plumes in the design of atrium smoke management systems, further study is desirable on the following areas:

1) The effect of atrium size on air entrainment: Complex atria and size of atria may affect air entrainment.
2) The effect of fire compartment size: The existing methods have not adequately addressed this issue.
3) The effect of geometric parameters: Parameters such as the breadth of the balcony, depth of fascia and length of balcony need to be studied in greater detail.

4) The effect of a sprinkler system in the fire compartment: The required capacity of a ventilation system in large atria can be adjusted if we know how the activation of sprinklers affects smoke generation and movement in the atrium.

5) The effectiveness of mechanical ventilation systems and natural ventilation systems: The most common smoke control system in atrium is mechanical ventilation. For tall atria, the amount of smoke that should be exhausted is large, and the effectiveness of mechanical ventilation system is questionable. It is necessary to verify these existing atrium smoke management systems under various conditions and explore alternative solutions for balcony spill plumes.

10 REFERENCES

Baum H R, McGrattan K B, Rehm R G. Large eddy simulations of smoke movement, Fire safety Journal V30, 1998.

Chow W K. CFD simulations on balcony spill plume. Journal of Fire Sciences, 16, 6, pp 468-485, 1998.

Chow W K. Numerical simulations on balcony spill plume. Fire and Materials, 23, 6, pp 91-99, 1999.

Chow W K, Li J. Simulation on natural smoke filling in atrium with a balcony spill plume. Journal of Fire Sciences, 19, 4, pp 258-277, 2001.

Gebhart B. Buoyancy-induced flows and transport, New York : Hemisphere Pub. Corp., 1988.

Harrison R. Smoke Control in Atrium Buildings: A Study of the Thermal Spill Plume (Master thesis) Department of Civil Engineering, University of Canterbury, July 2004.

Hansell G O. Heat and mass transfer process affecting smoke control in atrium buildings. PhD thesis, South Bank University, London, 1993.

Hansell G O. Morgan H P and Marshall N R. Smoke flow experiments in a model atrium. BRE Occasional Paper OP55, BRE, 1993.

International Code Council, Inc. International Building Code, Falls Church, VA, 2000.

Klote J H. An overview of atrium smoke management. Fire Protection Engineering, No 7, SFPE, pp 24-34, 2000.

Klote J H. Principles of smoke management, American Society of Heating, Refrigerating and Air-Conditioning Engineers Inc., 2002.

Law M. A note on smoke plumes from fires in multi-level shopping malls. Fire Safety Journal, 10, pp 197-202, 1986.

Law M. Measurements of balcony smoke flow. Fire Safety Journal, 24, pp 189-195, 1995.

Lee S, Emmons H W. A study of natural convection above a line fire. Journal of Fluid Mechanics, 11(3), pp 353-368, 1961.

Lougheed G D. Considerations in the Design of Smoke Management Systems for Atriums Construction Technology Update No. 48, Dec. 2000.

Lougheed G D, Hadjisophocleous G V. Smoke hazards from fires in high places ASHRAE Journal 2001.

Lougheed G D. Smoke Management Research at NRC, 2004.

Marshall N R, Harrison R. Experimental studies of thermal spill plumes. Building Research Establishment Occasional Paper, OP1, 1996.

McGrattan K B, Forney G P. Fire Dynamics Simulator (Version 4) - User Guide. NIST Special Publication 1019, National Institute of Technology and Standards, 2004.

McGrattan K B. Fire Dynamics Simulator (Version 4) - Technical Reference Guide. NIST Special Publication 1018, National Institute of Technology and Standards, 2004.

McWilliams J. Review of Airflow Measurement Techniques. LBNL-49747, Energy Performance of Buildings Group, Environmental Energy Technologies Division, Lawrence Berkeley National Laboratory, December 1, 2002.

Milke J A. Smoke management for covered malls and atria. Fire Technology, 26 (3), pp 223-243, 1990.

Milke J A. Smoke management in covered malls and atria. In: The SFPE Handbook of Fire Protection Engineering. Section 4/Chapter 13. DiNenno P J, Editor: 2002.

Miles S, Kumar S, Cox G. The balcony spill plume – Some CFD simulations. Fire Safety Science – Proceedings of the Fifth International Symposium, International Association of Fire Safety Science, pp 237-247, Melbourne, Australia. 1996.

Morgan H P, Marshall N R. Smoke hazards in covered multi-level shopping malls: an experimentally-based theory for smoke production. BRE Current Paper 48/75, BRE, 1975.

Morgan H P, Marshall N R. Smoke control measures in a covered two storey shopping mall having balconies and pedestrian walk ways. BRE Current paper 11/79, BRE, 1979.

Morgan H P. The horizontal flow of buoyant gases toward an opening. Fire Safety Journal, 11, pp 193-200, 1986.

Morgan H P, Hansell G O. Atrium buildings: calculating smoke flows in atria for smoke control design. Fire Safety Journal, 12, pp 9-35, 1987.

Morgan H P. Comments on "A note on smoke plumes from fires in multi-level shopping malls". Letters to the Editor, Fire Safety Journal, 12, pp 83-84, 1987.

Morgan H P, Ghosh B K, Garrad G, Pamlitschka R, De Smedt J-C and Schoonbaert L R. Design methodologies for smoke and heat exhaust ventilation. BRE Report 368, 1999.

National Fire Protection Association. Smoke management systems in malls, atria and large areas. 1991 edition. Publication No.92B. Quincy MA, USA, NFPA, 1991.

National Fire Protection Association. Smoke management systems in malls, atria and large areas. 2000 edition. Publication No.92B. Quincy MA, USA, NFPA, 2000.

Poreh M, Morgan H P, Marshall N R, Harrison R. Entrainment by two dimensional spill plumes in malls and atria. Fire Safety Journal, 30, pp 1-19, 1998.

Quintiere J G, Rinkinen W J, Jones W W. The effects of room openings on fire plume entrainment. Combustion Science and Technology, 26, pp 1983-201, 1981.

Thomas P H, Hinkley P L, Theobald C R, Simms D L. Investigations into the flow of hot gases in roof venting. Fire Research Technical Paper No 7, London, The Stationary Office, 1963.

Thomas P H. On the upward movement of smoke and related shopping mall problems. Fire Safety Journal, 12, pp 191-203, 1987.

Thomas P H, Morgan H P, Marshall N R. The spill plume in smoke control design. Fire Safety Journal, 30, pp 21-46, 1998.

Turner J S. Buoyancy effects in fluids. Publisher Cambridge [Eng.]: University Press, 1973.

Yokoi S. Study on the prevention of fire spread by hot upward current. Building Research Institute Report 34, Japan, 1960.

APPENDIX A. Code modification of FDS for calculating mass flow rate of smoke

1. MODS.F (data declaration)

```
---------- MODS.F
[111]  new data types "VALUEN,VALUEP" added
X,Y,Z,VALUE,VALUEN,VALUEP,DEPTH,DIAMETER,EMISSIVITY

[714] new FILE NUMBER "LU21=21,LU22=22" added
LU19=19,LU80=80,LU90=90,LU91=91,LU111=111,LU21=21,LU22=22
```

2. MAIN.F(main program)

```
[440]  CALL DUMP_N_TC(T_MIN)
[441]  CALL DUMP_P_TC(T_MIN)
[445]  THERMOCOUPLE(1:NTC)%VALUEN = 0.
[446]  THERMOCOUPLE(1:NTC)%VALUEP = 0.
```

3. DUMP.F(subroutine for writing and update thermocouple)

```
[3071]     REAL(EB) T,FLOW,FLOWN,FLOWP,HMFAC,DRAD,DTMP,
[3298]  FLOWN = 0.  (initialize)
[3315]  FLOWN = FLOWN + VEL*HMFAC*AREA
[3429]  TC%VALUEN = TC%VALUEN + FLOWN


[3297]  FLOWP = 0.
[3318]  FLOWP = FLOWP + VEL*HMFAC*AREA

[3310]
    SELECT CASE(IND)
    CASE(101:103) ;
     FLOW = FLOW + VEL*HMFAC*AREA
     if ( vel < 0 ) THEN
     FLOWN = FLOWN + VEL*HMFAC*AREA
     endif
     if ( vel > 0 ) THEN
     FLOWP = FLOWP + VEL*HMFAC*AREA
     endif
[3432]  TC%VALUEP = TC%VALUEP + FLOWP

-------------FILE WRITE(POSITIVE)------------
[148]     OPEN(LU21,FILE=FN21,FORM='FORMATTED',STATUS='OLD',RECL=5000,
[151]     OPEN(LU21,FILE=FN21,FORM='FORMATTED',STATUS='REPLACE',RECL=5000)
[152]     WRITE(LU21,'(I5)') NTC
[154]     WRITE(LU21,TCFORM) 'TIME',(TRIM(THERMOCOUPLE(N)%LABEL),N=1,NTC)
[156]     WRITE(LU21,TCFORM) 'TIME',
[159]     WRITE(LU21,TCFORM) 's',
[3490]     WRITE(LU21,TCFORM) T,(THERMOCOUPLE(N)%VALUEN/

----------------FILE WRITE(NEGATIVE)--------------
170]     OPEN(LU22,FILE=FN22,FORM='FORMATTED',STATUS='OLD',RECL=5000,
[173]     OPEN(LU22,FILE=FN22,FORM='FORMATTED',STATUS='REPLACE',RECL=5000)
[174]     WRITE(LU22,'(I5)') NTC
```

```
[176]   WRITE(LU22,TCFORM) 'TIME',(TRIM(THERMOCOUPLE(N)%LABEL),N=1,NTC)
[178]   WRITE(LU22,TCFORM) 'TIME',
[181]   WRITE(LU22,TCFORM) 's',
[3507]   WRITE(LU22,TCFORM) T,(THERMOCOUPLE(N)%VALUEP/
```

APPENDIX B. Example FDS input data

Simple modelling study

```
//Domain Test -Blow model, NOMirror
//evaluated temp and vel from 5 MW12NN --- Temp : 245'C
//                                        U-Vel : 2.22m/s
//                                        LayerDepth : 2m
//                                        Door Size : 12m
//                                        GridSize : 0.5m
//                                        Domain Size : Nsize ( 16.8, 20, 10)

&HEAD CHID='domainT-N',TITLE='domainT-N'/
&GRID IBAR=34, JBAR=40, KBAR=20/
&TIME TWFIN=300./5min
&MISC DATABASE='/jbod2/home/yko/database4/database4.data'/
//&MISC DATABASE='/site/home/yko/database3/database3.data'/

&PDIM XBAR0=0.000, XBAR= 16.8, YBAR0=-10, YBAR=10, ZBAR0= 0.000, ZBAR= 10.000/
//BLOWER/
&SURF ID='BLOWER', VEL=-2.22, TMPWAL=245, RGB=0.0, 1.0, 0.0/
//COMPUTATIONAL DOMAIN//
&VENT CB='ZBAR0', SURF_ID='CONCRETE'/floor
&VENT CB='ZBAR', SURF_ID='OPEN'/atriumceiling
&VENT CB='XBAR0', SURF_ID='OPEN'/
&VENT CB='XBAR',  SURF_ID='OPEN'/
&VENT CB='YBAR0', SURF_ID='OPEN'/centre
&VENT CB='YBAR', SURF_ID='OPEN'/
&VENT XB=0.000, 0.000, 6.00, 10.000, 0.000, 4.985/back
&VENT XB=0.000, 0.000, -6.00, -10.000, 0.000, 4.985/back
&VENT XB=0.000, 0.000, -10, 10.000, 4.985, 10.000, SURF_ID='OPEN'/ obove rm back

//DOOR-DOWNSTAND door centre point ( 0.0, (0.0), 0.0)  W=12, H=full=4.985/
&VENT XB=0.000, 0.000, -6, 6, 2.985, 4.985, SURF_ID='BLOWER'/door width 6m no fascia layerDepth 2m
&VENT XB=0.000, 0.000, -6, 6, 0.000, 2.985, SURF_ID='OPEN'/door width 12m no fascia

&OBST XB= 0.000, 4.195, -10.000, 10.000, 4.985, 5.085/ceiling+balcony:4.195

&THCP XB=0.000, 0.000, -6, 6.0 , 2.985, 4.985, QUANTITY='MASS FLOW', LABEL='@door through'/
&THCP XB=1.000, 1.000, -10, 10.0, 0.0, 4.985, QUANTITY='MASS FLOW', LABEL='x=1.0'/
&THCP XB=2.000, 2.000, -10, 10.0, 0.0, 4.985, QUANTITY='MASS FLOW', LABEL='x=2.0'/
&THCP XB=3.000, 3.000, -10, 10.0, 0.0, 4.985, QUANTITY='MASS FLOW', LABEL='x=3.0'/
&THCP XB=4.195, 4.195, -10, 10.0, 0.0, 4.985, QUANTITY='MASS FLOW', LABEL='x=4.2'/

&THCP XB=4.195, 16.8, -10.0, 10.0, 4.985, 4.985, QUANTITY='MASS FLOW', LABEL='z=0'/
&THCP XB=4.195, 16.8, -10.0, 10.0, 9.000, 9.000, QUANTITY='MASS FLOW', LABEL='z=4'/
&THCP XB=4.195, 16.8, -10.0, 10.0, 10.00, 10.00, QUANTITY='MASS FLOW', LABEL='z=5'/


&SLCF PBY=0.000,QUANTITY='VELOCITY' /centre of the atrium
&SLCF PBY=0.000,QUANTITY='U-VELOCITY' /
&SLCF PBY=0.000,QUANTITY='V-VELOCITY' /
&SLCF PBY=0.000,QUANTITY='W-VELOCITY' /
&SLCF PBY=0.000,QUANTITY='TEMPERATURE'/
&SLCF PBY=0.000,QUANTITY='DENSITY'/
&SLCF PBY=0.000,QUANTITY='PRESSURE' /
```

```
//Temp-Vel Test -Blow model, Mirror
//      Temp : 197'C
//      U-Vel : 2.65m/s
//      LayerDepth : 2m
//      Door Size  : 5m
//GridSize : 0.25m
//Domain Size : Nsize ( 16.8, 20, 10)


&HEAD CHID='TV3',TITLE='TV3'/

&GRID IBAR=68, JBAR=40, KBAR=40/
&TIME TWFIN=300./5min
//&MISC DATABASE='/jbod2/home/yko/database4/database4.data'/
&MISC DATABASE='/site/home/yko/database3/database3.data'/

&PDIM XBAR0=0.000, XBAR= 16.8, YBAR0=0, YBAR=10, ZBAR0= 0.000, ZBAR= 10.000/

//BLOWER/
&SURF ID='BLOWER', VEL=-2.65, TMPWAL=197, RGB=0.0, 1.0, 0.0/
//COMPUTATIONAL DOMAIN//
&VENT CB='ZBAR0', SURF_ID='CONCRETE'/floor
&VENT CB='ZBAR', SURF_ID='OPEN'/atriumceiling
/&VENT CB='XBAR0', SURF_ID='OPEN'/
&VENT CB='XBAR',  SURF_ID='OPEN'/
&VENT CB='YBAR0', SURF_ID='MIRROR'/centre
&VENT CB='YBAR', SURF_ID='OPEN'/
&VENT XB=0.000, 0.000, 2.5, 10.000, 0.000, 4.985/back
&VENT XB=0.000, 0.000, 0, 10.000, 4.985, 10.000, SURF_ID='OPEN'/ above rm back

//DOOR-fascia door centre point ( 0.0, (0.0), 0.0)  W=5, H=full=4.985/
&VENT XB=0.000, 0.000, 0, 2.5, 2.985, 4.985/
&VENT XB=0.000, 0.000, 0, 2.5, 0.000, 2.985, SURF_ID='OPEN'/door width 5m no fascia
&OBST XB= 0.000, 4.195, 0.000, 2.5, 2.985, 4.985/
&VENT XB= 4.195, 4.195, 0.000, 2.5, 2.985, 4.985,SURF_ID='BLOWER'/
&OBST XB= 0.000, 4.195, 0.000, 10.000, 4.985, 5.085/ceiling+balcony:4.195_______
//DRAFT CURTAIN//
&OBST XB=0.000, 4.195, 2.5, 2.7, 1.985, 4.985/draft curtain 3m


&THCP XB=4.195, 4.195, 0, 2.5, 0.0, 4.985, QUANTITY='MASS FLOW', LABEL='x=4.2'/
&THCP XB=0.00, 16.8, 0.0, 10.0, 4.985, 4.985, QUANTITY='MASS FLOW', LABEL='z=0'/
&THCP XB=0.00, 16.8, 0.0, 10.0, 6.0, 6.0, QUANTITY='MASS FLOW', LABEL='z=1'/
&THCP XB=0.00, 16.8, 0.0, 10.0, 7.0, 7.0, QUANTITY='MASS FLOW', LABEL='z=2'/
&THCP XB=0.00, 16.8, 0.0, 10.0, 8.0, 8.0, QUANTITY='MASS FLOW', LABEL='z=3'/
&THCP XB=0.00, 16.8, 0.0, 10.0, 9.000, 9.000, QUANTITY='MASS FLOW', LABEL='z=4'/
&THCP XB=0.00, 16.8, 0.0, 10.0, 10.00, 10.00, QUANTITY='MASS FLOW', LABEL='z=5'/

&SLCF PBY=0.000,QUANTITY='VELOCITY' /centre of the atrium
&SLCF PBY=0.000,QUANTITY='U-VELOCITY' /
&SLCF PBY=0.000,QUANTITY='V-VELOCITY' /
&SLCF PBY=0.000,QUANTITY='W-VELOCITY' /
&SLCF PBY=0.000,QUANTITY='TEMPERATURE'/
&SLCF PBY=0.000,QUANTITY='DENSITY'/
&SLCF PBY=0.000,QUANTITY='PRESSURE' /
```

CFD modelling of the balcony spill plume

```
///////Balconly spill plume –focused on under the balcony area-///////////

&HEAD
CHID='S2M12YY',TITLE='S2M12YY'/*********************************************************

&GRID IBAR=116, JBAR=40, KBAR=52/
&TIME TWFIN=400/5min
&MISC DATABASE='/jbod2/home/yko/database4/database4.data',DTCORE=390./
//&MISC DATABASE='/site/home/yko/database3/database3.data'/
//&MISC DATABASE='c:\nist\fds\database4\database4.data'/

// DOMAIN SIZE  23.17*20.00*9.97
&PDIM XBAR0= -6.09, XBAR= 16.78, YBAR0= 0.000, YBAR= 10.000, ZBAR0= 0.000, ZBAR= 9.97/

&TRNX CC=-1.36, PC=0.0, MESH_NUMBER=1/
&TRNX CC=9.09, PC=6.6,    MESH_NUMBER=1/
&TRNZ CC=2.3, PC=3, MESH_NUMBER=1/
&TRNZ CC=6.9, PC=6, MESH_NUMBER=1/

//COMPUTATIONAL DOMAIN//
&VENT CB='ZBAR0', SURF_ID='CONCRETE'/floor
&VENT CB='ZBAR', SURF_ID='OPEN'/atriumceiling
&VENT CB='XBAR0', SURF_ID='OPEN'/
&VENT CB='XBAR',  SURF_ID='OPEN'/
&VENT CB='YBAR0', SURF_ID='MIRROR'/
&VENT CB='YBAR', SURF_ID='OPEN'/

//fire4*250kw=2Mw/*****************************************************************************
******
&SURF ID='BURNER', HRRPUA=500, RGB=1,0,0/
//FIRE     fire centre point (-2.520, 0.0, 0.4572)4*500=2M//*****************************************

&OBST XB=-3.52, -1.52, -1.0, 1.0, 0.4572, 0.4572, SURF_IDS='BURNER', 'INERT', 'INERT'/

//FIRE COMPARTMENT//
&OBST XB= -5.040, 0.000, -6.800, -6.645, 0.000, 4.985/ left wall
&OBST XB= -5.040, 0.000, 6.645, 6.800, 0.000, 4.985/ right wall
&OBST XB= -5.140, 4.195, -6.800, 6.800, 4.985, 5.110/ceiling+balcony:4.195
&OBST XB= -5.140, -5.040, -6.800, 6.800, 0.000, 4.985/  rear wall
&OBST XB= -0.120, 0.000, -6.645, 6.645, 0.000, 4.985/ front wall

//DOOR-FASCIA door centre point ( 0.0, (0.0), 0.0)  W=12m, H=full=4.985/*****************************
&HOLE XB=-0.121, 0.001, -6.0, 6.0, 0.0, 3.385/door width 12m YES-FASCIA*******************************

//DRAFT CURTAIN//
&OBST        XB=0.000,        4.195,        -6.13,        -6.0,        1.985,        4.985/draft        curtain
3m*****************************************
&OBST        XB=0.000,        4.195,        6.0,        6.13,        1.985,        4.985/draft        curtain
3m*********************************************

&THCP XB=0.000, 0.000, -6.0, 6.0, 0.0, 3.385, QUANTITY='MASS FLOW', LABEL='@Door'/

&THCP XB=1.000, 1.000, -10.000, 10.000, 0.0, 4.985, QUANTITY='MASS FLOW', LABEL='@X=1.0'/
&THCP XB=2.000, 2.000, -10.000, 10.000, 0.0, 4.985, QUANTITY='MASS FLOW', LABEL='@X=2.0'/
&THCP XB=3.000, 3.000, -10.000, 10.000, 0.0, 4.985, QUANTITY='MASS FLOW', LABEL='@X=3.0'/
&THCP XB=4.195, 4.195, -10.000, 10.000, 0.0, 4.985, QUANTITY='MASS FLOW', LABEL='@X=4.2'/
```

```
&THCP XB=1.000, 1.000, -6.000, 6.000, 0.0, 4.985, QUANTITY='MASS FLOW', LABEL='@UB X=1.0'/
&THCP XB=2.000, 2.000, -6.000, 6.000, 0.0, 4.985, QUANTITY='MASS FLOW', LABEL='@UB X=2.0'/
&THCP XB=3.000, 3.000, -6.000, 6.000, 0.0, 4.985, QUANTITY='MASS FLOW', LABEL='@UB X=3.0'/
&THCP XB=4.195, 4.195, -6.000, 6.000, 0.0, 4.985, QUANTITY='MASS FLOW', LABEL='@UB X=4.2'/

&THCP XB=4.195, 16.78, -6.800, 6.800, 4.985, 4.985, QUANTITY='MASS FLOW', LABEL='@z' =0m'/

&THCP XB=4.195, 16.78, -10.000, 10.000, 4.985, 4.985, QUANTITY='MASS FLOW', LABEL='@z=0m'/
&THCP XB=4.195, 16.78, -10.000, 10.000, 6.00, 6.000, QUANTITY='MASS FLOW', LABEL='@z=1m'/
&THCP XB=4.195, 16.78, -10.000, 10.000, 7.0, 7.0, QUANTITY='MASS FLOW', LABEL='@z=2m'/
&THCP XB=4.195, 16.78, -10.000, 10.000, 8.0, 8.0, QUANTITY='MASS FLOW', LABEL='@z=3m'/
&THCP XB=4.195, 16.78, -10.000, 10.000, 9.0, 9.0, QUANTITY='MASS FLOW', LABEL='@z=4m'/
&THCP XB=4.195, 16.78, -10.000, 10.000, 9.97, 9.97, QUANTITY='MASS FLOW', LABEL='@z=5m'/

&THCP XYZ=-0.5, 0, 4.9, QUANTITY='TEMPERATURE', Label='Tc'/
&THCP XYZ=  0, 0, 3.2, QUANTITY='TEMPERATURE', Label='Tw'/
&THCP XYZ= 4.0, 0, 4.9, QUANTITY='TEMPERATURE', Label='Tb'/

&ISOF QUANTITY='MIXTURE_FRACTION', VALUE(1)=0.05, VALUE(2)=0.001/smoke isosurf

&SLCF PBY=0.00,QUANTITY='VELOCITY' /center line
&SLCF PBY=0.00,QUANTITY='U-VELOCITY' /
&SLCF PBY=0.00,QUANTITY='V-VELOCITY' /
&SLCF PBY=0.00,QUANTITY='W-VELOCITY' /
&SLCF PBY=0.00,QUANTITY='TEMPERATURE'/
&SLCF PBY=0.00,QUANTITY='DENSITY'/
&SLCF PBY=0.00,QUANTITY='PRESSURE' /

&SLCF PBY=3.0,QUANTITY='VELOCITY' /
&SLCF PBY=3.0,QUANTITY='U-VELOCITY' /
&SLCF PBY=3.0,QUANTITY='V-VELOCITY' /
&SLCF PBY=3.0,QUANTITY='W-VELOCITY' /
&SLCF PBY=3.0,QUANTITY='TEMPERATURE'/
&SLCF PBY=3.0,QUANTITY='DENSITY'/
&SLCF PBY=3.0,QUANTITY='PRESSURE' /

&SLCF PBX=0.000,QUANTITY='VELOCITY' /door through
&SLCF PBX=0.000,QUANTITY='U-VELOCITY' /
&SLCF PBX=0.000,QUANTITY='V-VELOCITY' /
&SLCF PBX=0.000,QUANTITY='W-VELOCITY' /
&SLCF PBX=0.000,QUANTITY='TEMPERATURE'/
&SLCF PBX=0.000,QUANTITY='DENSITY'/
&SLCF PBX=0.000,QUANTITY='PRESSURE' /

&SLCF PBX=1.000,QUANTITY='VELOCITY' /under balcony@1.0
&SLCF PBX=1.000,QUANTITY='U-VELOCITY' /
&SLCF PBX=1.000,QUANTITY='V-VELOCITY' /
&SLCF PBX=1.000,QUANTITY='W-VELOCITY' /
&SLCF PBX=1.000,QUANTITY='TEMPERATURE'/
&SLCF PBX=1.000,QUANTITY='DENSITY'/
&SLCF PBX=1.000,QUANTITY='PRESSURE' /

&SLCF PBX=2.000,QUANTITY='VELOCITY' /under balcony@2.0
&SLCF PBX=2.000,QUANTITY='U-VELOCITY' /
&SLCF PBX=2.000,QUANTITY='V-VELOCITY' /
&SLCF PBX=2.000,QUANTITY='W-VELOCITY' /
&SLCF PBX=2.000,QUANTITY='TEMPERATURE'/
&SLCF PBX=2.000,QUANTITY='DENSITY'/
&SLCF PBX=2.000,QUANTITY='PRESSURE' /
```

```
&SLCF PBX=3.000,QUANTITY='VELOCITY' /under balcony@3.0
&SLCF PBX=3.000,QUANTITY='U-VELOCITY' /
&SLCF PBX=3.000,QUANTITY='V-VELOCITY' /
&SLCF PBX=3.000,QUANTITY='W-VELOCITY' /
&SLCF PBX=3.000,QUANTITY='TEMPERATURE'/
&SLCF PBX=3.000,QUANTITY='DENSITY'/
&SLCF PBX=3.000,QUANTITY='PRESSURE' /

&SLCF PBX=4.2,QUANTITY='VELOCITY' /under balcony@4.2
&SLCF PBX=4.2,QUANTITY='U-VELOCITY' /
&SLCF PBX=4.2,QUANTITY='V-VELOCITY' /
&SLCF PBX=4.2,QUANTITY='W-VELOCITY' /
&SLCF PBX=4.2,QUANTITY='TEMPERATURE'/
&SLCF PBX=4.2,QUANTITY='DENSITY'/
&SLCF PBX=4.2,QUANTITY='PRESSURE' /

//upward spill plume//
&SLCF PBZ=5,QUANTITY='VELOCITY' /horizontal - ceiling level
&SLCF PBZ=5,QUANTITY='U-VELOCITY' /
&SLCF PBZ=5,QUANTITY='V-VELOCITY' /
&SLCF PBZ=5,QUANTITY='W-VELOCITY' /
&SLCF PBZ=5,QUANTITY='TEMPERATURE'/
&SLCF PBZ=5,QUANTITY='DENSITY'/
&SLCF PBZ=5,QUANTITY='PRESSURE' /

&SLCF PBZ=6.00,QUANTITY='VELOCITY' /horizontal - ceiling level
&SLCF PBZ=6.00,QUANTITY='U-VELOCITY' /
&SLCF PBZ=6.00,QUANTITY='V-VELOCITY' /
&SLCF PBZ=6.00,QUANTITY='W-VELOCITY' /
&SLCF PBZ=6.00,QUANTITY='TEMPERATURE'/
&SLCF PBZ=6.00,QUANTITY='DENSITY'/
&SLCF PBZ=6.00,QUANTITY='PRESSURE' /

&SLCF PBZ=7.00,QUANTITY='VELOCITY' /horizontal - ceiling level
&SLCF PBZ=7.00,QUANTITY='U-VELOCITY' /
&SLCF PBZ=7.00,QUANTITY='V-VELOCITY' /
&SLCF PBZ=7.00,QUANTITY='W-VELOCITY' /
&SLCF PBZ=7.00,QUANTITY='TEMPERATURE'/
&SLCF PBZ=7.00,QUANTITY='DENSITY'/
&SLCF PBZ=7.00,QUANTITY='PRESSURE' /

&SLCF PBZ=8.00,QUANTITY='VELOCITY' /horizontal - ceiling level
&SLCF PBZ=8.00,QUANTITY='U-VELOCITY' /
&SLCF PBZ=8.00,QUANTITY='V-VELOCITY' /
&SLCF PBZ=8.00,QUANTITY='W-VELOCITY' /
&SLCF PBZ=8.00,QUANTITY='TEMPERATURE'/
&SLCF PBZ=8.00,QUANTITY='DENSITY'/
&SLCF PBZ=8.00,QUANTITY='PRESSURE' /

&SLCF PBZ=9.00,QUANTITY='VELOCITY' /horizontal - ceiling level
&SLCF PBZ=9.00,QUANTITY='U-VELOCITY' /
&SLCF PBZ=9.00,QUANTITY='V-VELOCITY' /
&SLCF PBZ=9.00,QUANTITY='W-VELOCITY' /
&SLCF PBZ=9.00,QUANTITY='TEMPERATURE'/
&SLCF PBZ=9.00,QUANTITY='DENSITY'/
&SLCF PBZ=9.00,QUANTITY='PRESSURE' /

&SLCF PBZ=9.97,QUANTITY='VELOCITY' /horizontal - ceiling level
&SLCF PBZ=9.97,QUANTITY='U-VELOCITY' /
```

```
&SLCF PBZ=9.97,QUANTITY='V-VELOCITY' /
&SLCF PBZ=9.97,QUANTITY='W-VELOCITY' /
&SLCF PBZ=9.97,QUANTITY='TEMPERATURE'/
&SLCF PBZ=9.97,QUANTITY='DENSITY'/
&SLCF PBZ=9.97,QUANTITY='PRESSURE' /
```

APPENDIX C. Comparison of FDS predictions with experimental data

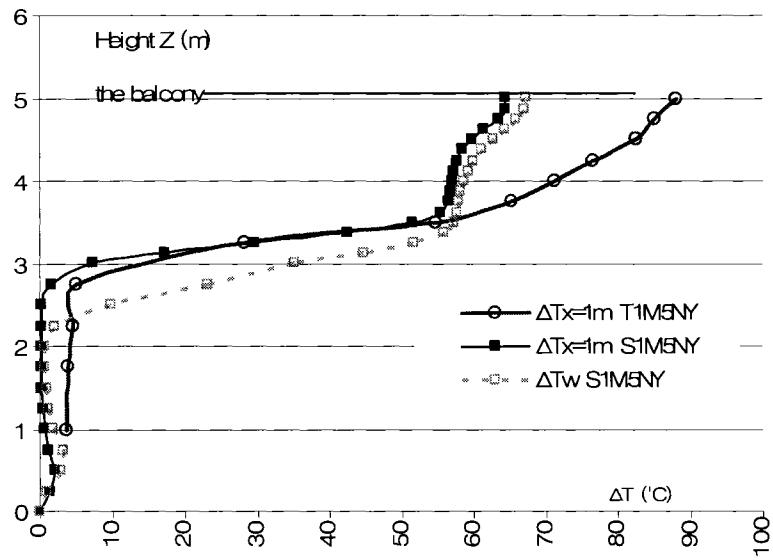

Fig 1 Temperature rise profiles at the opening (S1M5NY and T1MTNY)

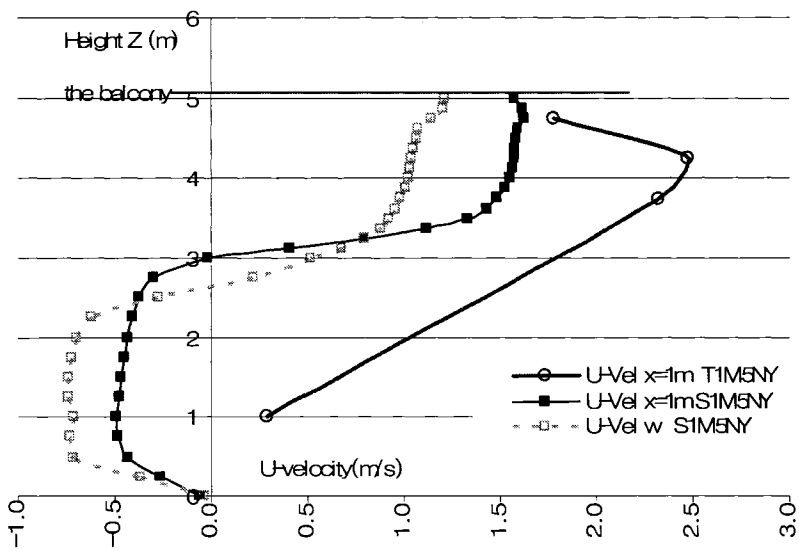

Fig 2 U-Velocity profiles at the compartment opening (S1M5NY and T1MTNY)

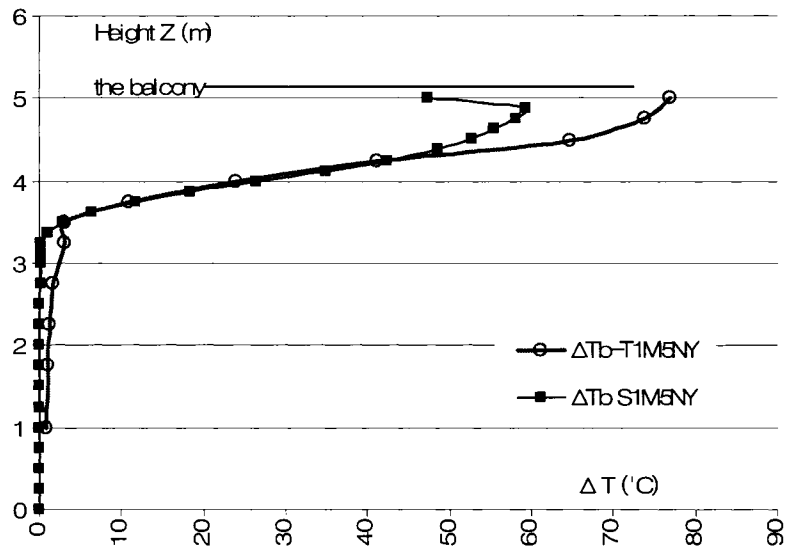

Fig 3 Temperature rise profiles at the balcony end (S1M5NY and T1MTNY)

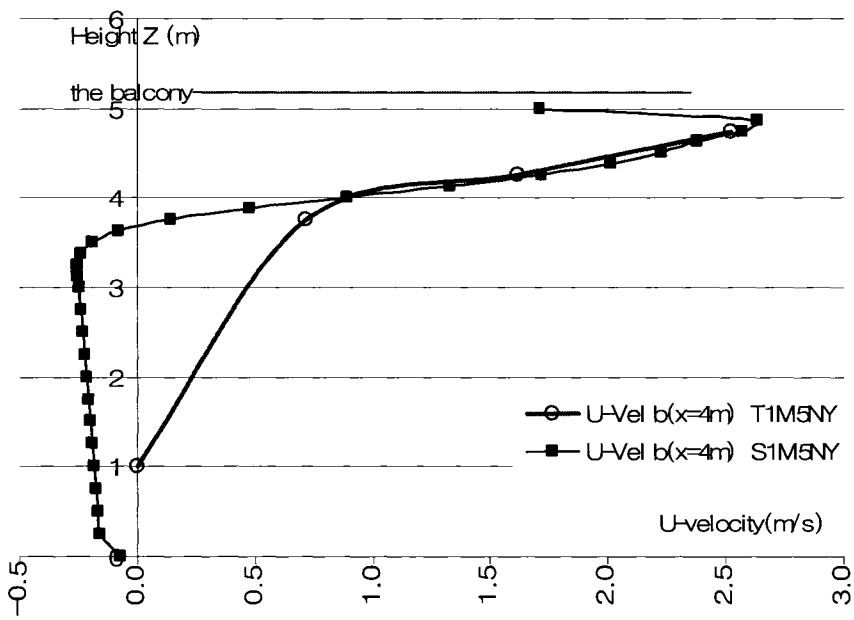

Fig 4 U- Velocity profiles at the balcony end (S1M5NY and T1MTNY)

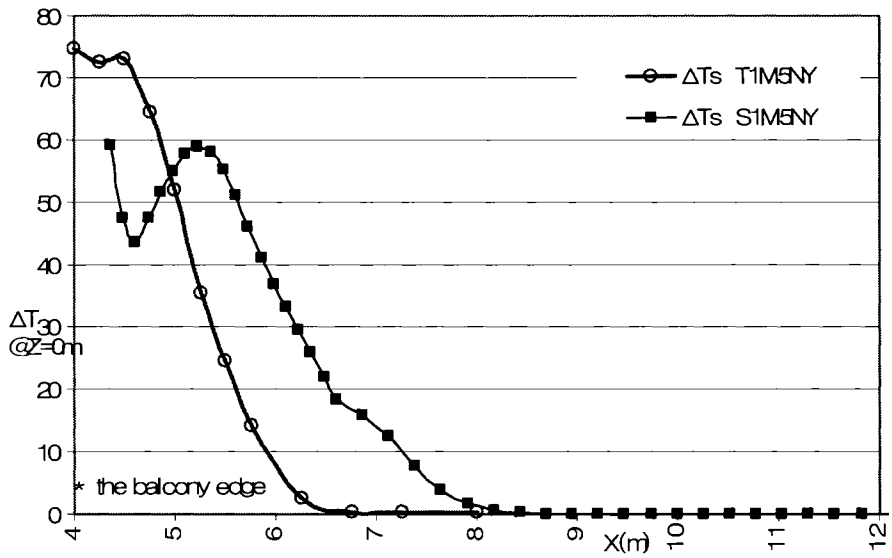

Fig 5 Temperature rise profiles at the balcony edge (S1M5NY and T1MTNY)

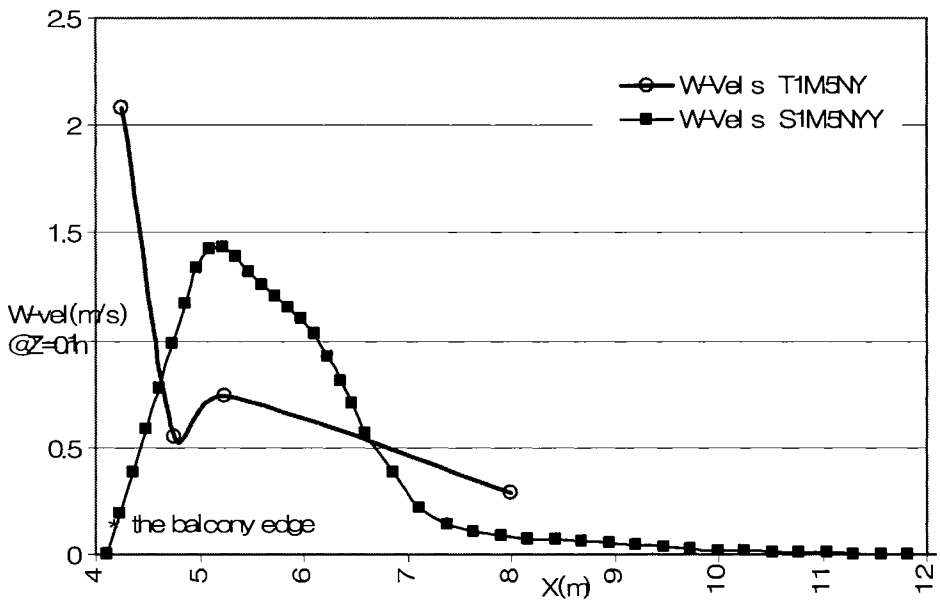

Fig 6 W-Velocity profiles of the vertical spill plume at the balcony edge (z=0m) (S1M5NY and T1MTNY)

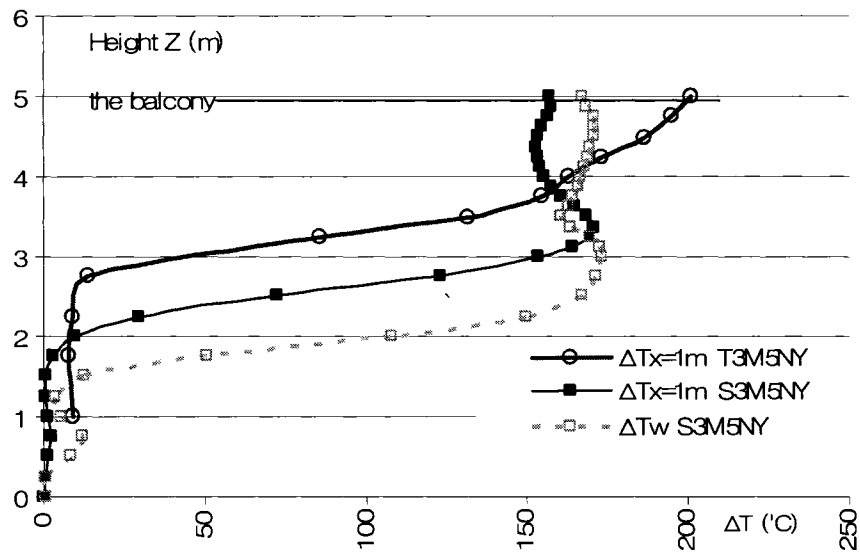

Fig 7 Temperature rise profiles at the opening (S3M5NY and T3M5NY)

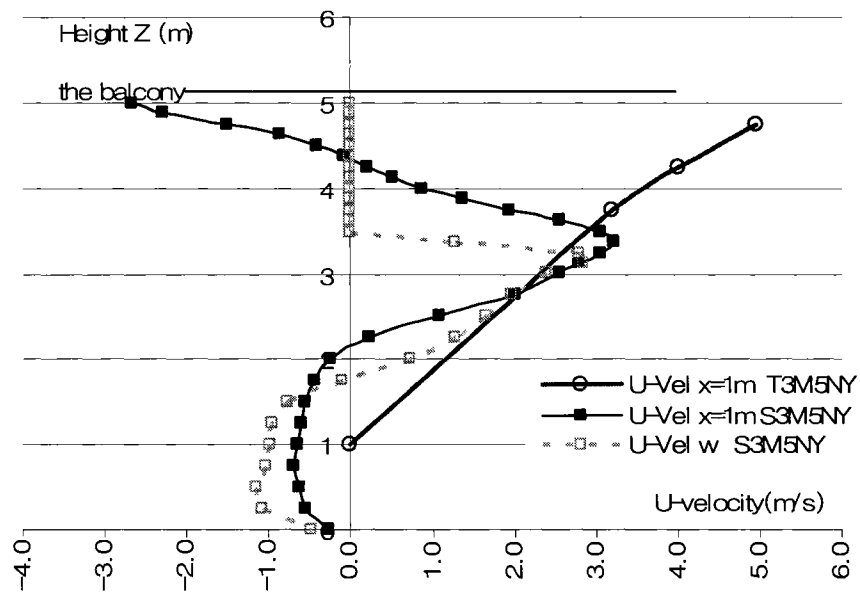

Fig 8 U -Velocity profiles at the opening (S3M5NY and T3M5NY)

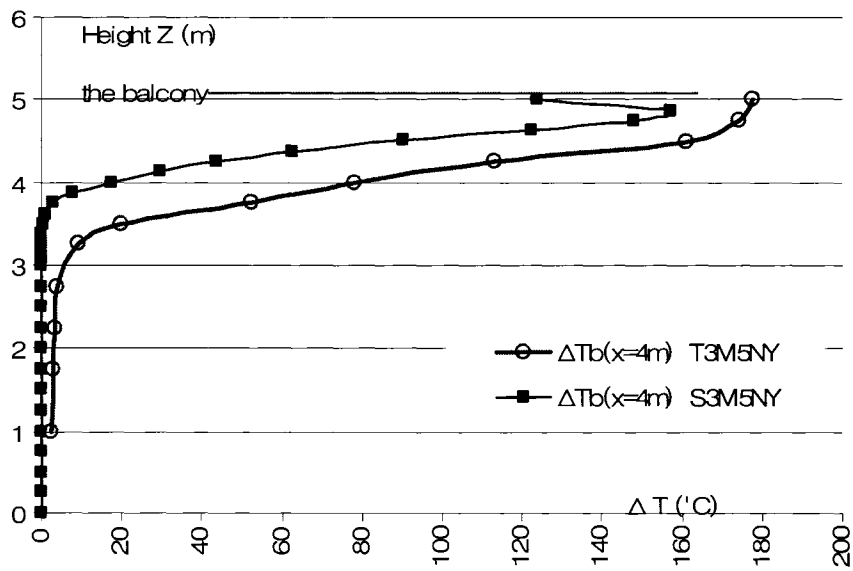

Fig 9 Temperature rise profiles at the end of the balcony (S3M5NY and T3M5NY)

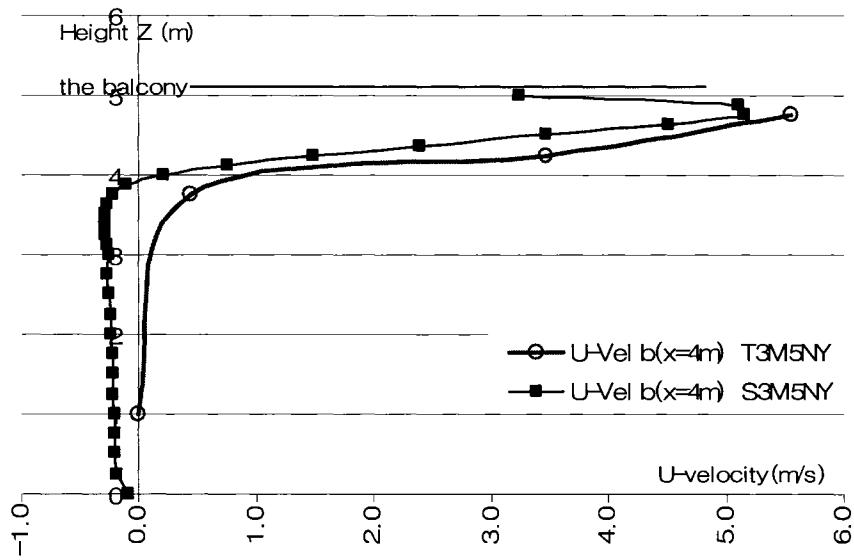

Fig 10 U-Velocity profiles at the end of the balcony (S3M5NY and T3M5NY)

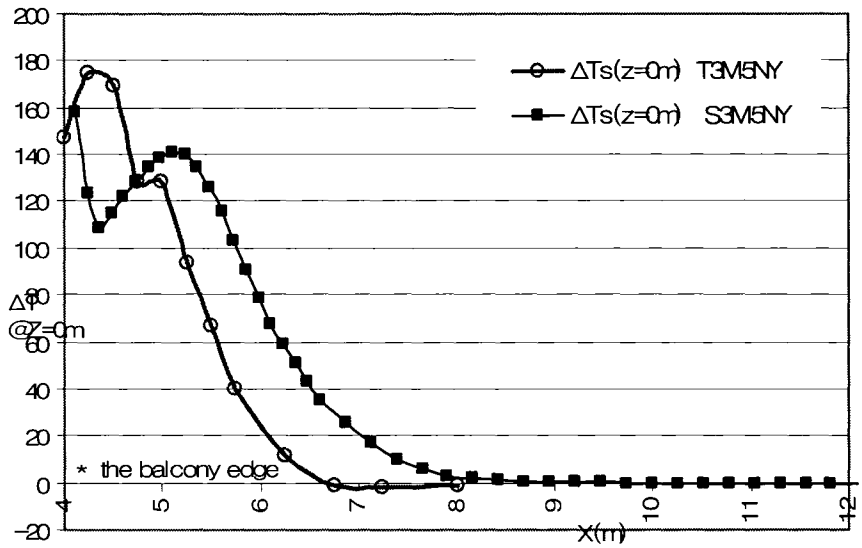

Fig 11 Temperature rise profiles at the balcony edge (S3M5NY and T3M5NY)

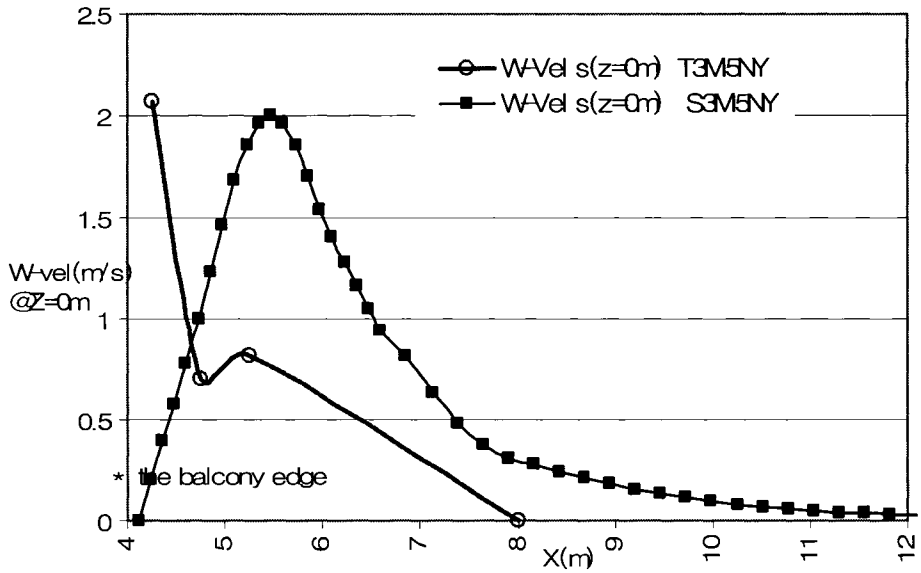

Fig 12 W-Velocity profiles at the balcony edge (S3M5NY and T3M5NY)

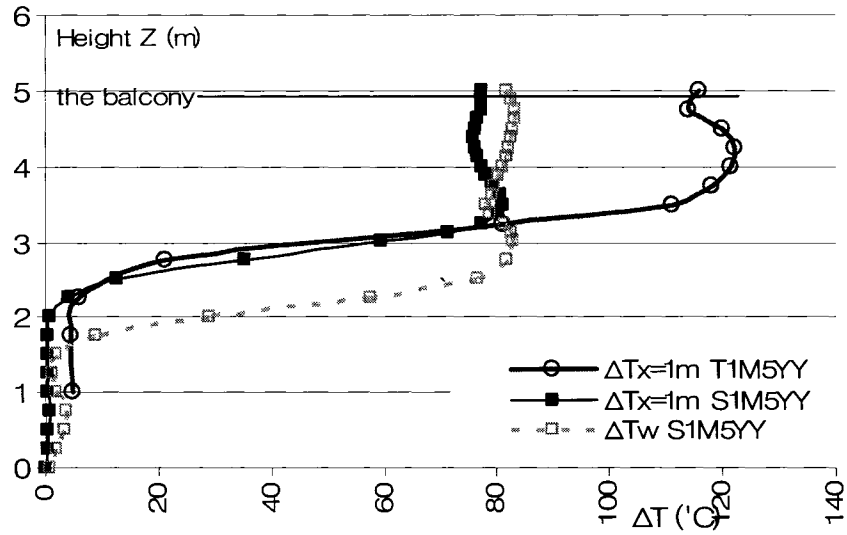

Fig 13 Temperature rise profiles at the opening (S1M5YY and T1M5YY)

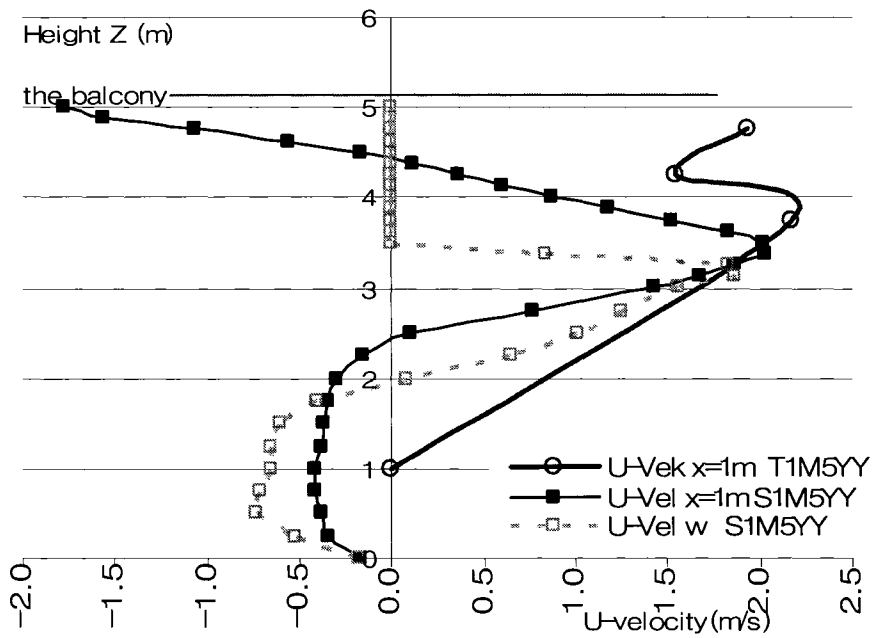

Fig 14 U-Velocity profiles at the opening (S1M5YY and T1M5YY)

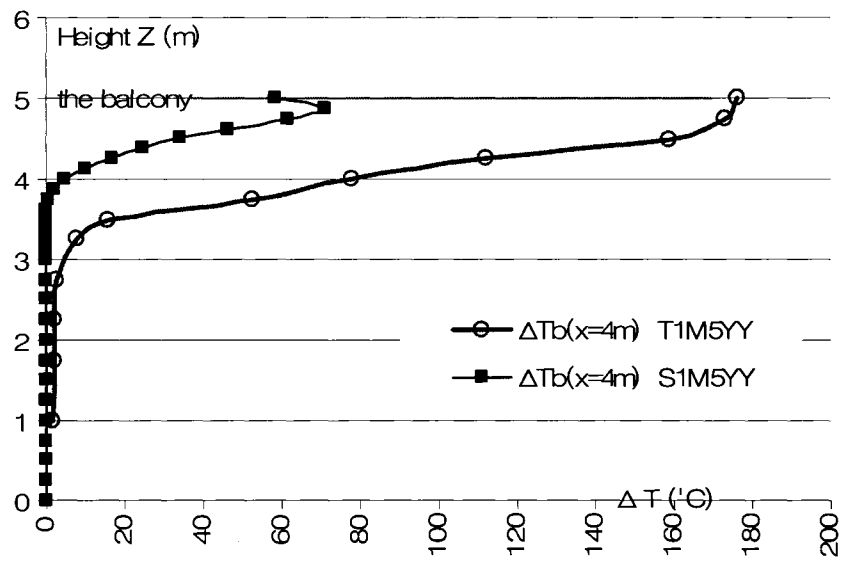

Fig 15 Temperature rise profiles at the end of the balcony (S1M5YY and T1M5YY)

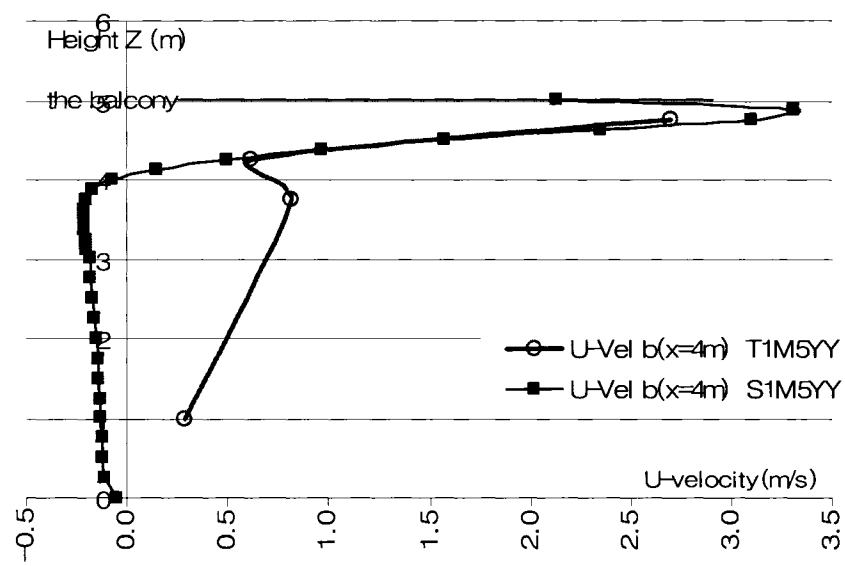

Fig 16 U-Velocity profiles at the end of the balcony (S1M5YY and T1M5YY)

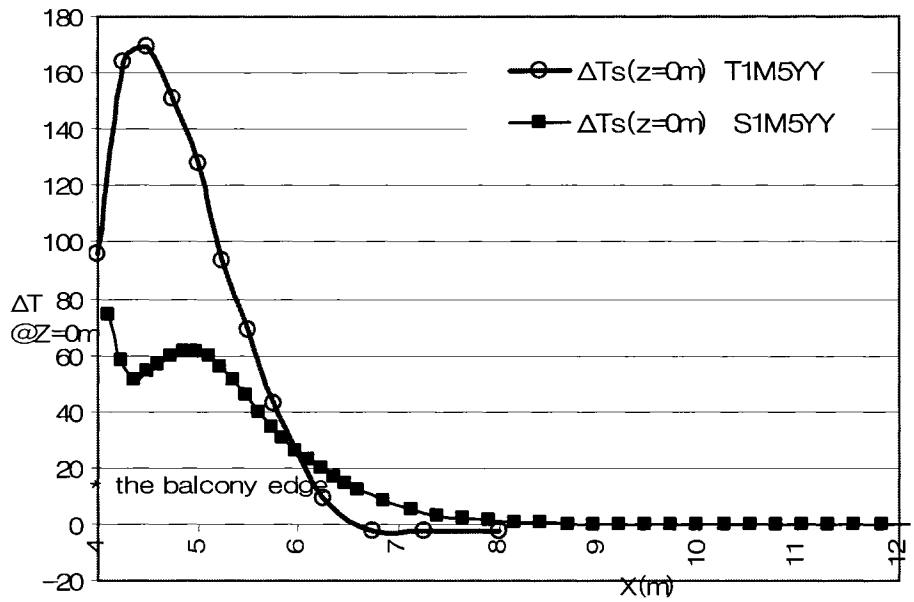

Fig 17 Temperature rise profiles at the edge of the balcony (S1M5YY and T1M5YY)

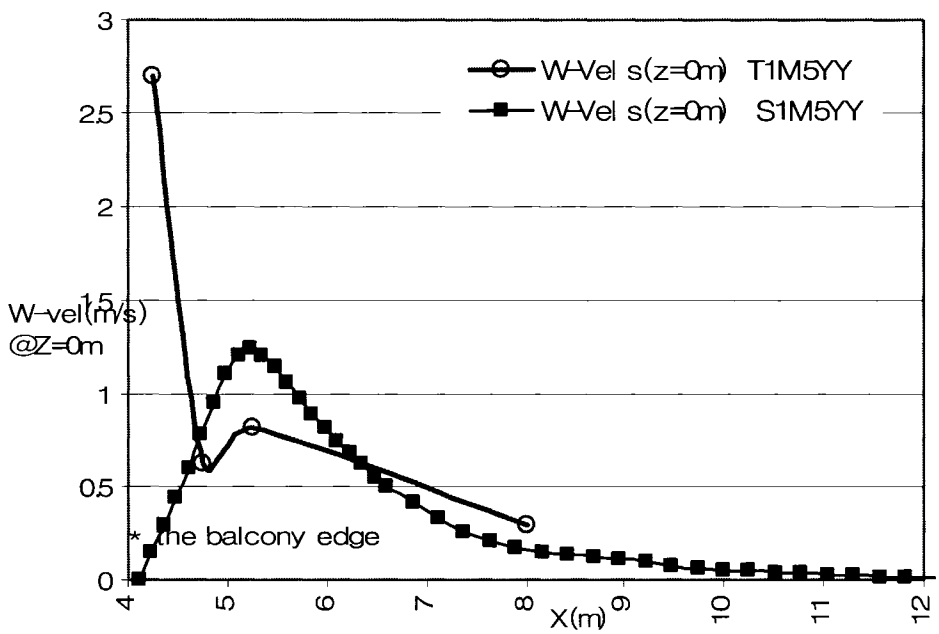

Fig 18 W-Velocity profiles at the edge of the balcony (S1M5YY and T1M5YY)

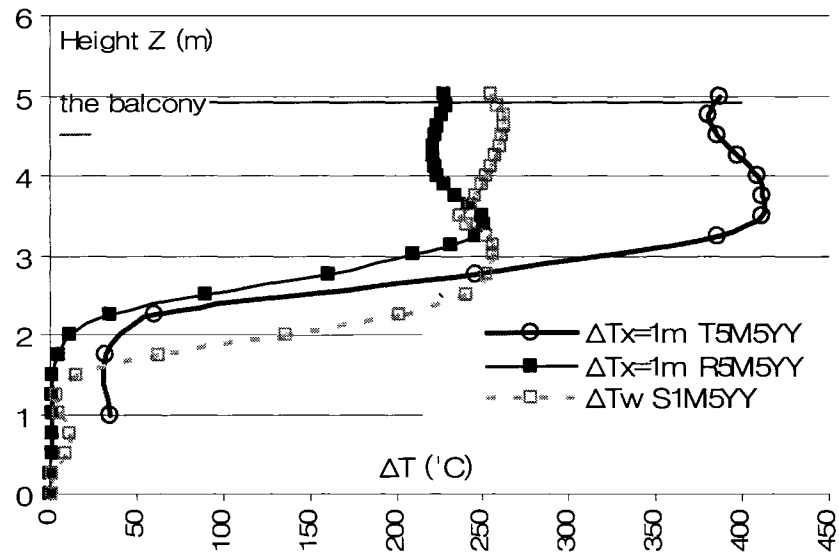

Fig 19 Temperature rise profiles at the opening (R5M5YY and T5M5YY)

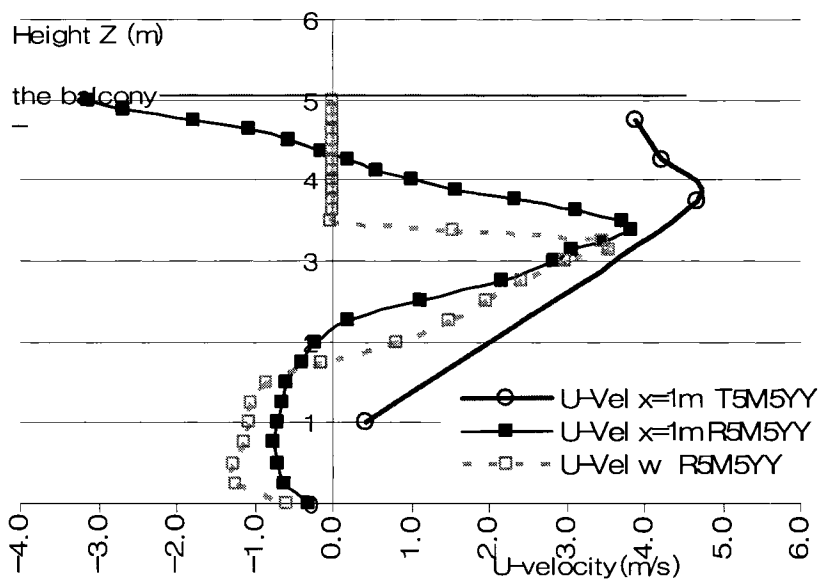

Fig 20 U-Velocity profiles at the opening (R5M5YY and T5M5YY)

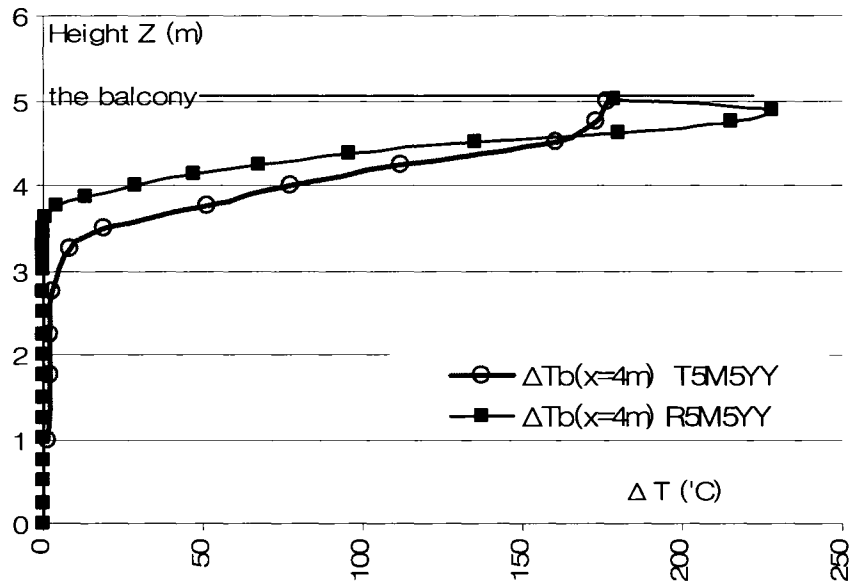

Fig 21 Temperature rise profiles at the end of the balcony (R5M5YY and T5M5YY)

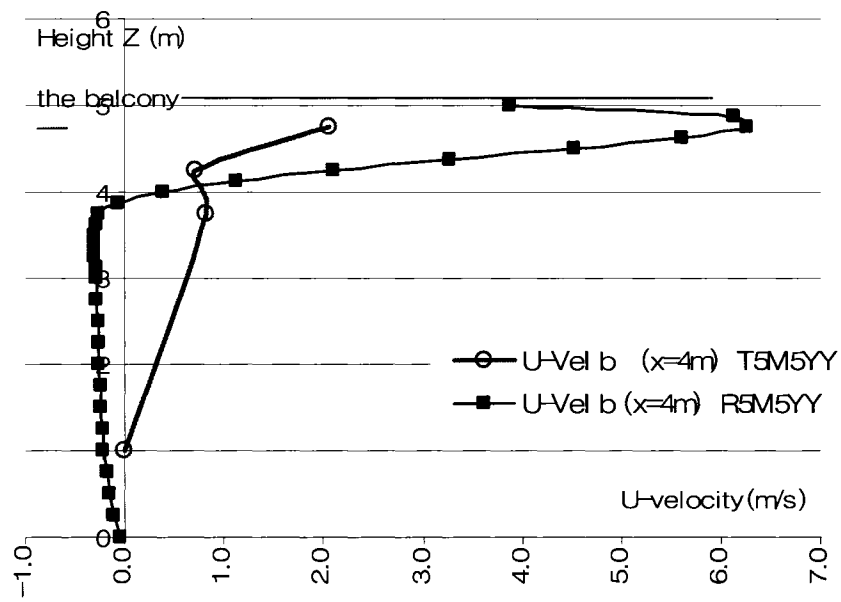

Fig 22 U-Velocity profiles at the end of the balcony (R5M5YY and T5M5YY)

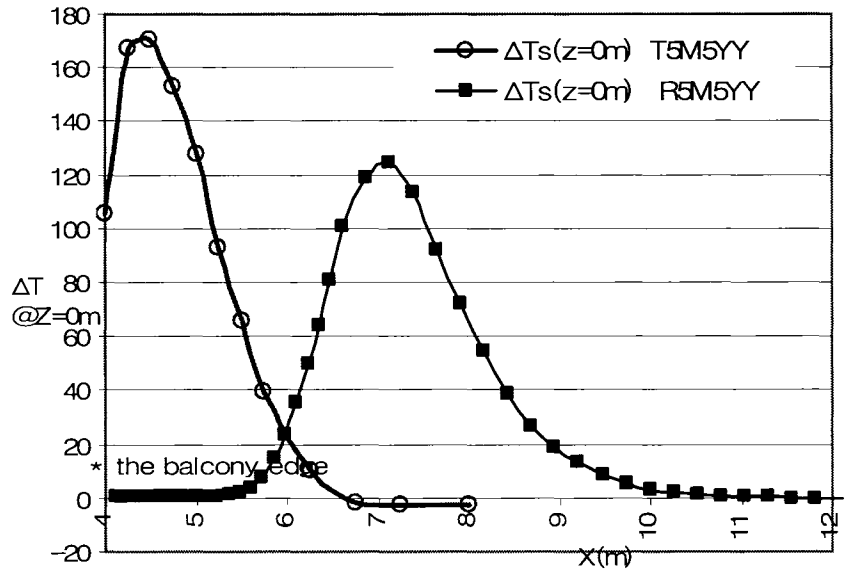

Fig 23 Temperature rise profiles at the edge of the balcony (R5M5YY and T5M5YY)

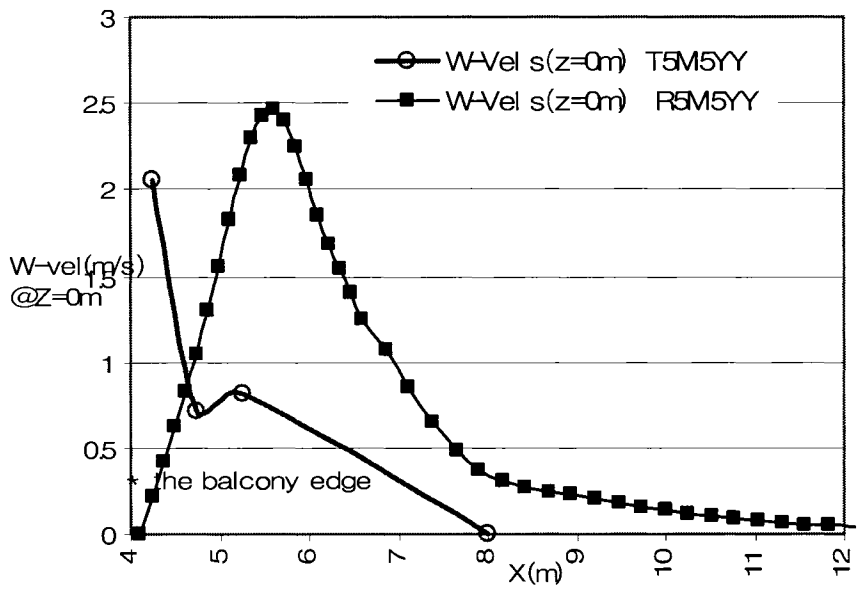

Fig 24 W-Velocity profiles at the edge of the balcony (R5M5YY and T5M5YY)

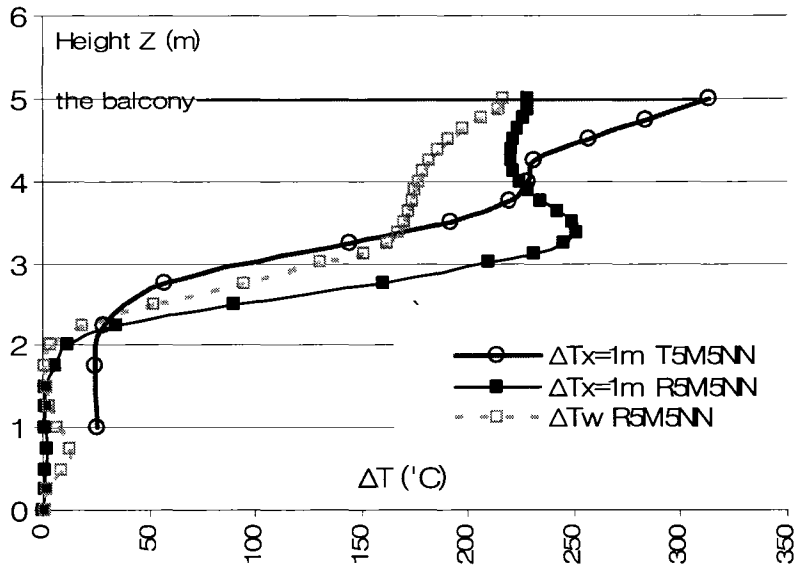

Fig 25 Temperature rise profiles at the opening (R5M5NN and T5M5NN)

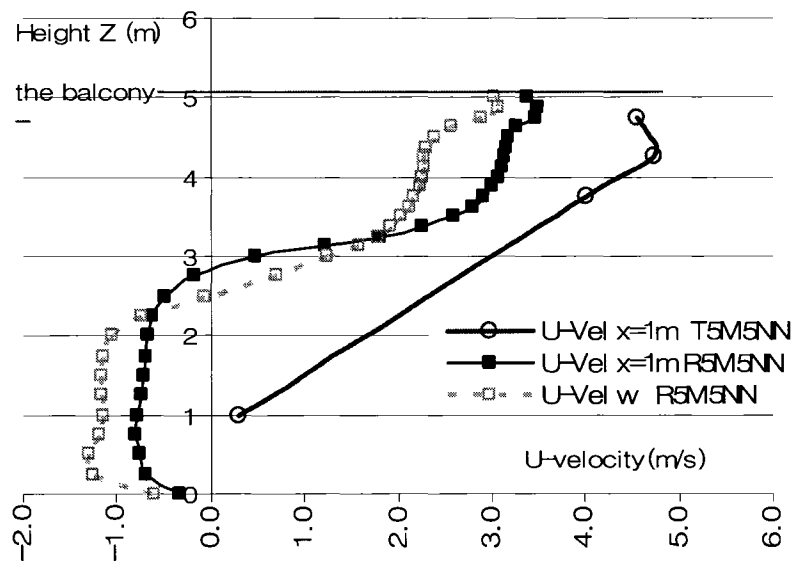

Fig 26 U-Velocity profiles at the opening ((R5M5NN and T5M5NN)

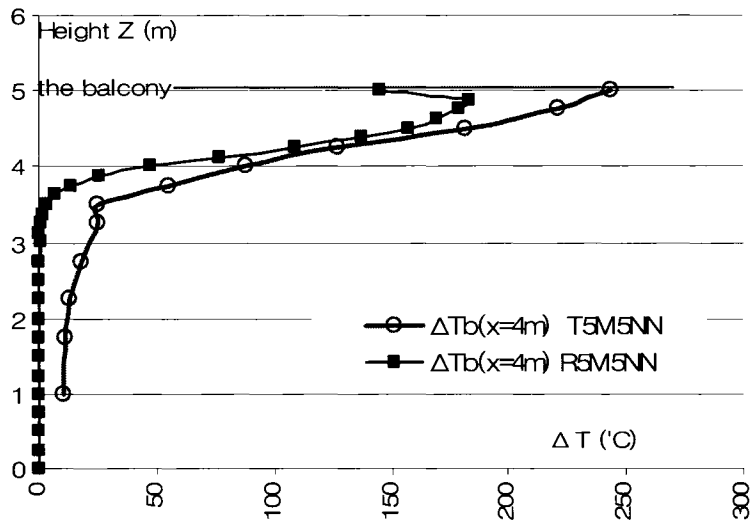

Fig 27 Temperature rise profiles at the end of the balcony (R5M5NN and T5M5NN)

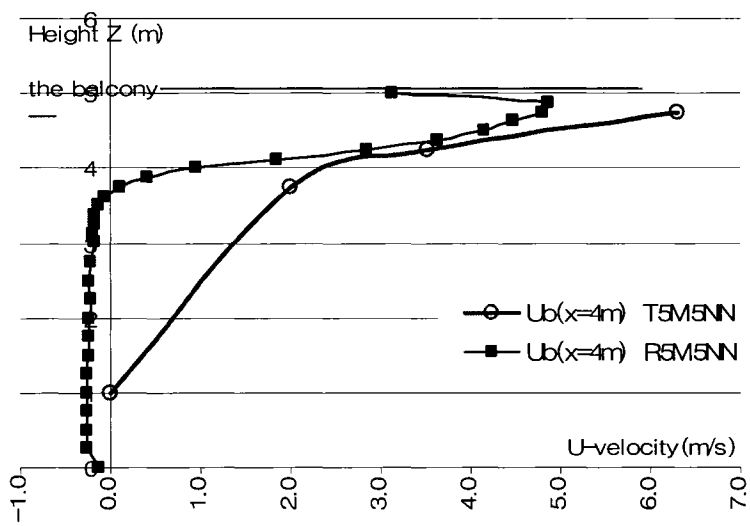

Fig 28 U-Velocity profiles at the end of the balcony (R5M5NN and T5M5NN)

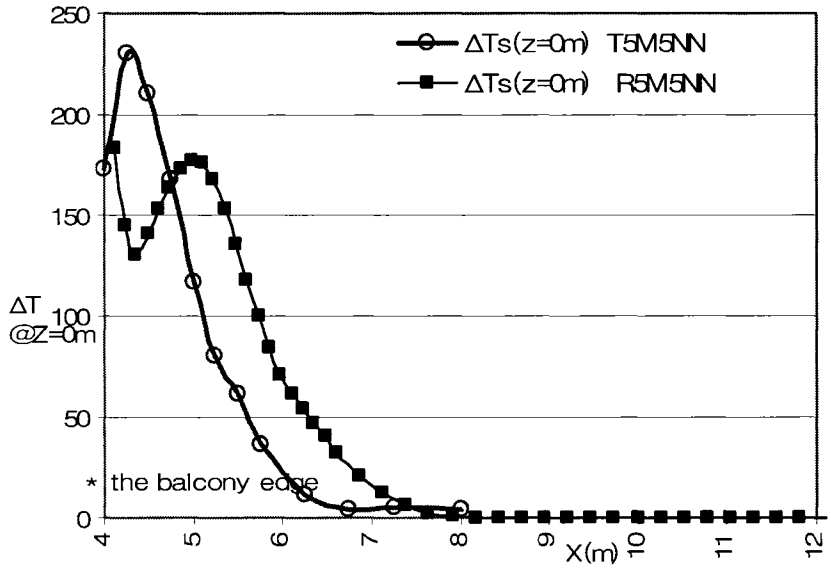

Fig 29 Temperature rise profiles at the edge of the balcony (R5M5NN and T5M5NN)

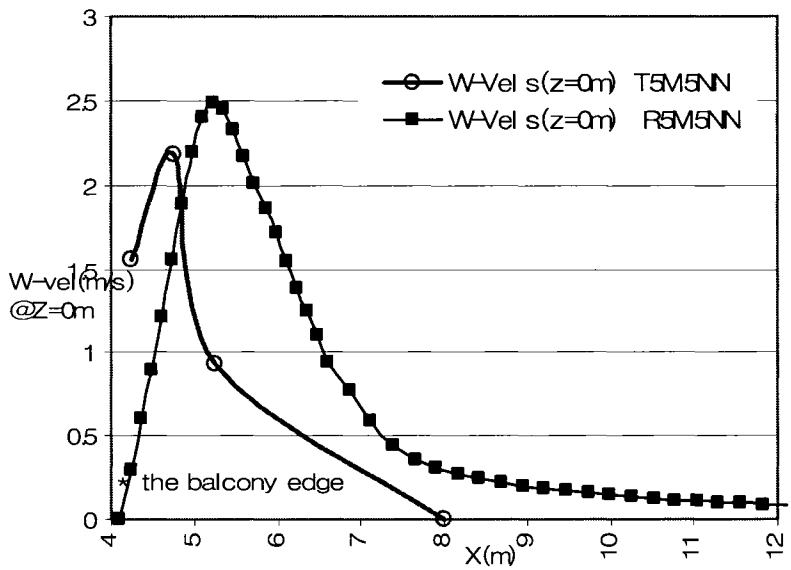

Fig 30 W-Velocity profiles at the edge of the balcony (R5M5NN and T5M5NN)

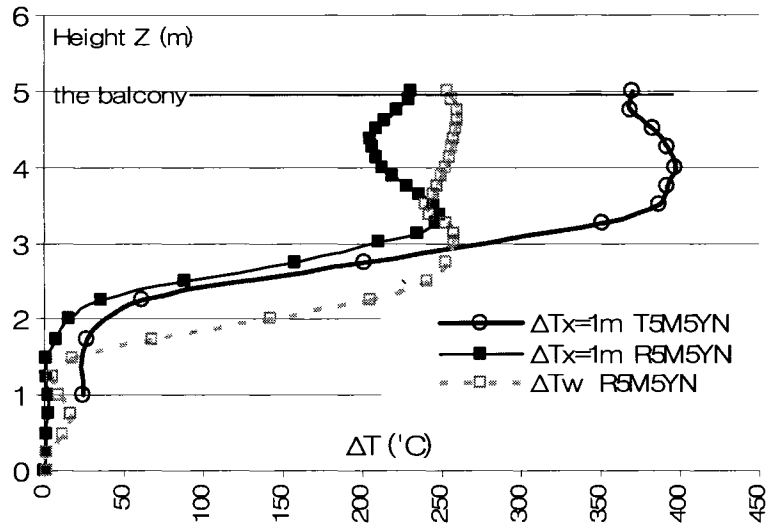

Fig 31 Temperature rise profiles at the opening (R5M5YN and T5M5YN)

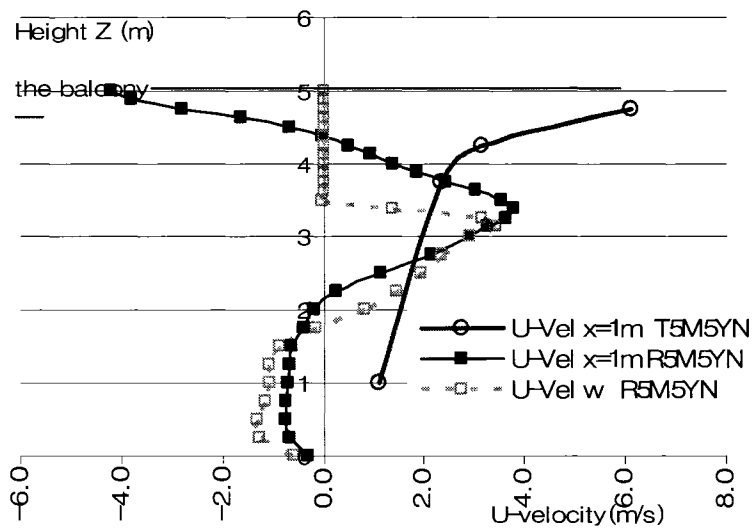

Fig 32 U-Velocity profilesat the opening(R5M5YN and T5M5YN)

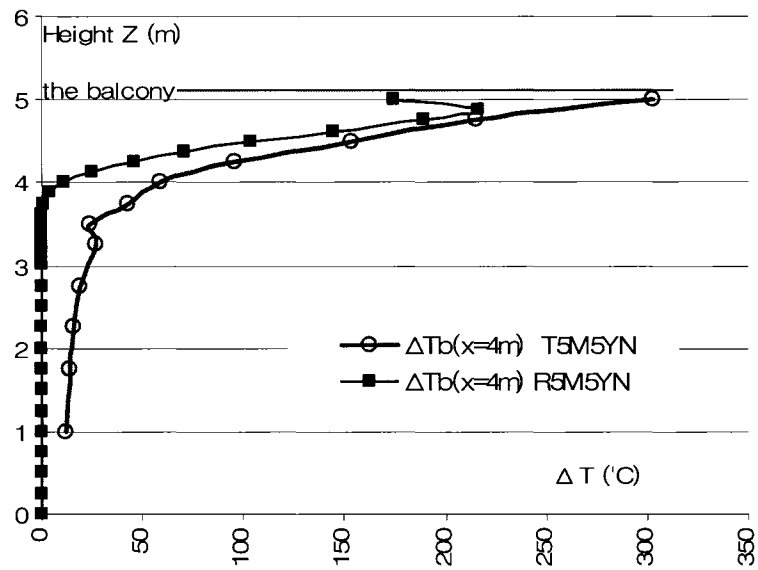

Fig 33 Temperature rise profiles at the end of the balcony (R5M5YN and T5M5YN)

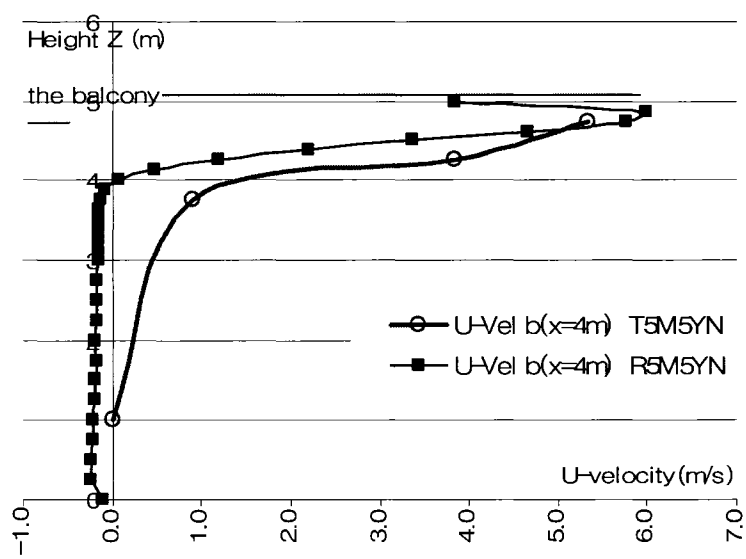

Fig 34 U-Velocity profiles at the end of the balcony (R5M5YN and T5M5YN)

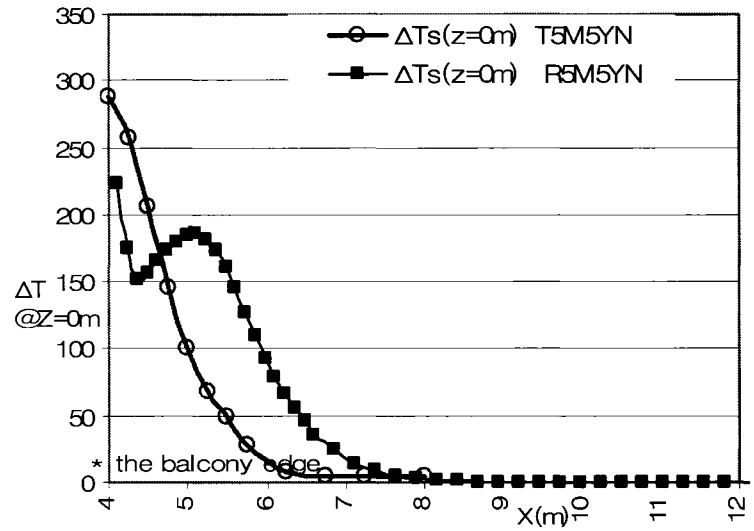

Fig 35 Temperature rise profiles at the edge of the balcony (R5M5YN and T5M5YN)

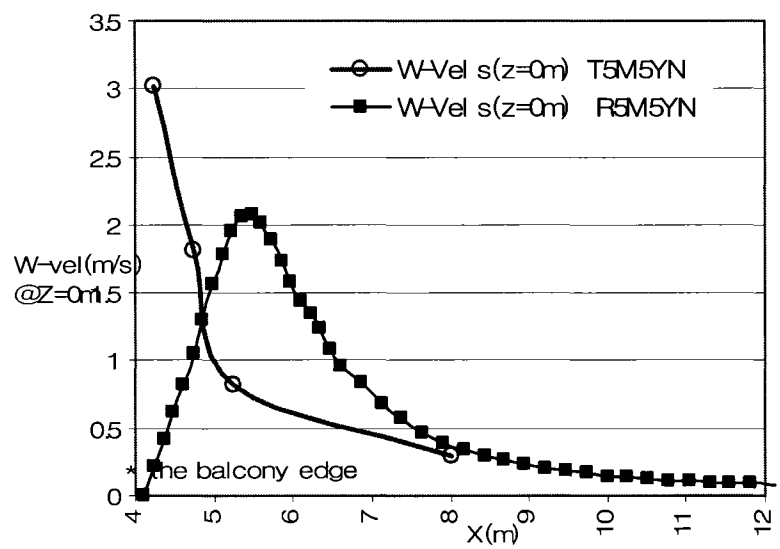

Fig 36 W-Velocity profiles at the edge of the balcony (R5M5YN and T5M5YN)

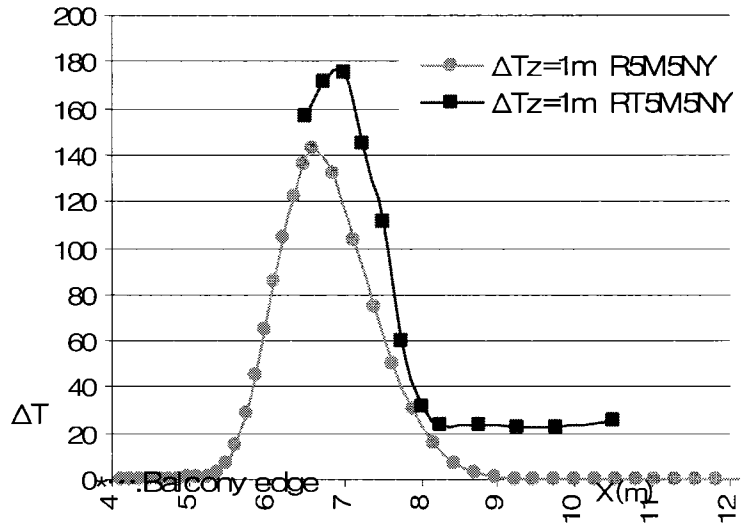

Fig 37 Temperature rise profiles at z=1 (RT5M5NY and R5M5NY)

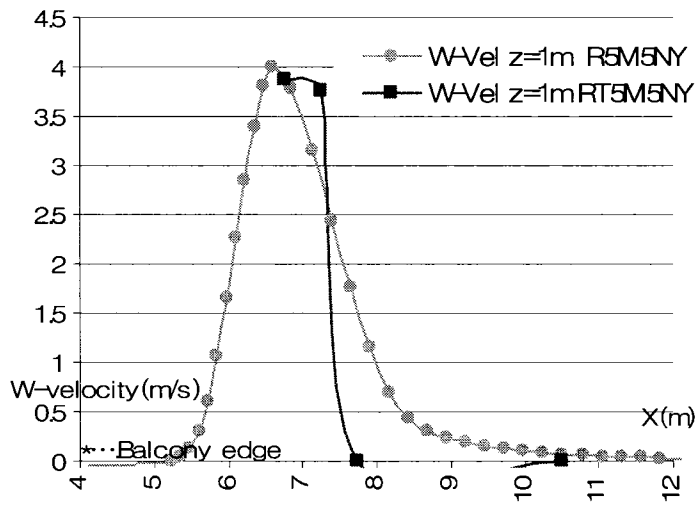

Fig 38 W-Velocity profiles at z=1 (RT5M5NY and R5M5NY)

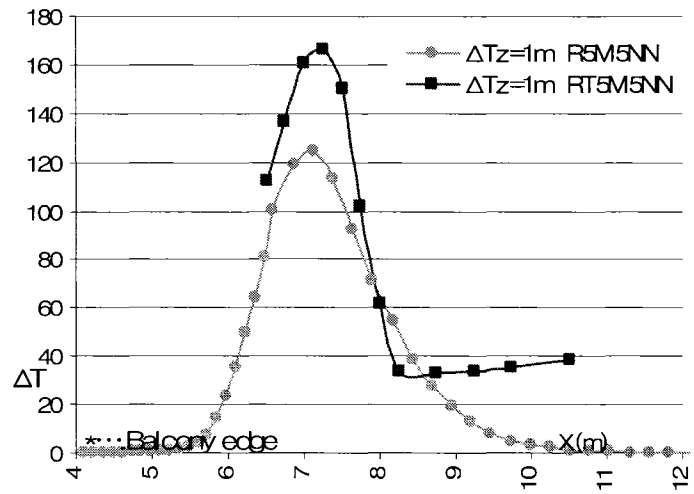

Fig 39 Temperature rise profiles at z=1 (RT5M5NN and R5M5NN)

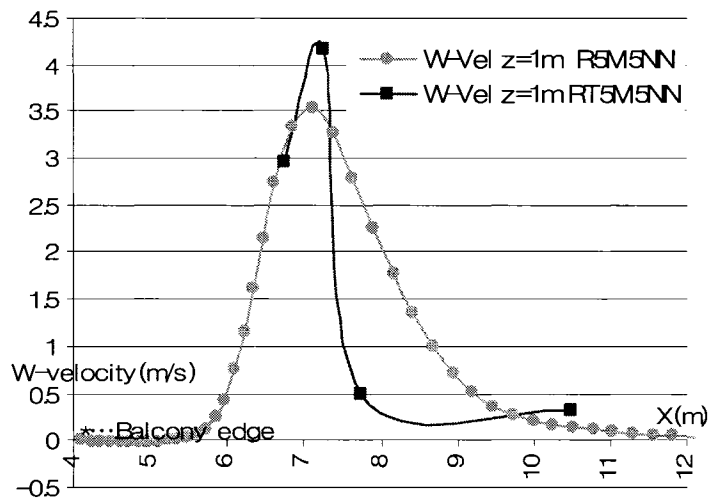

Fig 40 W-Velocity profiles at z=1 (RT5M5NY and R5M5NY)

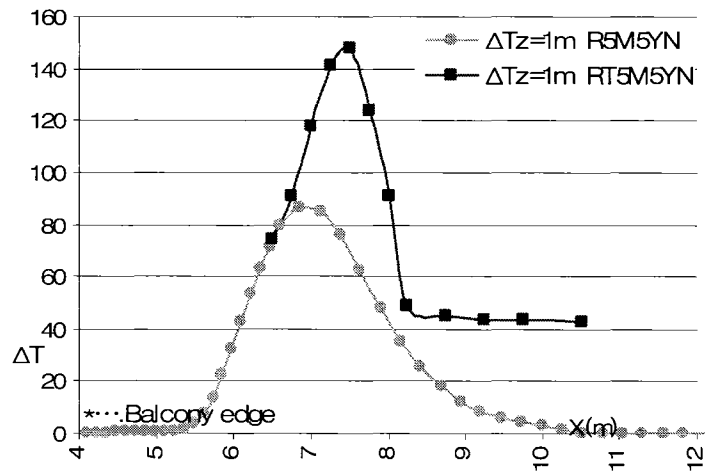

Fig 41 Temperature rise profiles at z=1 (RT5M5YN and R5M5YN)

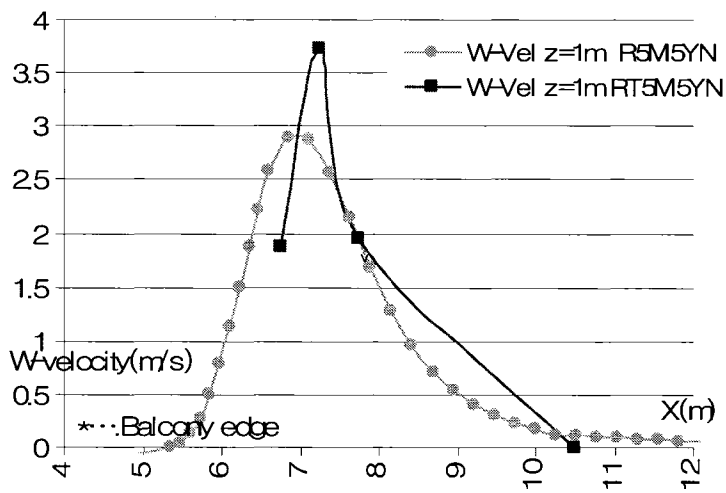

Fig 42 W-Velocity profiles at z=1 (RT5M5YN and R5M5YN)

APPENDIX D. Temperature correlation with Q/W : results from cases without draft curtain

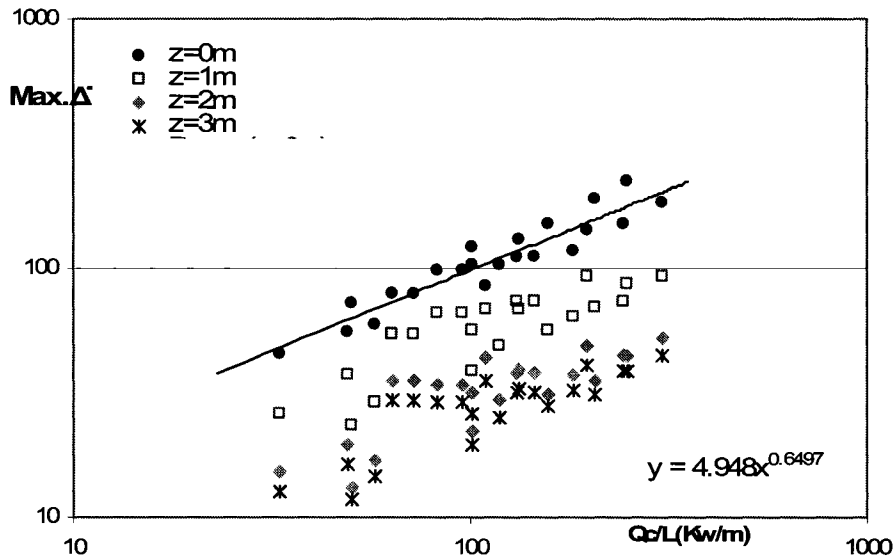

Figure A.1 Max. Temperature rise at every 1m above the balcony, plotted with respect to (Q_c/L) , (Simulation without draft curtain)

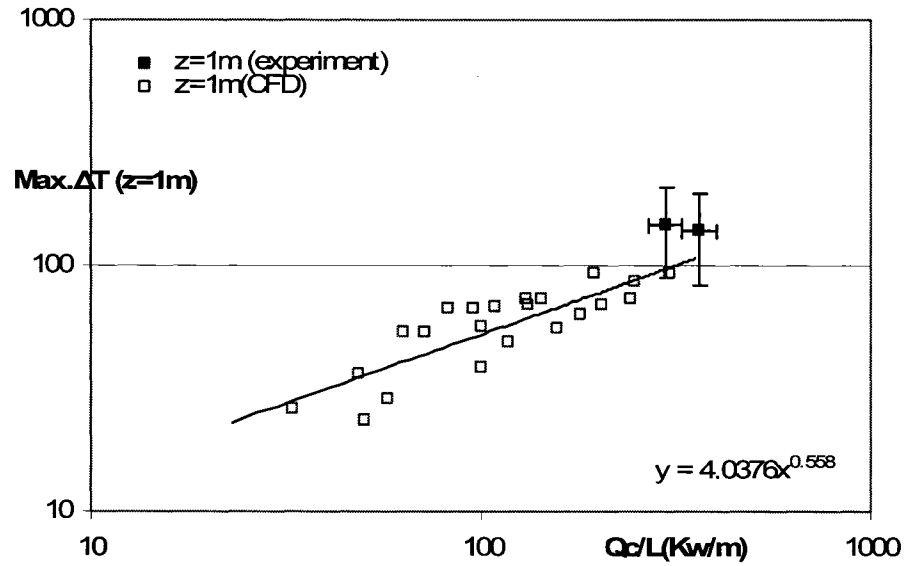

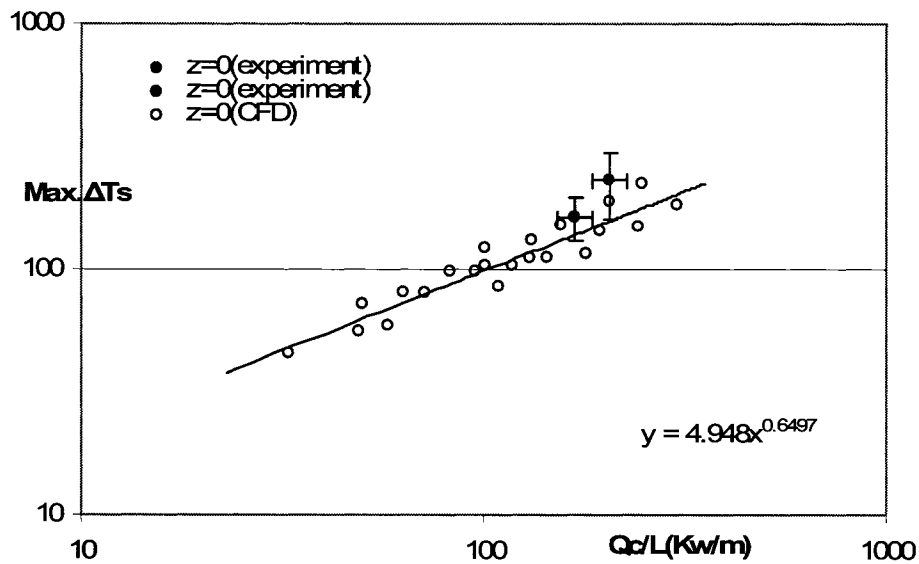

Figure A.2 Comparison of ΔT (at z=0m and 1m) between experiment and simulation (cases without draft curtain)